QUANTITATIVE FT-IRRS ANALYSIS OF THE EFFECTS OF SOLUTION CHEMISTRY ON AQUEOUS GLASS CORROSION

BY

GREG DARBY

A DISSERTATION PRESENTED TO THE GRADUATE SCHOOL
OF THE UNIVERSITY OF FLORIDA
IN PARTIAL FULFILLMENT OF THE REQUIREMENTS
FOR THE DEGREE OF DOCTOR OF PHILOSOPHY

UNIVERSITY OF FLORIDA

2000

ACKNOWLEDGEMENTS

The author wishes to express appreciation to all of his committee members for their invaluable input, and especially to his committee chairman, Dr. David E. Clark, for all his years of guidance and tutelage. Thanks are also extended to Diane Folz for all of her support and expertise, A.L. Dempere for her time and assistance in AFM training, and to M. Lambers, for her expertise in SIMS.

In addition, thanks are extended to Sherry Andrews for her invaluable moral support and encouragement.

Finally, the author wishes to thank his mother, Elizabeth Ann Darby, and his father, Greg Darby Sr., for their commitment in making his academic career go as smoothly as possible.

TABLE OF CONTENTS

	Page
ACKNOWLEDGEMENTS	ii
LIST OF TABLES.	v
LIST OF FIGURES	viii
ABSTRACT	xviii
CHAPTER 1 INTRODUCTION	1
A Brief History of Glass	1
Definition of Glass	4
The Silicate Glass Structure	5
Objectives	7
CHAPTER 2 BACKGROUND	10
An Overview of Aqueous Glass Corrosion	10
The Kinetics of Glass Leaching	11
The Effect of Solution pH	18
The Effects of Electrolytes in Solution	19
Characterization of Glass Corrosion	23
CHAPTER 3 FOURIER TRANSFORM INFRARED SPECTROSCOPY	25
Principles and Theory	25
Components and Instrumentation	29
Advantages of FT-IR over Dispersive Infrared Spectroscopy	36

CHAPTER 4 STATISTICAL ANALYSIS OF FT-IRRS DATA 38

Sample Preparation 38
Description of an FT-IRRS Spectrum 39
Effects of Surface Roughness 42
Experimental Design 46
Analysis of Variance 50
Discussion 140

CHAPTER 5 EFFECTS OF SOLUTION CHEMISTRY ON LEACHING BEHAVIOR OF SODA-LIME-SILICA GLASS 142

Introduction 142
Sample Preparation 143
The Leach Test 144
FT-IRRS Analysis of Glass Corrosion 146
pH Analysis 178
Solution Analysis 182
Depth Profiling 188
Discussion 199

CHAPTER 6 SUMMARY AND CONCLUSIONS 202

Statistical Analysis of FT-IRRS Data 204
Quantitative FT-IRRS Analysis of the Effects of Solution Chemistry on Glass Corrosion 205
Verification of the Validity of the FT-IRRS Data 206
Mechanisms of Glass Corrosion in Concentrated Electrolyte Solutions 207
Future Work 210

REFERENCES 211

BIOGRAPHICAL SKETCH 216

LIST OF TABLES

		Page
Table 2-1	Commonly used techniques for studying glass surfaces [LEE86].....	24
Table 4-1	FT-IRRS peak height and peak position of the left boundary of the corrected peak area of a 20/10/70 SLS glass for varying levels of polish during block one.....	53
Table 4-2	FT-IRRS peak height and peak position of the silica-oxygen stretching vibration within tetrahedra of a 20/10/70 SLS glass for varying levels of polish during block one.....	54
Table 4-3	FT-IRRS peak height and peak position of the "coupled" region in a 20/10/70 SLS glass for varying levels of polish during block one.....	55
Table 4-4	FT-IRRS peak height and peak position of the silica-nonbridging oxygen stretching vibration in a 20/10/70 SLS glass for varying levels of polish during block one.....	56
Table 4-5	FT-IRRS peak height and peak position of the right boundary of the corrected peak area in a 20/10/70 SLS glass for varying levels of polish during block one.....	57
Table 4-6	FT-IRRS peak height and peak position of the silica-bridging oxygen stretching vibration between tetrahedra in a 20/10/70 SLS glass for varying levels of polish during block one.....	58
Table 4-7	The corrected peak area in a 20/10/70 SLS glass for varying levels of polish during block one.....	59
Table 4-8	FT-IRRS peak height and peak position of the left boundary of the corrected peak area of a 20/10/70 SLS glass for varying levels of polish during block two.....	60

Table 4-9 FT-IRRS peak height and peak position of the silica-oxygen stretching vibration within tetrahedra of a 20/10/70 SLS glass for varying levels of polish during block two. 61

Table 4-10 FT-IRRS peak height and peak position of the "coupled" region in a 20/10/70 SLS glass for varying levels of polish during block two..... 62

Table 4-11 FT-IRRS peak height and peak position of the silica-nonbridging oxygen stretching vibration in a 20/10/70 SLS glass for varying levels of polish during block two..... 63

Table 4-12 FT-IRRS peak height and peak position of the right boundary of the corrected peak area in a 20/10/70 SLS glass for varying levels of polish during block two..... 64

Table 4-13 FT-IRRS peak height and peak position of the silica-bridging oxygen stretching vibration between tetrahedra in a 20/10/70 SLS glass for varying levels of polish during block two..... 65

Table 4-14 The corrected peak area in a 20/10/70 SLS glass for varying levels of polish during block two..... 66

Table 4-15 FT-IRRS peak height and peak position of the left boundary of the corrected peak area of a 20/10/70 SLS glass for varying levels of polish during block three..... 67

Table 4-16 FT-IRRS peak height and peak position of the silica-oxygen stretching vibration within tetrahedra of a 20/10/70 SLS glass for varying levels of polish during block three..... 68

Table 4-17 FT-IRRS peak height and peak position of the "coupled" region in a 20/10/70 SLS glass for varying levels of polish during block three..... 69

Table 4-18 FT-IRRS peak height and peak position of the silica-nonbridging oxygen stretching vibration in a 20/10/70 SLS glass for varying levels of polish during block three..... 70

Table 4-19 FT-IRRS peak height and peak position of the right boundary of the corrected peak area in a 20/10/70 SLS glass for varying levels of polish during block three..... 71

Table 4-20 FT-IRRS peak height and peak position of the silica-bridging oxygen stretching vibration between tetrahedra in a 20/10/70 SLS glass for varying levels of polish during block three..... 72

Table 4-21 The corrected peak area in a 20/10/70 SLS glass for varying levels of polish during block three..... 73

Table 4-22 ANOVA table template which was applied to spectral features..... 75

Table 4-23 ANOVA table for PH1 and PP1..... 76

Table 4-24 ANOVA table for PH2 and PP2..... 77

Table 4-25 ANOVA table for PH3 and PP3..... 78

Table 4-26 ANOVA table for PH4 and PP4..... 79

Table 4-27 ANOVA table for PH5 and PP5..... 80

Table 4-28 ANOVA table for PH6 and PP6..... 81

Table 4-29 A matrix representation of the coarsest surface roughness allowable before effects to spectral features become significant. 117

Table 5-1 pH after 12 hours of leaching in various solutions (95% confidence limits are included) 180

Table 6-1 Conclusions of this study..... 209

LIST OF FIGURES

		Page
Figure 1-1	The basic silica tetrahedra	5
Figure 1-2	The addition of alkali ions and the formation of non-bridging oxygens	8
Figure 1-3	A schematic representation of (a) a random silica network and (b) the structure of a sodium silicate glass. [KIN76]	9
Figure 2-1	A schematic representation of (a) bulk sodium silicate glass in contact with water, (b) ion-exchange reaction between surface sodium ions and $H^+(H_3O^+)$ in the water, and (c) the build-up of the alkali-depleted leached layer	14
Figure 2-2	A schematic representation of the reacted zones in a multi-component glass. [MEN84] and [CLA94]	15
Figure 3-1	A schematic representation illustrating specular and diffuse reflection from the surface of a sample. Adapted from Kingery [KIN76]	28
Figure 3-2	A simplified representation of the necessary components of an infrared spectrometer	30
Figure 3-3	Schematic diagram of a single-beam grating spectrometer. Adapted from Ferraro and Basile [FER78]	32
Figure 3-4	Schematic diagram of a Fourier transform infrared spectrometer. Adapted from Ferraro and Basile [FER78]	34
Figure 3-5	A schematic representation of the specular reflectance accessory	35

Figure 4-1 A typical FT-IRRS spectrum for a 20/10/70 SLS glass. (S indicates the location of the silicon-oxygen stretching vibration within a tetrahedra. SN indicates the location of the silicon-nonbridging oxygen stretching vibration. T indicates the location of the silicon-oxygen stretching vibration which occurs between neighboring tetrahedra)..... 40

Figure 4-2 Derivation of the Rayleigh criterion..... 44

Figure 4-3 A plot of the Rayleigh-criterion for rms surface roughness versus wavenumber..... 45

Figure 4-4 A representation of the effect of rms surface roughness on the reflectance of a 20/10/70 SLS FT-IRRS spectra..... 47

Figure 4-5 Labeling of the spectral features analyzed using ANOVA, as a function of surface polish and day-to-day variation..... 49

Figure 4-6 FT-IRRS spectra of a 20/10/70 SLS glass as a function of polishing. The spectra are overlaid upon one another in the top figure. The bottom figure offsets spectra by 5% for readability..... 74

Figure 4-7 The overall 3-day means (30 replicates) of % reflectance and wavenumber (cm^{-1}) for PH1 and PP1, respectively. (95% confidence bars drawn for reference)..... 83

Figure 4-8 The overall 3-day means (30 replicates) of % reflectance and wavenumber (cm^{-1}) for PH2 and PP2, respectively. (95% confidence bars drawn for reference)..... 84

Figure 4-9 The overall 3-day means (30 replicates) of % reflectance and wavenumber (cm^{-1}) for PH3 and PP3, respectively. (95% confidence bars drawn for reference)..... 85

Figure 4-10 The overall 3-day means (30 replicates) of % reflectance and wavenumber (cm^{-1}) for PH4 and PP4, respectively. (95% confidence bars drawn for reference)..... 86

Figure 4-11 The overall 3-day means (30 replicates) of % reflectance and wavenumber (cm^{-1}) for PH5 and PP5, respectively. (95% confidence bars drawn for reference)..... 87

Figure 4-12 The overall 3-day means (30 replicates) of % reflectance and wavenumber (cm^{-1}) for PH6 and PP6, respectively. (95% confidence bars drawn for reference)..... 88

Figure 4-13 The overall 3-day means (30 replicates) of the corrected peak area as a function of polishing. (95% confidence bars drawn for reference)..... 89

Figure 4-14 The overall 3-day means (30 replicates) of the PH2/PH4 peak height ratio as a function of polishing. (95% confidence bars drawn for reference) 90

Figure 4-15 The overall 3-day means (30 replicates) the PP2/PP4 peak position ratio as a function of polishing. (95% confidence bars drawn for reference)..... 91

Figure 4-16 Optical microscopy picture of the surface of a 20/10/70 SLS glass polished with 180 grit SiC paper. The EDS spectra shows the presense of Na, Ca and Si as expected. (Samples were coated in Au and Pd)..... 93

Figure 4-17 Optical microscopy picture of the surface of a 20/10/70 SLS glass polished with 240 grit SiC paper. The EDS spectra shows the presense of Na, Ca and Si as expected. (Samples were coated in Au and Pd)..... 94

Figure 4-18 Optical microscopy picture of the surface of a 20/10/70 SLS glass polished with 320 grit SiC paper. The EDS spectra shows the presense of Na, Ca and Si as expected. (Samples were coated in Au and Pd)..... 95

Figure 4-19 Optical microscopy picture of the surface of a 20/10/70 SLS glass polished with 400 grit SiC paper. The EDS spectra shows the presense of Na, Ca and Si as expected. (Samples were coated in Au and Pd)..... 96

Figure 4-20 Optical microscopy picture of the surface of a 20/10/70 SLS glass polished with 600 grit SiC paper. The EDS spectra shows the presense of Na, Ca and Si as expected. (Samples were coated in Au and Pd)..... 97

Figure 4-21 Optical microscopy picture of the surface of a 20/10/70 SLS glass polished with 9.5 micron Al_2O_3. The EDS spectra shows the presense of Na, Ca and Si as expected. (Samples were coated in Au and Pd)..... 98

Figure 4-22 Optical microscopy picture of the surface of a 20/10/70 SLS glass polished with 1.0 micron Al_2O_3. The EDS spectra shows the presense of Na, Ca and Si as expected. (Samples were coated in Au and Pd)..... 99

Figure 4-23 Optical microscopy picture of the surface of a 20/10/70 SLS glass polished with 0.3 micron Al_2O_3. The EDS spectra shows the presense of Na, Ca and Si as expected, plus the introduction of Al. (Samples were coated in Au and Pd)..... 100

Figure 4-24 Results of successive ANOVA tests on PH1.
(ALL: includes 180 grit through 0.3 micron polishing)
(180+: includes 180 grit through 1.0 micron polishing)
(240+: includes 240 grit through 1.0 micron polishing)
(320+: includes 320 grit through 1.0 micron polishing)
(400+: includes 400 grit through 1.0 micron polishing)
(600+: includes 600 grit through 1.0 micron polishing)..... 102

Figure 4-25 Results of successive ANOVA tests on PP1..... 103

Figure 4-26 Results of successive ANOVA tests on PH2..... 104

Figure 4-27 Results of successive ANOVA tests on PP2..... 105

Figure 4-28 Results of successive ANOVA tests on PH3..... 106

Figure 4-29 Results of successive ANOVA tests on PP3..... 107

Figure 4-30 Results of successive ANOVA tests on PH4..... 108

Figure 4-31 Results of successive ANOVA tests on PP4..... 109

Figure 4-32 Results of successive ANOVA tests on PH5..... 110

Figure 4-33 Results of successive ANOVA tests on PP5..... 111

Figure 4-34 Results of successive ANOVA tests on PH6..... 112

Figure 4-35 Results of successive ANOVA tests on PP6..... 113

Figure 4-36 The surface of a 20/10/70 SLS glass sample polished with 1.0 micron Al_2O_3 as measured by AFM..... 118

Figure 4-37 The surface of a 20/10/70 SLS glass sample polished with 9.5 micron Al_2O_3 as measured by AFM..... 119

Figure 4-38 The surface of a 20/10/70 SLS glass sample polished with 600 grit SiC as measured by AFM..... 120

Figure 4-39 The surface of a 20/10/70 SLS glass sample polished with 400 grit SiC as measured by AFM..... 121

Figure 4-40 The surface of a 20/10/70 SLS glass sample polished with 320 grit SiC as measured by AFM..... 122

Figure 4-41 The surface of a 20/10/70 SLS glass sample polished with 240 grit SiC as measured by AFM..... 123

Figure 4-42 The surface of a 20/10/70 SLS glass sample polished with 180 grit SiC as measured by AFM..... 124

Figure 4-43 The surface of a 20/10/70 SLS glass sample corroded for 12 hours in deionized water as measured by AFM..... 125

Figure 4-44 AFM measurements of a 20/10/70 SLS glass sample polished with 1.0 micron Al_2O_3..... 126

Figure 4-45 AFM measurements of a 20/10/70 SLS glass sample polished with 9.5 micron Al_2O_3..... 127

Figure 4-46 AFM measurements of a 20/10/70 SLS glass sample polished with 600 grit SiC..... 128

Figure 4-47 AFM measurements of a 20/10/70 SLS glass sample polished with 400 grit SiC..... 129

Figure 4-48 AFM measurements of a 20/10/70 SLS glass sample polished with 320 grit SiC..... 130

Figure 4-49 AFM measurements of a 20/10/70 SLS glass sample polished with 240 grit SiC..... 131

Figure 4-50 AFM measurements of a 20/10/70 SLS glass sample polished with 180 grit SiC..... 132

Figure 4-51 AFM measurements of a 20/10/70 SLS glass sample corroded for 12 hours in deionized water..... 133

Figure 4-52 Calculated and measured FT-IRRS spectra for a 20/10/70 SLS glass polished at 180 grit..... 134

Figure 4-53 Calculated and measured FT-IRRS spectra for a 20/10/70 SLS glass polished at 240 grit..... 135

Figure 4-54 Calculated and measured FT-IRRS spectra for a 20/10/70 SLS glass polished at 320 grit..... 136

Figure 4-55 Calculated and measured FT-IRRS spectra for a 20/10/70 SLS glass polished at 400 grit..... 137

Figure 4-56 Calculated and measured FT-IRRS spectra for a 20/10/70 SLS glass polished at 600 grit..... 138

Figure 4-57 Comparison of the measured σ values to those which were calculated via curve fitting. 139

Figure 5-1 Schematic of the experimental arrangement for static aqueous leaching.

Figure 5-2 FT-IRRS spectra as a function of time for a 20/10/70 SLS glass sample immersed in 0.1M KCl. The spectra have not been transformed to correct for surface roughness resulting from corrosion..... 147

Figure 5-3 FT-IRRS spectra as a function of time for a 20/10/70 SLS glass sample immersed in 0.1M KNO_3. The spectra have not been transformed to correct for surface roughness resulting from corrosion..... 148

Figure 5-4 FT-IRRS spectra as a function of time for a 20/10/70 SLS glass sample immersed in 0.1M LiCl. The spectra have not been transformed to correct for surface roughness resulting from corrosion..... 149

Figure 5-5 FT-IRRS spectra as a function of time for a 20/10/70 SLS glass sample immersed in 0.1M $LiNO_3$. The spectra have not been transformed to correct for surface roughness resulting from corrosion..... 150

Figure 5-6 FT-IRRS spectra as a function of time for a 20/10/70 SLS glass sample immersed in 1.0M KCl. The spectra have not been transformed to correct for surface roughness resulting from corrosion..... 151

Figure 5-7 FT-IRRS spectra as a function of time for a 20/10/70 SLS glass sample immersed in 1.0M KNO_3. The spectra have not been transformed to correct for surface roughness resulting from corrosion..... 152

Figure 5-8 FT-IRRS spectra as a function of time for a 20/10/70 SLS glass sample immersed in 1.0M LiCl. The spectra have not been transformed to correct for surface roughness resulting from corrosion..... 153

Figure 5-9 FT-IRRS spectra as a function of time for a 20/10/70 SLS glass sample immersed in 1.0M $LiNO_3$. The spectra have not been transformed to correct for surface roughness resulting from corrosion..... 154

Figure 5-10 FT-IRRS spectra as a function of time for a 20/10/70 SLS glass sample immersed in deionized water. The spectra have not been transformed to correct for surface roughness resulting from corrosion..... 155

Figure 5-11 Plot of surface area of polished glass samples as measured by AFM versus rms roughness (σ) as calculated for each of the polished samples using Equation 4-1..... 157

Figure 5-12 The surface of a 20/10/70 SLS glass sample corroded for 12 hours in 0.1M KCl. Surface Area: 402.77 μm^2..... 158

Figure 5-13 The surface of a 20/10/70 SLS glass sample corroded for 12 hours in 0.1M KNO_3. Surface Area: 405.00 μm^2..... 159

Figure 5-14 The surface of a 20/10/70 SLS glass sample corroded for 12 hours in 0.1M LiCl. Surface Area: 403.77 μm^2..... 160

Figure 5-15 The surface of a 20/10/70 SLS glass sample corroded for 12 hours in 0.1M $LiNO_3$. Surface Area: 403.27 μm^2..... 161

Figure 5-16 The surface of a 20/10/70 SLS glass sample corroded for 12 hours in 1.0M KCl. Surface Area: 404.45 μm^2..... 162

Figure 5-17 The surface of a 20/10/70 SLS glass sample corroded for 12 hours in 1.0M KNO_3. Surface Area: 401.97 μm^2 163

Figure 5-18 The surface of a 20/10/70 SLS glass sample corroded for 12 hours in 1.0M LiCl. Surface Area: 403.16 μm^2 164

Figure 5-19 The surface of a 20/10/70 SLS glass sample corroded for 12 hours in 1.0M $LiNO_3$. Surface Area: 402.36 μm^2 165

Figure 5-20 The surface of a 20/10/70 SLS glass sample corroded for 12 hours in deionized water. Surface Area: 404.19 μm^2 166

Figure 5-21 FT-IRRS spectrum of the unleached surface polished to 9.5 μm Al_2O_3 compared to the transformed spectrum of the same sample leached in 0.1M KCl for 12 hours..... 167

Figure 5-22 FT-IRRS spectrum of the unleached surface polished to 9.5 μm Al_2O_3 compared to the transformed spectrum of the same sample leached in 0.1M KNO_3 for 12 hours..... 168

Figure 5-23 FT-IRRS spectrum of the unleached surface polished to 9.5 μm Al_2O_3 compared to the transformed spectrum of the same sample leached in 0.1M LiCl for 12 hours..... 169

Figure 5-24 FT-IRRS spectrum of the unleached surface polished to 9.5 μm Al_2O_3 compared to the transformed spectrum of the same sample leached in 0.1M $LiNO_3$ for 12 hours..... 170

Figure 5-25 FT-IRRS spectrum of the unleached surface polished to 9.5 μm Al_2O_3 compared to the transformed spectrum of the same sample leached in 1.0M KCl for 12 hours..... 171

Figure 5-26 FT-IRRS spectrum of the unleached surface polished to 9.5 μm Al_2O_3 compared to the transformed spectrum of the same sample leached in 1.0M KNO_3 for 12 hours..... 172

Figure 5-27 FT-IRRS spectrum of the unleached surface polished to 9.5 μm Al_2O_3 compared to the transformed spectrum of the same sample leached in 1.0M LiCl for 12 hours..... 173

Figure 5-28 FT-IRRS spectrum of the unleached surface polished to 9.5 μm Al_2O_3 compared to the transformed spectrum of the same sample leached in 1.0M $LiNO_3$ for 12 hours..... 174

Figure 5-29 FT-IRRS spectrum of the unleached surface polished to 9.5 μm Al_2O_3 compared to the transformed spectrum of the same sample leached in deionized water for 12 hours. 175

Figure 5-30 Peak position (PP2) differences between the leached glass and the unleached glass with 95% confidence bars superimposed. The error bars for 0.1M LiCl, 1.0M KCl and 1.0M $LiNO_3$ are too small to be seen on the graph..... 176

Figure 5-31 pH correction curves for the various electrolyte solutions..... 181

Figure 5-32 Normalized mass loss of Na after 12 hours of immersion in various solutions..... 185

Figure 5-33 Normalized mass loss of Ca after 12 hours of immersion in various solutions..... 186

Figure 5-34 Normalized mass loss of Si after 12 hours of immersion in various solutions..... 187

Figure 5-35 SIMS depth profiling of a 20/10/70 SLS glass sample immersed in 0.1M KCl for 12 hours..... 189

Figure 5-36 SIMS depth profiling of a 20/10/70 SLS glass sample immersed in 0.1M KNO_3 for 12 hours..... 190

Figure 5-37 SIMS depth profiling of a 20/10/70 SLS glass sample immersed in 0.1M LiCl for 12 hours..... 191

Figure 5-38 SIMS depth profiling of a 20/10/70 SLS glass sample immersed in 0.1M $LiNO_3$ for 12 hours..... 192

Figure 5-39 SIMS depth profiling of a 20/10/70 SLS glass sample immersed in 1.0M KCl for 12 hours..... 193

Figure 5-40 SIMS depth profiling of a 20/10/70 SLS glass sample immersed in 1.0M KNO_3 for 12 hours..... 194

Figure 5-41 SIMS depth profiling of a 20/10/70 SLS glass sample immersed in 1.0M LiCl for 12 hours..... 195

Figure 5-42 SIMS depth profiling of a 20/10/70 SLS glass sample immersed in 1.0M $LiNO_3$ for 12 hours..... 196

Figure 5-43 SIMS depth profiling of a 20/10/70 SLS glass sample immersed in deionized water for 12 hours..... 197

Abstract of Dissertation Presented to the Graduate School
of the University of Florida in Partial Fulfillment of the
Requirements for the Degree of Doctor of Philosophy

QUANTITATIVE FT-IRRS ANALYSIS OF THE EFFECTS OF SOLUTION CHEMISTRY ON AQUEOUS GLASS CORROSION

By

Greg Darby

December, 2000

Chairman: Dr. David E. Clark
Major Department: Materials Science and Engineering

A statistical analysis of Fourier transform infrared reflection spectroscopy (FT-IRRS) spectra was performed in order to identify spectral features unaffected significantly by day-to-day variation and surface roughness. It was determined that the Si-O-Si stretching vibration peak was unaffected significantly by day-to-day variation and surface roughness. The Si-O-Si peak was used in subsequent analyses to characterize the surfaces of glass exposed to solutions of varying electrolyte composition. A wave scattering equation derived for rough surfaces which exhibit a Gaussian distribution of surface height irregularities was applied to the spectra of glass samples of varying surface roughnesses. A good fit was observed between calculated and measured spectra, which yielded much insight into the FT-IRRS spectral dependence on surface roughness. This technique may be applied in order to transform the spectra of rough samples into theoretically smooth

samples. The consequence of this is that spectral changes may be attributed directly to structural and compositional changes, and not to surface roughness.

Soda-lime-silicate glass samples were prepared, polished smooth, and immersed in various electrolyte solutions. These solutions were of varying concentration, consisted of varying electrolyte cation species, and consisted of varying electrolyte anion species. FT-IRRS analysis revealed no significant anion or cation effect of the aqueous corrosion of soda-lime-silica glass. FT-IRRS did reveal a significant concentration effect on corrosion rates. The Si-O-Si peak shift indicated a reduction of proton exchange with glass alkali. Inductively coupled plasma spectroscopy (ICP) and secondary ion mass spectrometry (SIMS) analyses supported the observations of FT-IRRS. Based upon these analyses, it was believed that electrolyte cation exchange was occurring with the sodium in the glass, thereby reducing the amount of proton exchange taking place. In this short term leach test, the reduction of proton exchange limited the number of Si-OH groups forming in the glass, which, upon dehydration of the glass surface, resulted in the observation via FT-IRRS of a decrease in the Si-O-Si peak shift, as the dehydration reaction was limited by the decreased amount of Si-OH groups. It was concluded that FT-IRRS could serve as a powerful primary surface characterization tool as long as the appropriate statistical analysis is performed on spectral features, and the effects of surface roughening are well understood and accounted for.

CHAPTER 1
INTRODUCTION

A Brief History of Glass

Glasses have been used by man from the earliest times of which there is archeological record. The use of the natural glass, obsidian, was widespread by people of Stone Age culture for the purpose of fashioning arrow-heads, spear-heads and knives. The ease by which obsidian could be broken into sharp, elongated pieces lent itself well to these early applications. It is not well known when glass was first manufactured artificially. The historical accounts of Morey [MOR38] do yield some insight into the beginnings of glass manufacture. One notion offered by Morey was that glass production owes its beginning to accident. Lightning strikes in fields of grain would result in fire. The burning of the grain and subsequent fusion of the ash would produce masses of glass, which the peasants referred to as "lightning stones" [VEL78]. Another account of the origin of glass manufacture was related by Pliny [BOS57, p. 379], describing the accidental discovery by Phoenician traders:

> The story is, that a ship, laden with nitre, being moored upon this spot, the merchants, while preparing their repast upon the seashore, finding no stones at hand for supporting their cauldrons, employed for the purpose some lumps of nitre which they had taken from the vessel. Upon its being subjected to the action of the fire, in combination with the sand of the sea-shore, they beheld transparent streams flowing forth of a liquid hitherto unknown: this, it is said, was the origin of glass.

Although these accounts may heighten the romanticism of the science, the fact remains that earlier glass has been found whose dating is unquestionable [MOR38]. According to Sir W.M. Flinders Petrie, the earliest known glaze dates back to 12,000 B.C. Egypt, and the earliest known pure glass dates back to 7,000 B.C. Egypt. Both of these occurrences were believed to have originated in Asia, before subsequent importation into ancient Egypt [PET25]. Although there is some question as to the actual dating of these occurrences and whether or not these occurrences represented glass at all, it does remain undisputed as to the dating of "rich blue glass beads" found in the coffin of Mait, child queen of King Mentuhotpe (2196-2172 B.C.) [WIN21].

Since man-made glass would have surpassed the rarity of natural gemstones during these early times, glass appears to have first been used as a gem [MOR38]. The pressing of glass into open molds, to form hollow containers, evolved around 1200 B.C. Although some of the products made by this process were of excellent craftmanship and intricate design, the process was a laborious one, and therefore was somewhat restricted in its scope.

The event which, in large part, caused the rapid expansion of glass manufacture and transformed it from a luxury into a necessity was the invention of glass blowing. The glass blowing process made it possible to produce more glasses of quality, more cheaply. Again, it is not certain as to the time and place of the first blown glass. It appears that, in general, glass blowing was believed to have been invented around 20 B.C., or perhaps even a little earlier [KIS08]. The glass blowing revolution resulted in an improvement of glass quality. It was during the early Roman Empire that glass usage for drinking vessels superseded that of silver and gold [BOS57].

The history of glass manufacture becomes unclear in the period from the fall of Rome to the eleventh century [MOR38]. It was not until the eleventh century that glass manufacture entered back into significant development. This re-emergence of glass manufacture occurred in Venice, which soon became the center of the glass industry, a distinction it maintained for at least the next four centuries.

In 1612, a priest, Neri, published a book in Florence entitled, L'Arte Vetraria [NER12]. This book not only recounted the history of glassmaking in detail, it served to usher in a new scientific approach to glass technology. Subsequent progress in the techniques and processes of glass manufacture was rapid. During this time, most of the advances in glass technology were accomplished by empirical observations, rather than through basic scientific understanding [DOR73]. Michael Faraday, in the early nineteenth century, was among the first to study glass in a more fundamental way. Faraday's description of glass as "rather as a solution of different substances one in another than as a strong chemical compound" [FAR30, p. 1] still holds today. Nearly a century later, knowledge of the structure of glass was expanded upon by the papers of Zachariasen [ZAC32] and Warren [WAR38]. Their random-network models are still used to describe glass structure today.

The modern applications of glass have far outgrown its early uses as decorative beads and containers. Today, glass may be recognized in applications ranging from flat glass for windows, to glass electrodes for ion-specific measurement, to microelectronic packaging, to glass lasers used to perform microsurgery, to transoceanic telecommunication lines, and to glass used to safely store radioactive wastes. Glass lends

itself to excel at these various applications due to some of its unique properties, which shall be discussed in a subsequent section.

Definition of Glass

The word "glass" is a broad term which may be used to describe a host of different types of materials. In its most general sense, a glass describes a material which is non-crystalline, or amorphous, in nature, and while it may exhibit some short-range order on the atomic level, it exhibits no long-range order. The ASTM Standards for Glass defines glass as "an inorganic product of fusion which has been cooled to a rigid condition without crystallization." This definition is somewhat restricted in its scope, however, as it is not necessary for a glass to be formed by cooling from the liquid state. Glass coatings may be formed by vapor deposition, for example. Also, the "cooling" of the glass isn't a requirement either. The sol-gel process is a technique which can result in the formation of a glass at room temperature. Glasses do not necessarily need to be inorganic materials either. Organic polymers may exhibit the characteristics of the absence of long-range order, and therefore could be classified as being a glass. Various materials which may be classified as being a glass include, but are not limited to, splat-cooled metals, glassy polymers, electronically conducting glasses of various metal-halide compositions, and oxide glasses. Oxide compositions account for more than 99% of the commercial tonnage of glass [VAR94]. A great percentage of these oxide compositions are silica-based. For the purposes of this dissertation, the term glass will refer to an inorganic, silica-based oxide material, which has been cooled from the liquid state in such a manner that an

amorphous solid material has formed, which exhibits no long-range atomic order. A description and more complete definition of the structure of silicate glasses and their properties will be detailed in the following section.

The Silicate Glass Structure

Glass is a thermodynamically metastable material, characterized by a three-dimensional amorphous structure exhibiting only short-range order corresponding to the hybridization and bonding of its component elements [EBE94]. The tetrahedral arrangement of silicon in silicate glasses generates a three-dimensional polymeric network of ≡Si-O-Si≡ bonds. The bond lengths and bond angles are constrained in individual tetrahedra; however, long-range order is not present. The silica glass structure is the simplest of all glass structures [VAR94]. The basic unit (tetrahedra) is depicted in Figure 1-1.

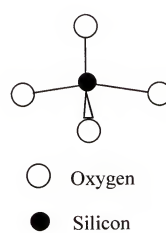

Figure 1-1. The basic silica tetrahedra.

A silica glass consists of these slightly distorted SiO_4 tetrahedra joined at the corners. The oxygen atoms act as a "bridge" between tetrahedra and are thus referred to as bridging oxygens (BO). In silica glass, practically all of the oxygens are classified as bridging oxygens, with the exception of some defect sites and impurities. The disorder of the glass structure is attributed to the variations in the bond angle between two neighboring tetrahedra as well as the torsion/rotation angles between two neighboring tetrahedra [VAR94].

Other elements may also be introduced into the silicate network. These elements will be disruptive to this network due to their different ionic sizes and charges (valence). These two factors, size and valence, to some extent determine how a particular element will be incorporated into the glass network [EBE94]. The addition of monovalent alkali and divalent alkaline earth cations terminates the network structure. These components act as network modifiers, occupying interstitial sites. In terms of charge balance, each alkali ion is expected to create one non-bridging oxygen (NBO) by breaking the "bridge" and incorporating an oxygen (from the alkali oxide) to the broken bridge (Figure 1-2). Likewise, each alkaline earth is expected to create two non-bridging oxygens. An increase in the number of non-bridging oxygens in the glass network is associated with a reduction of connectivity in the glass structure [VAR94]. This reduction in connectivity is also associated with changes in other properties of the glass, such as an increase in thermal expansion coefficient, a decrease in processing temperature, an increase in electrical conductivity, an increase in diffusion, a reduction in viscosity, and in regards to the topic of this dissertation, an increase in the susceptibility of the glass to chemical corrosion. The next chapter will discuss the phenomenon of glass corrosion in much more detail.

Figure 1-3 shows a schematic representation of both a random silica network and a silica network with the incorporation of a monovalent alkali cation.

Objectives

The objectives of this research were the following: (1) obtain statistical data from glass surfaces using Fourier transform infrared reflection spectroscopy (FT-IRRS), (2) to develop a quantitative model of the effects of surface roughness on infrared reflection, (3) to apply this quantitative technique to evaluate the effects of solution electrolyte chemistry on glass corrosion, (4) to verify the validity of this quantitative data with complementary characterization techniques, and (5) to evaluate the general mechanisms of corrosion when a glass is immersed in solutions of varying electrolytes and ionic strength.

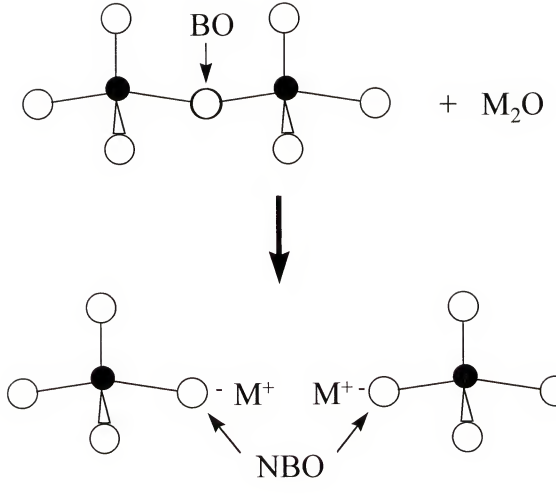

Figure 1-2. The addition of alkali ions and the formation of non-bridging oxygens.

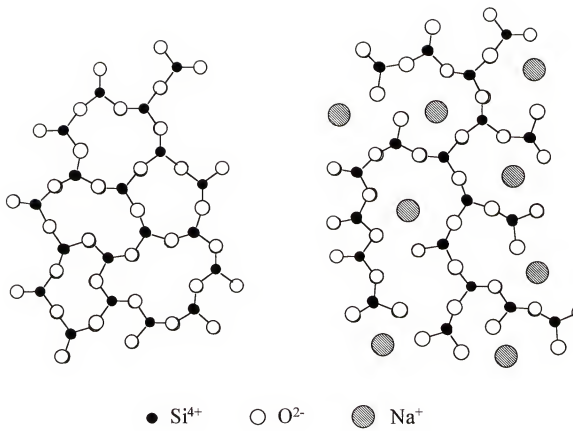

Figure 1-3. A schematic representation of (a) a random silica network and (b) the structure of a sodium silicate glass. [KIN76].

CHAPTER 2
BACKGROUND

An Overview of Aqueous Glass Corrosion

When a silicate glass is first placed into contact with water, two things start to happen immediately. First, a process of ion exchange between alkali metal ions within the glass and protons from the water occurs (Equation 2-1a). Equation 2-1 represents the basic reaction; however, it is unlikely that an unhydrolyzed proton is stable in either the solution or in the glass. Equation 2-1b and Equation 2-1c are alternatives to Equation 2-1a which have been expressed by different authors [EBE94]. Second, hydrolysis reactions at the glass surface begin, which result in direct dissolution of the silica matrix (Equations 2-2 and 2-3).

$$\equiv SiO\text{-}M + H^+ = \equiv SiO\text{-}H + M^+ \quad (2\text{-}1a)$$

$$\equiv SiO\text{-}M + H_3O^+ = \equiv SiO\text{-}H + M^+ + H_2O \quad (2\text{-}1b)$$

$$\equiv SiO\text{-}M + H_2O = \equiv SiO\text{-}H + M^+ + OH^- \quad (2\text{-}1c)$$

$$\equiv SiOSi + H_2O = \equiv SiOH + HO\text{-}Si \quad (2\text{-}2)$$

$$\equiv SiO\text{-}Si(OH)_3 + H_2O = \equiv SiOH + H_4SiO_4(aq) \quad (2\text{-}3)$$

where M^+ represents an alkali metal ion and ≡SiO-H represents a silanol group. Again, Equation 2-1a gives the basic reaction for the ion exchange process. The continued release of alkali metal ions into solution requires protons to continue to diffuse into the glass to exchange with more alkali ions. Equation 2-2 represents the network hydrolysis reaction, which is thought to be responsible for the deterioration of the silicate network [EBE94]. The hydrolysis of the silicate network may result from the nucleophilic attack on a silicon atom by either molecular water (Equation 2-2) or hydroxide. Equation 2-3 represents the network dissolution reaction, which, again, may occur by reaction with molecular water (Equation 2-3) or hydroxide. The extent of corrosion in silicate glasses is typically measured in rates of release of it's components ([M+], [Si] or [H_4SiO_4]). Various models which have been proposed to describe the kinetics of glass corrosion are outlined in the following section.

The Kinetics of Glass Leaching

There are several mathematical models dealing with aqueous corrosion of glass. Each subsequent model tends to refine and to better explain deficiencies in the previous model, or to take into account additional complexities. This section will briefly outline the more relevant of these various models and their evolution to the most current models on aqueous glass corrosion.

The earliest theories were focused in terms of leach rate, a process of ion exchange governed by the diffusion of H^+ (or H_3O^+) into the glass with the simultaneous diffusion of more soluble/leachable ions out of the glass [CLA92] (See Figure 2-1). Fick's law in one dimension may be used to describe this process:

$$dC/dt = d/dx(D\ dC/dx) \qquad (2\text{-}4)$$

where D is the diffusivity of the ion leaching out of the glass. The solution of the above equation, assuming a planar interface and constant diffusivity yields the observed parabolic rate law, given in simple empirical form:

$$\text{Rate (moles cm}^{-2}) = k_o + k_p t^{1/2} \qquad (2\text{-}5)$$

where k_p is the rate constant, and k_o is a constant non-zero term associated with the rapid initial ion-exchange on or near the glass surface. This simple model has its deficiencies. The above equation describes a reaction which continues without limit, ending only when the entire glass sample has been leached. Also the leaching of ions from the glass surface may lead to a build-up of ions in solution, which then may exceed the solubility limit of secondary reaction products which may then precipitate.

It is observed that the process of ion-exchange is comprised of (1) a diffusion component where leachable ions must diffuse out through the depleted leach layer (Figure 2-1) and (2) the dissolution of the leach layer itself [BOU94]. It is recognized that the parabolic kinetics observed during the early stages of glass corrosion shift to linear kinetics after long times [CLA92], [RAN61]. This is expressed empirically by an equation of the form:

$$Q = at^{1/2} + bt \quad (2\text{-}6)$$

$$R_a = dQ/dt = a / (2t^{1/2}) + b \quad (2\text{-}7)$$

where Q is the amount of alkali extracted from the glass, t is exposure time, a and b are experimentally determined constants and R_a is the rate of alkali extraction [CLA92], [CLA94], [ELS72], [ELS72a]. In the early stages of corrosion, the ion-exchange reaction controls the rate of the process, and the removal of the leachable alkali ions is dependent on the square root of time (the first term in the above equation). An alkali-depleted layer, sometimes referred to as the gel layer, develops (Figure 2-2). In simple glasses the structure and composition of this layer is almost identical to vitreous silica [SAN74]. As this alkali-depleted surface layer continues to grow, the rate of alkali extracted by ion exchange decreases. Simultaneously, at the gel/water interface, alkali ions are removed from the glass surface through the slower direct dissolution of the silica matrix. This rate of removal is linearly dependent on time (the second term in Equation 2-6). Eventually, this reaction reaches steady-state, where the rates of the two processes are equal and further corrosion is controlled by the slower (linear) silica matrix dissolution [CLA94]. Unlike the previous model based simply upon Fick's Law, this model takes into account the growth of and diffusion through the alkali-depleted layer. This model still has some deficiencies. It does not take into account the pH of the solution or any drift in pH of the solution as leachable ions are extracted. For example, if the pH of the solution is high, the second term of the equation may dominate over the entire duration of exposure. For simple glasses, this could result in the absence of a surface layer as the silica matrix is congruently dissolved into solution.

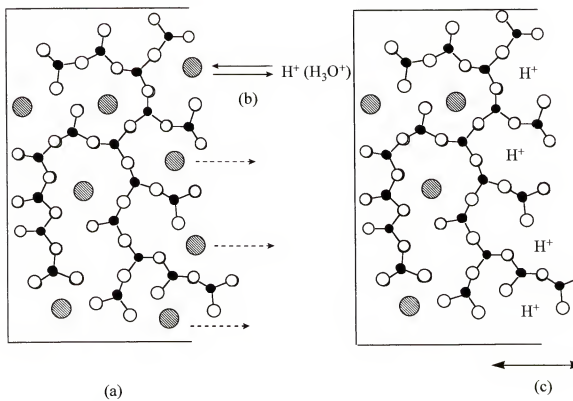

Figure 2-1. A schematic representation of (a) bulk sodium silicate glass in contact with water, (b) ion-exchange reaction between surface sodium ions and $H^+(H_3O^+)$ in the water, and (c) the build-up of the alkali-depleted leached layer.

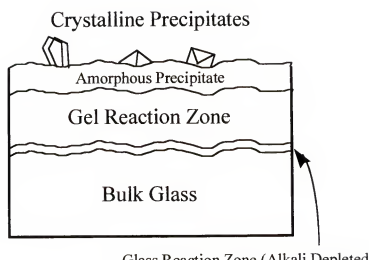

Figure 2-2. A schematic representation of the reacted zones in a multi-component glass. [MEN84] and [CLA94]

In 1983, Pederson, Buckwalter and McVay [PED83] presented static leaching test results which clearly indicated that the glass alteration rate decreased as the dissolved silica concentration increased [ADV98]. This led to the Savannah River Laboratory (SRL) Leachability model which was proposed by Wallace and Wicks [WAL83]. This empirical kinetic relation is given by the following equation:

$$R_{si} = K(C_s - C) / (1 + K\,l/D) \qquad (2\text{-}8)$$

where K is an initial rate constant, C_s is the concentration at silica saturation, C is the dissolved silica concentration, l is the alteration layer thickness and D is the diffusion coefficient. This relation is based on a three-stage corrosion process: (1) an ion-exchange process takes place between the leachable ions in the glass and the protons in the water, (2) matrix/silica dissolution then occurs and is controlled by both the pH and silica saturation concentration of the leachate, and (3) surface layer formation may occur after longer times, through which dissolved silica at the gel/glass interface must be transported through the gel layer to solution [CLA94]. With this model, the surface layers may be protective (acting as a barrier to further corrosion), or they may not be protective (where the rate of silica dissolution will only be dependent on its saturation concentration and its actual concentration in solution).

Three years later, Grambow proposed a geochemical approach for modeling glass/water interactions [GRA85]. Grambow's method involves reaction path modeling through the use of computer codes, taking into account glass/solution composition, pH, Eh, temperature, surface area to volume ratios, pCO_2 and flow rate [CLA94]. Once an

accurate reaction path has been identified, the GLASSOL computer code performs the time dependence calculations. The general equation for this model is the following:

$$R_m = K_+(D/L(K^*a) + R_f) / ((D/L)K^* + K_+) \qquad (2\text{-}9)$$

where R_m is the matrix dissolution rate, K^* is a stability constant for the rate limiting reaction, R_f is the final rate after silica saturation, K_+ is a rate constant for the forward reaction, D is the diffusion coefficient, L is the layer thickness and a is the silicic acid activity. The major differences between Grambow's model and the Wallace-Wicks equation are the following: (1) while concentrations are used in the Wallace-Wicks equation, activities are used in the Grambow model, and (2) the Grambow model accounts for R_f, the very low but nonzero alteration rate even after silica saturation, which is still not presently well understood [ADV98], [CLA94].

Finally, based upon earlier work done by Newton and Paul [NEW80], a thermodynamic approach to model and predict the long-term durability of nuclear waste glasses was developed by Jantzen and Plodinec [JAN83], [CLA94]. This model is expressed mathematically as the following:

$$\Delta G^{o}_{hyd} = \Sigma\, x_i\, (\Delta G_{hyd})_i \qquad (2\text{-}10)$$

where ΔG_{hyd} is the total free energy and $(\Delta G_{hyd})_i$ is the free energy change of the thermodynamically most stable hydration reaction of component i at mole fraction x. The assumption being made here is that the total free energy of hydration is equal to the weighted sum of the hydration energies of the individual components. The major shortcoming of this model is it's inability to model the time dependence of the corrosion

rate that results from changes in the silicic acid concentrations in the leachate. However, it is being used to control the process at the Defense Waste Processing Facility used for fabricating nuclear waste glass at the Savannah River Plant in Aiken, South Carolina.

These were some of the more prominent models of aqueous glass corrosion to date. These models take into account such variables as glass composition, temperature, pH, Eh, flow rate, and the surface area of the sample to volume of solution. The question arises, how do the mechanisms and kinetics of aqueous corrosion change as a function of solution chemistry, or as the electrolyte composition in the surrounding aqueous solution is changed? There are a host of applications in which glass is exposed to various aqueous electrolyte solutions, but there exists to date no complete understanding or model that adequately describes the corrosion processes under these conditions.

The Effect of Solution pH

When a soda-lime-silica (Na_2O-CaO-SiO_2) or alkali-silicate glass is placed in an aqueous solution, two main reactions take place, (1) the ion exchange between alkali ions in the glass with protons in the solution, and (2) the direct dissolution of silica by the breakdown of the siloxane bonds at the glass/solution interface [ELS72a]. A silica-rich leached layer is usually formed due to the alkali extraction occurring at a faster rate than silica dissolution, and this layer plays a large role in determining the overall corrosion rate of the glass. With the alkali ion exchange forming alkali hydroxide (strong base) in solution and the silica dissolution resulting in hydrosilicic acid (weak acid), it is inevitable that the glass corrosion process will result in pH changes in the solution. El-Shamy, Lewins and Douglas [ELS72a] studied the effects of solution pH on the corrosion rates of

some simple binary alkali-silicate glasses and various soda-lime-silica glasses. They found that alkali extraction from the glass into solution was relatively constant from pH 1 to pH 9. They associated this observation with all surface sites at the glass/water interface being associated with hydrogen. Above pH 9, however, they noticed a drastic decrease in alkali extraction. This was attributed to the decrease in hydrogen ion activity and corresponding increase in alkali ion activity in the solution. Interestingly, El-Shamy et al. found just the opposite behavior in regards to silica extraction. From pH 1 to pH 9, silica extraction was found to be relatively constant; however, at approximately pH 9, silica extraction increased substantially. They attributed this to the increase of $\equiv SiO^-$ groups on the hydrated silica surface, whose repulsive forces would presumably result in the breakdown of the silica structure [ELS72a].

The Effects of Electrolytes in Solution

In 1987, Dunken and Doremus [DUN87] measured the corrosion rates of a soda-lime-silica (SLS) glass in the following solutions: H_2O, 0.1M NaCl, 1.0M NaCl and 1.0M $NaNO_3$. They characterized the corrosion rates of the SLS glasses exposed to various temperatures and leaching times by using infrared absorbance and pH measurements of the leaching solutions. Dunken and Doremus observed that the corrosion rates were higher in the salt solutions as compared to the water. Their explanation was that the salt electrostatically "masks" the silicate species in solution, leading to a higher effective solubility of the silicate. They also measured higher resultant pH's in the water systems as compared to the salt systems for all times and temperatures. A higher resultant pH in the water would tend to indicate that a greater extent of ion exchange was occurring in the

water as compared to the salt solutions, which seems to contradict their observations of higher corrosion rates in the salt solutions. No elemental analysis of the solution was performed following leaching, and there appears to have been no discussion on possible pH measurement inadequacies within the high concentration salt solutions.

In 1992, Pederson et al. [PED93] measured the corrosion rates of a lithium disilicate, sodium trisilicate and potassium trisilicate immersed in concentrated solutions of their respective alkali chlorides (LiCl, NaCl and KCl). They observed a decrease in reaction rate as the electrolyte concentration increased. One proposed mechanism is that the electric surface potential might influence glass reaction rates in water through an enhancement in the alkali ion drift velocity [MUL79]. This particular mechanism, however, has been shown to be of negligible importance [SUL83]. It is known that the electrical charge on an oxide surface immersed in water will decrease in the presence of electrolytes [HEA77], [HUN71]. Pederson et al found that the initial rates of sodium/hydrogen ion exchange in sodium trisilicate glass, which is negatively charged for pH values greater than the isoelectric point (pH 2.3), were reliably lower in saturated sodium chloride solution than in deionised water [PED93]. The sodium chloride electrolyte was believed to lower the near surface concentration of hydrogen ions through lowering of the negative surface potential, thereby lowering the rate of ion exchange. The bulk and surface concentrations of hydrogen ions should be identical and independent of electrolyte concentration at the isoelectric point, resulting in the expected similar reaction rates in the two different solutions. The binary glasses which were studied by Pederson et al. were leached only in electrolytes of their respective alkali chlorides. For example, there

were no such experiments of leaching lithium disilicate in a concentrated sodium choloride solution, to differentiate between effects of cation.

In 1994, Feng et al. [FEN94] published a paper on the effects of salt solutions on the dissolution of a nuclear waste glass. They immersed 1 gram of powdered West Valley nuclear waste reference glass in deionised water, 0.1M KNO_3, 0.1M $CsNO_3$, 0.1M $Ba(NO_3)_2$, and 0.05M $Ba(NO_3)_2$, and held each system at 90°C. Feng et al. measured silicon release into solution and solution pH as a function of time. In general, they observed that the leach rates in the salt solutions were consistently lower than those of glasses immersed in deionised water. They attributed this to kinetic ion exchange. What they proposed was that the cations in the salt solutions were taking part in ion exchange to some extent. This meant that fewer H^+ ions were participating in ion exchange with alkali in the glass, which could result in the lower pH values that they observed in those salt solutions. They also noticed that salt solutions consisting of cations of greater aqueous mobility resulted in lower corrosion rates in glasses immersed in them. This also supports their theory of kinetic ion exchange. Feng et al observed no change in silicon release as the concentration of the salt solution increased, which is inconsistent with the findings of Pederson. Feng performed this study on a rather complicated glass. Therefore it was difficult to measure the release rate of alkali in the glass and relate that to any kinetic ion exchange which may have been occuring. Also the salt solutions they immersed their glasses in consisted of cations which were already present in their glasses, which eliminated any possibility of characterizing the surface of their leached samples to observe the presence of solution cations in the surface.

In 1996, Ahmed and Youssof [AHM97] published a paper on the corrosion of soda-lime-silica glass exposed to various acidic solutions. They filled commercial glass bottles with either citric acid, acetic acid, oxalic acid, hydrochloric acid, or deionised water, and measured pH and Na^+ and Si^{4+} release as a function of time. What they found was that silica release was greatest in the bottles filled with deionised water. They attributed this to pH effects. Comparing the "protective" effects of the various acids, they observed that variations in the amount of Na^+ released from the glass by the various solutions was found to be best related to the solubilities of the corresponding sodium salts, as opposed to pH. Therefore, they concluded that the anions in the solution played a major role in determining corrosion rate.

Referring to the above accounts, solution chemistry plays a major role in glass corrosion. The exact nature of this role, however, is not completely understood. There seem to be varying theories, each of which appears to have validity under the scope by which the corresponding experiments were carried out. To briefly summarize, electrolytes in solution may affect glass corrosion rates in the following manner: (1) by electrostatically masking the silicate species in solutions, thereby increasing its effect solubility, (2) by decreasing the surface potential at the glass surface, thereby lowering the effective number of H^+ ions available for ion exchange, (3) kinetic ion exchange of solution cations with alkali in the glass, and, (4) solubility limits for glass alkali and solution anion species. A systematic study on the aqueous leaching of a simple three component, soda-lime-silica glass, immersed in electrolyte solutions of varying cations, anions and varying concentration should shed much light on the mechanisms of the effects of solution chemistry on glass corrosion rates.

Characterization of Glass Corrosion

In order to adequately evaluate the effects of solution chemistry on glass corrosion kinetics, suitable characterization techniques must be employed in order to analyze both structural and chemical changes which occur in the glass surface. A host of characterization techniques exist to analyze the basic mechanisms of glass leaching. Table 2-1 lists commonly used techniques for studying glass surfaces [LEE86].

Due to the insulating nature of glasses and to the mobility of non-network cations, there are difficulties which may arise when applying certain surface analysis techniques to glasses. All of the techniques listed in table 2-1 except for the optical and infrared techniques employ the use of electrons, x-rays, or ions which bombard the glass surface. Atomic species within the glass surface are subject to local electric fields, thermal excitation and atomic collision processes. These processes may result in undesirable charging, electromigration and surface damage which may complicate analysis. These effects become exaggerated with higher beam energy and smaller spot sizes of analysis. In addition, sampling times and costs of operation must be considered in the selection of a suitable surface characterization technique.

In this study, FT-IRRS is used to study glass structure and composition as a function of aqueous corrosion environment. FT-IRRS offers several advantages over other surface analysis techniques. It requires minimum sample preparation, it has no vacuum requirements, it requires no energetic particles, it is non-destructive, and the analysis of samples using this technique are rapid [CLA77]. In combination with a suitable

solution analysis technique, such as inductively coupled plasma atomic emission spectroscopy (ICP-AE), FT-IRRS can be a powerful, inexpensive tool for the analysis of surface-environmental interactions. A detailed description of FT-IRRS will be included in the next chapter.

Table 2-1. Commonly used techniques for studying glass surfaces [LEE86]

Surface Composition

Auger Electron Spectroscopy w/ Ion Milling
Secondary Ion Mass Spectroscopy
Energy Dispersive Spectroscopy
Electron Spectroscopy for Chemical Analysis w/Ion Milling
Electron Microprobe Analysis
Nuclear Reaction Analysis
Sputter-Induced Photon Spectroscopy
Ion Scattering Spectroscopy
Rutherford Backscattering
Particle Induced X-ray Emission

Surface Morphology

Scanning Electron Microscopy
Scanning Auger Microscopy
Optical Microscopy

Surface Structure

Infrared Reflection Spectroscopy
Fourier Transform Infrared Reflection Spectroscopy (FT-IRRS)
Fourier Transform Infrared Diffuse Reflectance Spectroscopy
Small Angle X-ray Scattering
Transmission Electron Microscopy

CHAPTER 3
FOURIER TRANSFORM INFRARED SPECTROSCOPY

Principles and Theory

When exposed to infrared radiation, a material can transmit, absorb, or reflect (scatter) the incident radiation. When the frequency of the incident radiation is equal to the frequency of vibration of a corresponding molecular vibration, it may be absorbed, and the corresponding molecules may be excited into higher-energy vibrational states. This makes infrared spectroscopy a useful tool in the characterization of materials, because many functional groups vibrate at or near the same frequency regardless of their molecular environment. According to the ASM Handbook on Materials Characterization [ASM86], infrared spectroscopy has the following general uses: (1) the identification and determination of structure of both organic and inorganic materials, (2) the quantitative determination of molecular components in mixtures, (3) the identification of surface-absorbed molecular species, (4) the determination of molecular orientation, and, (5) the determination of molecular conformation/stereochemistry.

Typically, infrared spectra are reported in terms of intensity versus wavenumber (cm^{-1}). The wavenumber unit is simply an inverse wavelength, or frequency, unit reported in inverse centimeters. Most infrared spectrometers do not measure the entire infrared radiation range, which consists of wavelengths between 0.78 and 1000 microns (or 12,820 to 10 cm^{-1}). Infrared spectrometers typically measure only the region where

most fundamental vibrational modes occur, the mid-infrared region, from 2.5 to 25 microns (or 4000 to 400 cm^{-1}) [ASM86].

The intensity may be expressed in percent transmittance (%T), absorbance (A), or percent reflectance (%R). Traditionally, infrared spectra have been produced by transmission. This is accomplished by transmitting light through a sample and measuring the light intensity at the detector. This would then be compared, as a function of wavelength (or wavenumber), to the intensity obtained with no sample in the path of the light. Therefore, if I_o represents the radiant energy reaching the infrared detector with no sample in the path of the beam, and I represents the radiant energy reaching the detector after passing through a sample, transmittance and percent transmittance may be expressed as the following:

$$T = I / I_o \qquad (3\text{-}1)$$

$$\%T = 100\ (I / I_o) \qquad (3\text{-}2)$$

Other infrared spectroscopy techniques have become more common within the last couple decades. These include techniques such as attenuated total reflectance, diffuse reflectance, specular reflectance, and reflection-absorption spectroscopy. The research in this dissertation revolves around specular infrared reflectance. Specular reflectance is useful in obtaining surface information in a material. Specifically, specular reflectance refers to the component of incident light that reflects off the surface of the sample at an angle equal to the incident angle. In simplified terms, the fraction of specularly reflected light, R, may be expressed as:

$$R = [(n-1)^2 + k^2] / [(n+1)^2 + k^2] \qquad (3\text{-}3)$$

where n refers to the refractive index of the material, and k refers to the index of absorption. Consider an infrared beam, passing through a series of polished mirrors, whereby 100% of the radiant energy reaches the detector. This may be represented as I_o. Now, replace one of those polished mirrors with a polished sample. The radiant energy now reaching the detector may be represented as I. Reflectance and percent reflectance may now be expressed as the following:

$$R = I / I_o \qquad (3\text{-}4)$$

$$\%R = 100\ (I / I_o) \qquad (3\text{-}5)$$

In contrast to specular reflectance, diffuse reflectance refers to the component of light that is reflected (or scattered) at angles different than the incident beam. To visualize, compare a high-gloss material to a low-gloss material. The high-gloss material has a large component of specularly reflected light. On the other hand, the low-gloss material has a large component of diffusely reflected light. Two main factors which govern the relative amounts of specular to diffuse reflectance in a material are its index of refraction and surface roughness [KIN76]. Figure 3-1 illustrates the differences between specular and diffuse reflectance.

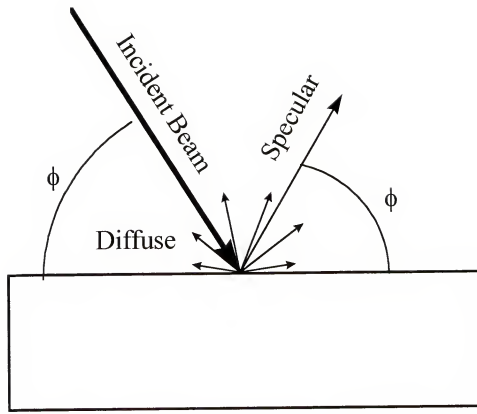

Figure 3-1. A schematic representation illustrating specular and diffuse reflection from the surface of a sample. Adapted from Kingery [KIN76].

As mentioned previously, the intensity, as a function of wavelength/wavenumber, of the specularly reflected infrared radiation is going to depend on the following: (1) the index of refraction of the sample, (2) the surface roughness of the sample, and, (3) the vibrational frequencies and fundamental vibrations of the molecules interacting with the incident radiation. Molecular vibrations may be calculated using normal coordinate analysis, however, it is not a trivial matter, as individual bond vibrations are often highly coupled to one another. These bond vibrations may be classified as either being stretching vibrations, bending vibrations or rocking vibrations, rotational vibrations, or some combination. Fortunately, certain functional groups and bonds result in reflections at similar wavenumbers regardless of the surrounding molecular environment. The vibrational frequencies of various modes as relevant to soda-lime-silica glass will be described in another chapter.

Components and Instrumentation

The essential components of any infrared spectrometer can be simplified into three main parts, as shown in figure 3-2. The source is where the broad-band infrared beam is generated. It may contain the necessary power supplies and various alignment components required to direct the beam into the sampling area. It is in the sampling area where the broad-band infrared beam interacts with the sample. Again, the method of interaction may vary: transmission, attenuated total reflectance, diffuse reflectance, specular reflectance, etc. Many sampling accessories exist on the market, and today, it is as easy as plugging in a sampling accessory, placing your sample, and generating a

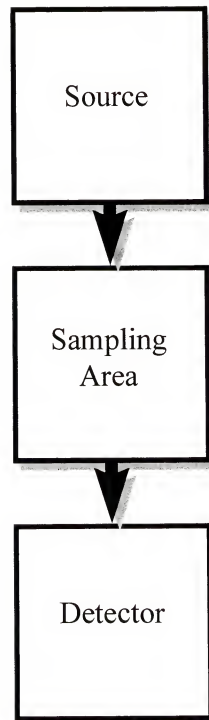

Figure 3-2. A simplified representation of the necessary components of an infrared spectrometer.

spectra. After the broad-band infrared beam interacts with the sample, it is directed towards the detector. The detector basically records the intensities of the broad-band infrared radiation reaching it. A computer may be attached for data processing.

A primary function of an infrared spectrometer is the ability to detect intensity changes as a function of wavenumber. There exists two main categories of spectrometers which have this ability to separate infrared light into single infrared wavenumber intervals: (1) the dispersive spectrometer, or commonly referred to as the grating spectrometer, and, (2) the Fourier transform spectrometer. The instrumentation of both will be described in this section, with focus on the Fourier transform spectrometer, as this was used for this research. The advantages of using one type of spectrometer over the other will be detailed in the next section.

In dispersive infrared spectroscopy, a dispersing element, such as a prism, a diffraction grating, or variable filter rotates within a monochromator to allow a mechanical slit to select individual wavenumber intervals in sequence. Figure 3-3 shows a schematic representation of one possible configuration of a single-beam grating spectrometer [FER78]. The infrared source generates radiation which is then focused through the sample and onto the entry slit. The collimated beam is dispersed by a diffraction grating, and radiation of a certain narrow frequency range is then directed through an exit slit and chopper before reaching the detector. A plot of detector response versus wavelength may be obtained by means of a calibrated mechanical linkage to the grating.

In Fourier transform infrared spectroscopy, an interferometer is used to modulate the intensity of each wavelength of light. The most common is the Michelson interferometer. Figure 3-4 shows a schematic representation of a Fourier transform

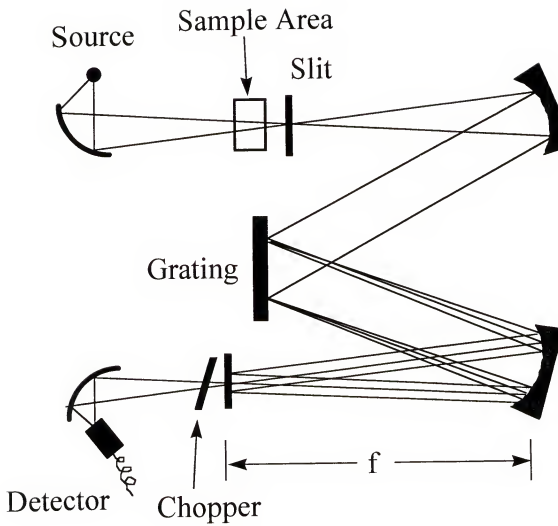

Figure 3-3. Schematic diagram of a single-beam grating spectrometer. Adapted from Ferraro and Basile [FER78].

infrared spectrometer. The infrared radiation is generated from a broad-band source and is divided into two optical paths by a beam splitter. One beam goes to a moving mirror, while the other is directed to a stationary mirror. When the the two beams recombine at the beam splitter, a modulated optical path difference is generated. Constructive and destructive interference may occur depending on the instantaneous optical path difference of a particular wavelength. For example, if the optical path difference is equal to an integral multiple of the wavelength, constructive interference will occur. This reconstructed beam exits the beam splitter and is directed to the sample and then focused onto the detector. The resulting signal at the detector represents signal intensity as a function of moving mirror position. A laser beam which experiences the same changes in optical path as the infrared beam is used to reference the mirror position, which is then used in the collection of data points. This resulting signal reaching the detector is referred as the interferogram. The interferogram must be Fourier transformed by a computer to obtain a single-beam infrared spectrum.

The Fourier transform infrared spectrometer (FT-IR) which was used in this research was a Nicolet, Impact 410, laboratory model. It functions by the same principles stated above, and figure 3-4 is a adequate representation of its components. For the purposes of this dissertation, only surface modification in the glass samples were of interest. Therefore, Fourier transform infrared reflectance (specular) spectroscopy (FT-IRRS) was used. This resulted in the sampling of only a thin layer (on the order of half a micron) of the glass surface by the infrared beam. Changes in beam intensity would reflect changes in the molecular structure of this thin layer. Figure 3-5 is a schematic

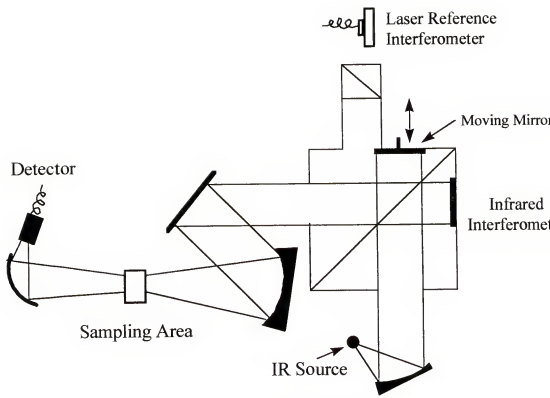

Figure 3-4. Schematic diagram of a Fourier transform infrared spectrometer. Adapted from Ferraro and Basile [FER78].

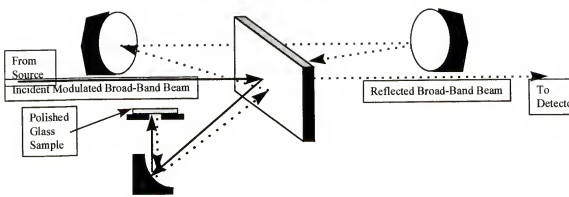

Figure 3-5. A schematic representation of the specular reflectance accessory.

representation of the specular reflectance accessory used in the sampling area (refer to figure 3-4) of the spectrometer. The modulated beam, as generated by the interferometer, is directed through a series of polished mirrors so that it impinges upon the sample surface at near normal incidence. The reflected portion of the beam is then directed back through the series of polished mirrors towards the detector, where the interferogram is generated, and then Fourier transformed into a resultant single-beam infrared spectra.

Advantages of FT-IR over Dispersive Infrared Spectroscopy

One of the main advantages that FT-IR has over dispersive infrared spectroscopy is in sampling time. The interferogram contains information on the entire infrared spectrum to be analyzed. This is in contrast to the dispersive spectrometer, which only allows one wavelength of the spectrum to be analyzed at a time. Sampling times in FT-IR are on the order of one second. This advantage is referred to as the multiplex, or Felgett's, advantage [FEL58]. Jacquinot's advantage [JAC60] refers to the high optical throughput of the FT-IR spectrometer as compared to dispersive spectrometers, since no slit is required. Also, with FT-IR, precise referencing of the wavenumber position is possible because a laser controls the sampling of the interferogram. This is referred to as Connes's advantage [CON66]. Finally, since a computer is a necessary part of any FT-IR system, it is available for data processing. Robust FT-IR systems may be purchased now relatively inexpensively (as compared to other characterization systems), and the ease and speed of data collection makes them quite an attractive characterization tool. There is some question, however, on the usefulness of information extracted from specular

reflectance spectra [ASM86], as the intensities are highly affected by the quality of the surface of sample. This will be addressed in a subsequent chapter.

CHAPTER 4
STATISTICAL ANALYSIS OF FT-IRRS DATA

Sample Preparation

The soda-lime-silicate (SLS) glasses used for this research were prepared by thoroughly mixing reagent grade carbonates of Na and Ca with 5 μm Min-U-Sil (SiO_2) with the following target composition in mind: 20 mol% Na_2O, 10 mol% CaO, 70 mol% SiO_2 – 20/10/70 SLS. These mixtures were homogenized at 1400°C for 24 hours in a high-temperature electric furnace. After 24 hours of homogenization, the molten glass was cast into approximately 1.30 cm x 1.30 cm x 10 cm bars using a graphite mold. Immediately following casting, the bars were placed into a small annealing furnace, maintained at 450°C for 4 hours and furnace-cooled to room temperature. Following annealing, the cast bars were stored in a drying oven held at 110°C. Melting was carried out in platinum crucibles to minimize potential contamination during the process. Between melts, the platinum crucible was cleaned thoroughly in a 60/40 HF/H_2O bath.

The annealed glass bars were cut into 0.4 cm thick samples using a slow speed diamond-impregnated wafering saw. For the purposes of the statistical analysis of FT-IRRS spectral features, a single sample was polished in the following grit sequence: 180 grit, 240 grit SiC, 320 grit SiC, 400 grit SiC, 600 grit SiC, 9.5 μm Al_2O_3, 1.0 μm Al_2O_3, and 0.3 μm Al_2O_3. All polishing was done dry, to minimize glass surface interactions with

water. The sample was rinsed in ethanol and wiped with lint-free paper in order to clean the surface between polishing steps. Ten independent FT-IRRS spectra were obtained after each level of polish, rinsing the surface of the sample in ethanol between measurements. The samples were marked such that sample placement on the specular reflectance accessory was the same for each measurement. This process was repeated a total of three times, on three different days, using the same sample. The purpose of repeatedly polishing the same sample day-to-day was to ensure compositional invariability while studying the effects of surface roughness and day-to-day variation on FT-IRRS spectral features.

Description of an FT-IRRS Spectrum

Figure 4-1 is an FT-IRRS spectrum of a 20/10/70 SLS glass, polished through 9.5 μm Al_2O_3. Percent reflectance is plotted on the vertical axis. Wavenumber is plotted on the horizontal axis. The spectral range displayed is from 1400 cm^{-1} to 600 cm^{-1}, which represents the range where the features of interest reside [SAN74]. Referring to this figure, feature -S- corresponds to symmetric silicon-oxygen stretching vibration (within tetrahedra) in the alkali environment [SAN74]. This is found at about 1050 cm^{-1}. The silicon-nonbridging oxygen vibration (-SN-) occurs at approximately 950 cm^{-1}. The small valley between between the S and SN peaks is often referred to as the coupled region [SAL94]. The small peak, -T-, located at about 750 cm^{-1} is attributed to the silicon-oxygen stretching vibration between tetrahedra [HUS90]. Both the intensity and

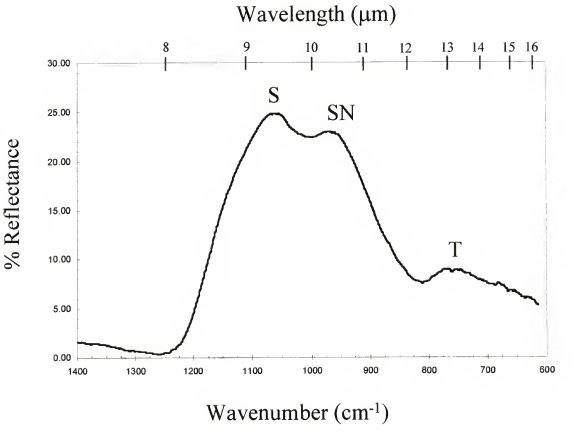

Figure 4-1. A typical FT-IRRS spectrum for a 20/10/70 SLS glass. (S indicates the location of the silicon-oxygen stretching vibration within a tetrahedra. SN indicates the location of the silicon-nonbridging oxygen stretching vibration. T indicates the location of the silicon-oxygen stretching vibration which occurs between neighboring tetrahedra)

frequency location of the S peak are proportional to the relative SiO_2 concentration in the glass surface. Likewise, both the intensity and frequency of the SN peak are proportional to the alkali concentration in the glass surface. In general, as corrosion proceeds, an ion exchange process occurs (Equation 2-1a, Chapter 2), involving alkali leaching out of the glass. This effectively decreases the relative alkali concentration in the glass surface, resulting in a shift and decrease in the SN peak. As corrosion proceeds it has also been observed that the S peak shifts and increases in magnitude. This would be indicative of an increase in the relative Si-O-Si bond concentration within the glass surface. Olbert [OLB82] proposed that the SiOH groups within the surface of a glass may decompose to molecular water and Si-O-Si (the reverse reaction of Equation 2-2 in Chapter 2), which would support this observation. The coupled region would also show a corresponding decrease and change in frequency as the S and SN peaks separate. It may be difficult to interpret the corrosion process using FT-IRRS in that the corrosion process itself may lead to extensive roughening of the sample's surface. It has been noted that surface roughening may lead to a decrease in the reflectance in a sample [SAN72]. An extensive statistical analysis on various spectral features as affected by surface roughening is required in order to achieve confidence in interpreting FT-IRRS corrosion results.

Effects of Surface Roughness

It has been previously demonstrated [BEN61] that for relatively smooth surfaces, the reflectance from a rough surface at normal incidence can be expressed by the following equation:

$$R_s = R_o \exp [-(4\pi\sigma/\lambda)^2] \qquad (4\text{-}1)$$

In the above equation, R_s is the observed specular reflectance, R_o is the reflectance of a perfectly smooth surface of the same material, σ is the root mean square roughness (rms height of the surface irregularities) and λ is the wavelength of incident radiation. This equation is based upon the assumption that an approximately Gaussian height distribution exists in the surface roughness and that the rms roughness is small as compared to the incident wavelength of the radiation. Rayleigh formulated a relation involving the peak-to-valley height (h) of surface irregularities, the angle of incidence of the radiation, and the wavelength of the radiation (Figure 4-2) [BEC63]. Referring to this figure, the path difference between ray 1 and ray 2 is given by:

$$\Delta r = 2h \sin \gamma \qquad (4\text{-}2)$$

making the phase difference equal to:

$$\Delta\phi = 2\pi/\lambda \; \Delta r = 4\pi h/\lambda \sin \gamma \qquad (4\text{-}3)$$

Therefore, if the phase difference, $\Delta\phi$, is small, ray 1 and ray 2 will be practically in phase, as the case with a perfectly smooth surface. As $\Delta\phi$ increases, the two rays will interfere until $\Delta\phi = \pi$. At this point they will be in phase opposition and cancel. It can be said for $\Delta\phi = \pi$, the surface scatters and hence is rough. In order to differentiate between a "smooth" and "rough" surface, Rayleigh arbitrarily selected a value half-way between the two cases ($\Delta\phi = \pi/2$). By substituting into Equation 4-3 for an normal angle of incidence (case used in this research), the "Rayleigh criterion" for a smooth surface becomes:

$$h < \lambda / 8 \qquad (4\text{-}4)$$

If the peak-to-valley height (h) is assumed to be $2\sqrt{2}\sigma$ (the case of a Gaussian height distribution), then, the criterion becomes the following: $\sigma/\lambda < 1 / 16\sqrt{2}$. Figure 4-3 shows a plot of this criterion versus wavenumber (and λ), showing the maximum rms roughness allowable for the S peak, if the above equation is to hold. For example, if σ for the surface is greater than 0.419, the criterion is not met for the S peak (the equation does not hold), however, the criterion may still be met for higher wavelengths. In terms of interpreting FT-IRRS reflectance spectra during glass corrosion, the above description has two main consequences: (1) at a given peak position (wavenumber, cm^{-1}), the increasing roughness of the surface due to corrosion will have a significant effect on the relative amount of specularly reflected light, and, (2) for a given uniform surface roughness, the

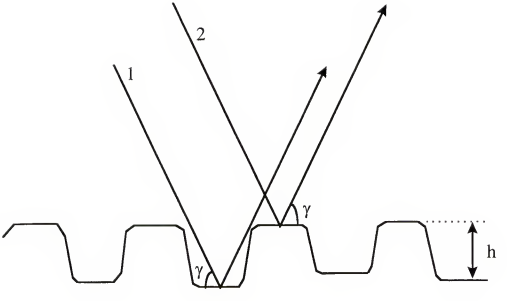

Figure 4-2. Derivation of the Rayleigh criterion.

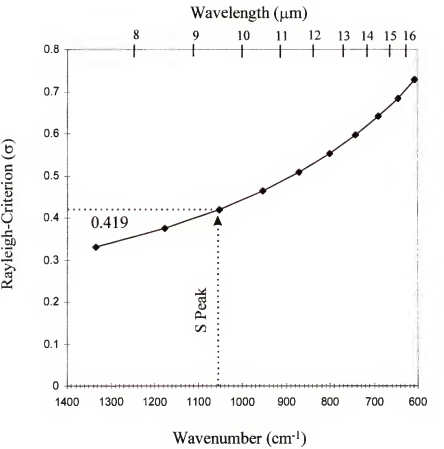

Figure 4-3. A plot of the Rayleigh-criterion for rms surface roughness versus wavenumber.

relative amount of specularly reflected light is an exponential function of λ. These two consequences increase the complexity of correlating changes in FT-IRRS spectral features with surface compositional changes. Figure 4-4 is a representation of how the spectra in Figure 4-1 will vary as a function of σ. In this figure the spectra were calculated using Equation 1 and assuming different values of σ. R_o was taken to be the reflectance after polishing with 9.5 μm Al_2O_3 powder. In a subsequent section, it was revealed that this level of polish achieved a maximum reflectivity in the sample. It should be noted, that in Figure 4-4, the Rayleigh criterion is not met for all wavelengths at certain values of σ (refer to Figure 4-3), however, the overall trends should give a good indication of how surface roughness will affect the FT-IRRS spectra. Peaks occurring at higher wavenumbers (smaller wavelengths) decrease more rapidly than those at lower wavenumbers in accordance with Equation 4-1.

Experimental Design

In 1984, Hench et al published a paper describing the suitability of using FT-IRRS in establishing boundaries for acceptance or rejection of samples based upon easily measured spectral features [HEN84]. They related the statistically significant variations in these spectral features to such applications as the leach sensitivity of a nuclear waste glass, and to the end-use behavior of PZT ceramics. In terms of this dissertation, an analysis of variance (ANOVA) technique was employed to examine the effects of treatment and the effects of experimental blocking on various spectral features. In this case, treatment refers to the successive levels of polishing each sample was exposed to. Composition was held

$$R_s = R_o \exp[-(4\pi\sigma/\lambda)^2$$

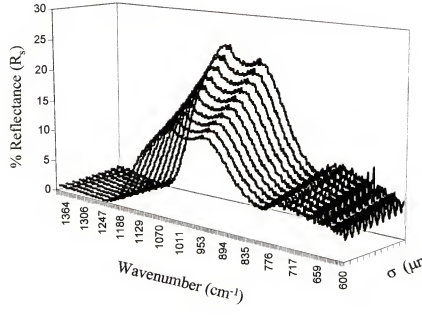

where, λ (in microns) = 10000 / Wavenumber

Z-Axis: 0.0 μm - 0.45 μm rms height

Figure 4-4. A representation of the effect of rms surface roughness on the reflectance of a 20/10/70 SLS FT-IRRS spectra.

constant, so that any statistically significant differences in spectral features could be directly attributed to changes in surface roughness (polishing was the only treatment). Experimental blocking refers to the repetition of this analysis on different days (day-to-day variation). Blocking effects may arise from operator error/inconsistency, instrument variability, inconsistency in polishing from day to day, temperature/atmospheric considerations, as well as any day-to-day variation which cannot be anticipated by the experimenter. The statistical design used in this analysis was a complete block design. The implication of this design is that any effects of treatment, any effects of blocking, and any treatment-blocking interaction effects will be resolved. Ten replicates of FT-IRRS spectra were obtained from each successive level of polishing. Between each of the ten measurements, the sample was rinsed in ethanol in order to avoid any water condensation interactions with the surface which could alter the surface composition of the glass sample. Successive polishes of 180 grit, 240 grit, 320 grit, 400 grit, 600 grit, 9.5 micron, 1.0 micron and 0.3 micron represented the sample treatment. For example, ten FT-IRRS spectra were obtained at a 180 grit polish of the 20/10/70 SLS glass surface; then, ten FT-IRRS spectra were obtained at a 240 grit polish of the 20/10/70 SLS glass surface. This entire procedure (ten replicates at each of eight levels of surface polish) was repeated on three separate days (three blocks). Figure 4-5 displays the spectral features analyzed using this ANOVA technique. Referring to Figure 4-5, PH2 and PP2 correspond to the peak height (% reflectance) and peak position (cm^{-1}) of the silicon-oxygen stretching vibration. PH4 and PP4 correspond to the peak height and peak position of the silicon-nonbridging oxygen stretching vibration. PH3 and PP3 correspond to the coupled "peak". PH6 and PP6 correspond to the silicon-oxygen stretching vibration that exists between tetrahedra.

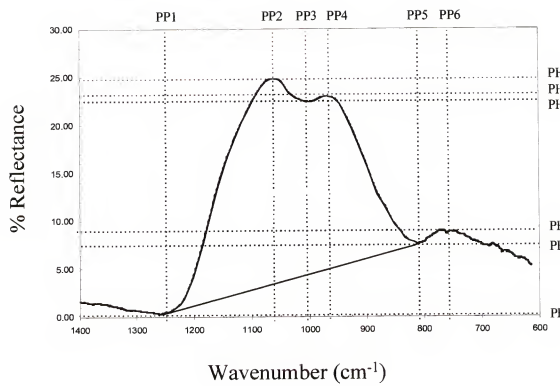

Figure 4-5. Labeling of the spectral features analyzed using ANOVA, as a function of surface polish and day-to-day variation.

The corrected peak area represents the integrated area under the curve, bounded by PP1 and PP5 at the corresponding minima. This peak area is labeled as "corrected" due to the baseline connecting PP1 and PP5, that is subtracted out. All of these peak heights, peak positions and the corrected peak area were recorded for each of the 10 replicates, for each of the 8 polishing steps, and for each of the 3 days during which these experiments were run (10 x 8 x 3 = 240 spectra measured). These spectral features were examined statistically in order to determine the following: (1) which features are significantly affected by surface treatment, and, (2) which features are significantly affected by day-to-day variation. Those features which are not significantly affected will be used to analyze FT-IRRS spectra in subsequent corrosion studies. Table 4-1 through Table 4-21 shows the data collected corresponding to the above features, as a function of level of polish and block. Figure 4-6 shows a representation of FT-IRRS spectra recorded after each polishing step.

Analysis of Variance

The analysis of variance is a statistical technique used to test the significance of differences between multiple sampling means. This study may be viewed as a two-factor experiment with replication. Here, the two factors were surface roughness treatment and day-to-day blocking. The replication corresponded to the ten spectra obtained for each level of surface roughness, on each day. The appropriate model describing the variance in each set of sample measurements (PH1, PP1, PH2, PP2, PH3, PP3, PH4, PP4, PH5, PP5, PH6, PP6 and PArea) is the following [SPI99]:

$$X_{jkl} = \mu + \alpha_j + \beta_k + \gamma_{jk} + \varepsilon_{jkl} \qquad (2)$$

where j, k and l correspond to the jth treatment, the kth block, and the lth replication. Here X_{jkl} simply represents the actual measurement of the lth replication, of the jth treatment, of the kth block. For example, for the analysis of variance of PH1, there were a total of 10 x 8 x 3, or 240 X_{jkl}'s. The term μ represents the population grand mean, the term α_j refers to the part of X_{jkl} due to the treatment effects, the term β_k refers to the part of X_{jkl} due to the blocking effects, the term ε_{jkl} refers to the part of X_{jkl} due to chance/error (commonly referred to as the residual), and the term γ_{jk} refers to the treatment-block interaction effect. The summations of each the treatment effects, the blocking effects, the error term and the interaction effects sum to zero. The X_{jkl} values are also assumed to be normally distributed with mean μ and variance σ^2. The total variation, V, of all data can be expressed as treatment variation V_T, block variation V_B, interaction variation V_I and random error V_E. Below are the relevant equations:

$$V = V_T + V_B + V_I + V_E \qquad (4\text{-}5)$$

$$V = \sum_{jkl} (X_{jkl} - \mu)^2 \qquad (4\text{–}6)$$

$$V_T = bc\sum_{j=1,a} (\mu_j - \mu)^2 \qquad (4\text{-}5)$$

$$V_B = ac\sum_{k=1,b} (\mu_k - \mu)^2 \qquad (4\text{-}6)$$

$$V_I = c\sum_{jk} (\mu_{jk} - \mu_j - \mu_k + \mu)^2 \qquad (4\text{-}7)$$

$$V_E = \sum_{jkl} (X_{jkl} - \mu_{jk})^2 \qquad (4\text{-}8)$$

where a is the total number of treatments (8), b is the total number of blocks (3) and c is the total number of replications (10). Again, μ represents the grand mean of the entire population. The subscripts associated with μ merely indicate treatment means (j), block means (k), or means of block/treatment (jk). Table 4-22 represents the template for the ANOVA tables which were used to examine the significance of various spectral features. The F column in this table represents the calculated F-statistic. This calculated F-statistic was compared to the interpolated critical value for the F distribution, which is read from a reference table displaying the 95th percentile values for the F distribution [SPI99]. If the calculated F-statistic was greater than the critical value of the F distribution, it may be said that there was a significant difference (with a 95% confidence) in that particular treatment, block or interaction. Likewise, if the calculated F-statistic was less than the critical value of the F distribution, it may be said that there was no significant difference in that particular treatment, block or interaction. The "Reject" column merely clarifies whether: (1) "YES," there was an effect, or, (2) "NO," there was no effect. The term "Reject" refers to the "rejection" of the NULL hypothesis of there being no significant effect. F(0.95) was interpolated to be 2.03 from the tables [SPI99] for treatment , 3.03 for block effects, and 1.71 for interaction effects. The calculated ANOVA tables for each spectral feature are displayed in Table 4-23 through Table 4-28.

Table 4-1. FT-IRRS peak height and peak position of the left boundary of the corrected peak area of a 20/10/70 SLS glass for varying levels of polish during block one.

-BLOCK ONE- PH1: Peak Height One (% Reflectance)

Polish										
180 Grit	0.484	0.439	0.389	0.485	0.418	0.519	0.398	0.231	0.457	0.304
240 Grit	0.553	0.674	0.576	0.365	0.632	0.295	0.429	0.543	0.528	0.327
320 Grit	0.340	0.270	0.369	0.511	0.181	0.331	0.312	0.130	0.384	0.332
400 Grit	0.180	0.428	0.375	0.433	0.331	0.209	0.481	0.588	0.429	0.278
600 Grit	0.265	0.372	0.484	0.294	0.307	0.309	0.453	0.389	0.587	0.486
9.5 Micron	0.358	0.402	0.388	0.407	0.540	0.236	0.384	0.177	0.517	0.462
1.0 Micron	0.314	0.401	0.359	0.374	0.265	0.506	0.481	0.481	0.407	0.423
0.3 Micron	0.713	0.615	0.119	0.506	0.419	0.616	0.570	0.556	0.438	0.380

-BLOCK ONE- PP1: Peak Position One (cm^{-1})

Polish										
180 Grit	1237.411	1239.972	1237.411	1237.411	1236.771	1239.972	1237.411	1236.771	1239.972	1237.411
240 Grit	1239.972	1239.972	1237.411	1236.771	1239.972	1239.972	1237.411	1239.972	1239.972	1239.972
320 Grit	1241.607	1240.398	1237.980	1240.398	1240.398	1240.398	1237.980	1239.189	1240.398	1237.980
400 Grit	1240.398	1239.189	1239.189	1237.980	1239.189	1239.189	1237.980	1240.398	1237.980	1239.189
600 Grit	1239.189	1237.980	1236.771	1239.189	1239.189	1239.189	1237.980	1237.980	1239.189	1239.189
9.5 Micron	1240.398	1239.189	1241.607	1240.398	1239.189	1239.189	1239.189	1237.980	1239.189	1239.189
1.0 Micron	1237.980	1239.189	1239.189	1237.980	1239.189	1240.398	1239.189	1239.189	1240.398	1239.189
0.3 Micron	1239.189	1237.980	1237.980	1236.771	1239.189	1239.189	1240.398	1240.398	1239.189	1240.398

Table 4-2. FT-IRRS peak height and peak position of the silica-oxygen stretching vibration within tetrahedra of a 20/10/70 SLS glass for varying levels of polish during block one.

-BLOCK ONE- PH2: Peak Height Two (% Reflectance)

Polish										
180 Grit	5.116	5.178	5.290	4.426	4.634	4.681	5.077	4.937	4.796	5.158
240 Grit	13.347	13.489	13.087	12.511	12.978	14.063	12.729	13.266	12.920	12.769
320 Grit	14.886	15.125	13.915	14.115	13.960	13.865	15.191	14.815	14.992	14.995
400 Grit	18.517	19.595	18.350	17.781	18.473	17.571	17.833	17.087	17.834	17.661
600 Grit	23.093	23.244	22.355	22.655	22.570	23.105	23.620	22.107	21.357	22.560
9.5 Micron	23.381	23.893	23.596	23.291	22.948	23.903	23.179	23.677	22.657	23.308
1.0 Micron	22.910	23.407	23.064	22.882	22.442	22.334	22.383	22.472	22.462	22.685
0.3 Micron	19.532	18.661	21.950	20.522	21.034	21.032	22.771	22.854	23.265	22.054

-BLOCK ONE- PP2: Peak Position Two (cm^{-1})

Polish										
180 Grit	1050.569	1051.778	1051.778	1050.569	1051.778	1049.360	1049.360	1051.778	1049.360	1050.569
240 Grit	1051.778	1051.778	1051.778	1052.987	1052.987	1051.778	1052.987	1052.987	1051.778	1051.778
320 Grit	1054.196	1052.987	1054.196	1054.196	1052.987	1055.405	1052.987	1052.987	1055.405	1054.196
400 Grit	1054.196	1054.196	1052.987	1052.987	1052.987	1054.196	1054.196	1054.196	1052.987	1054.196
600 Grit	1052.987	1054.196	1052.987	1052.987	1054.196	1054.196	1055.405	1054.196	1055.405	1055.405
9.5 Micron	1052.987	1055.405	1055.405	1054.196	1055.405	1052.987	1055.405	1054.196	1054.196	1052.987
1.0 Micron	1052.987	1054.196	1054.196	1054.196	1055.405	1055.405	1055.405	1055.405	1052.987	1055.405
0.3 Micron	1052.987	1052.987	1051.778	1051.778	1051.778	1051.778	1051.778	1051.778	1051.778	1052.987

Table 4-3. FT-IRRS peak height and peak position of the "coupled" region in a 20/10/70 SLS glass for varying levels of polish during block one.

-BLOCK ONE- PH3: Peak Height Three (% Reflectance)

Polish										
180 Grit	5.039	4.545	4.902	4.560	4.570	4.493	4.864	4.787	5.042	4.824
240 Grit	12.720	12.006	11.954	11.241	11.704	12.941	11.886	12.050	11.910	11.696
320 Grit	13.392	13.799	12.619	13.043	13.028	12.737	13.378	13.343	13.627	14.012
400 Grit	17.458	17.622	16.015	16.195	16.665	16.222	16.367	15.308	16.027	16.133
600 Grit	20.958	21.215	20.099	20.226	20.365	20.816	20.817	19.980	19.457	20.481
9.5 Micron	21.101	21.300	21.260	20.863	20.504	21.233	21.025	21.015	20.240	20.824
1.0 Micron	20.293	21.097	20.660	20.469	19.992	19.459	19.899	20.340	19.926	20.172
0.3 Micron	18.012	17.098	19.522	18.814	18.684	18.674	20.504	21.125	20.718	19.888

-BLOCK ONE- PP3: Peak Position Three (cm^{-1})

Polish										
180 Grit	1000.996	1000.996	1003.414	1002.215	1003.414	1000.996	1002.215	1003.414	1002.215	1003.414
240 Grit	1002.215	1002.215	1003.414	1003.414	1002.215	1002.215	1003.414	1003.414	1002.215	1003.414
320 Grit	1003.414	1002.215	1000.996	1003.414	1003.414	1000.996	1003.414	1002.215	1002.215	1001.849
400 Grit	1002.215	1001.849	1002.215	1001.849	1003.414	1003.414	1004.623	1003.414	1002.215	1003.414
600 Grit	1003.414	1003.414	1003.414	1002.215	1002.215	1002.215	1003.414	1002.215	1003.414	1003.414
9.5 Micron	1003.414	1003.414	1002.215	1002.215	1003.414	1003.414	1002.215	1003.414	1002.215	1002.215
1.0 Micron	1002.215	1002.215	1003.414	1002.215	1003.414	1001.849	1003.414	1002.215	1002.215	1003.414
0.3 Micron	1005.832	1003.414	1003.414	1003.414	1003.414	1002.215	1003.414	1002.215	1002.215	1002.215

Table 4-4. FT-IRRS peak height and peak position of the silica-nonbridging oxygen stretching vibration in a 20/10/70 SLS glass for varying levels of polish during block one.

-BLOCK ONE- PH4: Peak Height Four (% Reflectance)

Polish										
180 Grit	5.499	5.239	5.547	5.354	5.126	4.960	5.625	5.248	5.032	5.471
240 Grit	13.520	13.621	13.282	12.799	13.289	14.113	13.412	13.395	13.335	12.750
320 Grit	14.770	15.303	14.351	14.253	14.421	14.164	15.281	14.481	14.848	15.177
400 Grit	18.638	19.353	18.189	17.699	17.758	17.232	17.371	16.534	17.286	17.419
600 Grit	22.647	21.586	21.227	21.291	21.259	22.009	22.046	20.721	19.788	21.308
9.5 Micron	21.351	22.186	21.933	21.790	21.350	22.094	21.848	21.901	21.010	22.070
1.0 Micron	20.869	21.501	21.248	21.002	20.504	20.244	20.495	20.335	20.862	21.046
0.3 Micron	19.819	18.711	21.075	20.415	19.959	19.851	21.888	22.115	22.097	21.245

-BLOCK ONE- PP4: Peak Position Four (cm^{-1})

Polish										
180 Grit	944.168	944.168	942.959	944.168	942.959	944.168	942.959	944.168	945.377	945.377
240 Grit	952.642	950.640	950.640	952.642	946.586	946.586	947.795	946.586	950.640	947.795
320 Grit	953.201	950.640	951.920	950.640	953.201	950.640	951.920	953.201	950.640	950.640
400 Grit	957.041	954.481	955.761	957.041	954.481	955.761	957.041	955.761	955.761	955.761
600 Grit	959.602	959.602	957.468	957.041	959.602	957.041	956.259	957.041	957.041	959.602
9.5 Micron	961.095	961.095	961.095	961.095	962.304	959.886	960.882	958.677	959.886	960.882
1.0 Micron	961.095	961.095	962.304	962.304	963.513	961.095	961.095	961.095	959.886	962.304
0.3 Micron	956.259	953.841	955.050	956.259	954.468	957.468	957.468	958.677	957.468	957.468

Table 4-5. FT-IRRS peak height and peak position of the right boundary of the corrected peak area in a 20/10/70 SLS glass for varying levels of polish during block one.

-BLOCK ONE- PH5: Peak Height Five (% Reflectance)

Polish										
180 Grit	2.374	2.461	2.408	2.278	2.366	2.434	2.427	2.352	2.793	2.192
240 Grit	4.825	5.076	5.130	4.801	5.140	5.602	4.878	5.312	5.188	5.074
320 Grit	5.386	5.709	5.614	5.603	5.361	5.315	5.984	5.701	5.595	5.495
400 Grit	6.883	6.574	6.464	6.146	6.640	5.994	6.602	6.278	6.415	6.564
600 Grit	6.928	6.918	7.027	6.676	6.701	7.462	7.602	6.836	6.582	6.885
9.5 Micron	6.889	7.429	7.442	7.402	6.723	7.487	6.722	6.873	6.941	7.225
1.0 Micron	6.597	7.011	6.980	6.920	6.930	6.313	6.256	6.545	6.865	6.816
0.3 Micron	7.930	7.559	8.204	8.241	7.622	7.769	7.964	8.065	8.407	7.932

-BLOCK ONE- PP5: Peak Position Five (cm^{-1})

Polish										
180 Grit	809.959	807.255	809.959	805.121	808.749	808.535	807.539	807.539	809.815	808.535
240 Grit	807.539	808.535	809.959	808.535	811.166	808.535	811.166	807.539	808.535	811.166
320 Grit	808.535	809.959	811.166	811.166	808.535	808.535	811.166	811.166	811.166	808.535
400 Grit	811.166	809.959	807.539	809.959	809.959	811.166	806.330	809.959	809.959	809.959
600 Grit	808.535	811.166	807.539	807.255	807.255	807.539	809.959	808.535	808.535	808.535
9.5 Micron	807.255	809.959	808.749	808.535	809.815	811.166	808.749	811.166	808.535	807.255
1.0 Micron	807.539	811.166	813.585	809.959	811.166	811.166	811.095	811.095	808.749	811.166
0.3 Micron	807.539	809.959	811.166	809.959	809.959	808.749	811.166	808.535	811.166	808.749

Table 4-6. FT-IRRS peak height and peak position of the silica-bridging oxygen stretching vibration between tetrahedra in a 20/10/70 SLS glass for varying levels of polish during block one.

-BLOCK ONE- PH6: Peak Height Six (% Reflectance)

Polish										
180 Grit	3.475	3.443	3.380	3.366	3.032	3.354	3.418	3.547	3.492	3.430
240 Grit	6.534	7.045	6.668	6.431	6.964	7.414	7.017	7.071	6.843	7.031
320 Grit	6.985	7.677	7.027	7.495	6.552	6.527	7.389	6.522	7.743	7.063
400 Grit	8.514	8.622	8.220	7.839	7.736	7.571	7.484	7.226	7.690	8.422
600 Grit	8.749	9.053	8.395	8.187	8.491	8.558	8.953	8.205	8.315	8.389
9.5 Micron	8.938	9.388	8.963	9.142	8.796	9.157	8.741	8.487	8.512	8.878
1.0 Micron	8.643	8.456	8.680	8.641	8.653	7.939	8.400	8.253	8.677	8.414
0.3 Micron	10.187	9.218	11.062	9.968	9.947	9.690	10.412	9.996	10.412	9.887

-BLOCK ONE- PP6: Peak Position Six (cm^{-1})

Polish										
180 Grit	745.875	754.339	751.920	747.084	745.875	739.829	744.666	731.366	743.457	745.875
240 Grit	750.711	748.293	747.084	744.666	744.666	747.084	745.875	745.875	748.293	745.875
320 Grit	747.084	747.084	749.502	745.875	744.666	747.084	748.293	745.875	744.666	747.084
400 Grit	749.502	747.084	747.084	749.502	750.711	749.502	748.293	749.502	748.293	749.502
600 Grit	749.502	750.711	751.920	745.875	751.920	748.293	750.711	749.502	749.502	748.293
9.5 Micron	751.920	750.711	749.502	749.502	749.502	749.502	748.293	750.711	749.502	749.502
1.0 Micron	751.920	750.711	749.502	749.502	748.293	750.711	749.502	749.502	750.711	749.502
0.3 Micron	749.502	749.502	749.502	747.084	750.711	747.084	749.502	749.502	748.293	748.293

Table 4-7. The corrected peak area in a 20/10/70 SLS glass for varying levels of polish during block one.

-BLOCK ONE- Corrected Peak Area

Polish										
180 Grit	1011.169	929.669	986.275	914.258	931.069	896.559	972.221	984.992	979.276	990.497
240 Grit	2846.385	2749.500	2674.190	2655.793	2682.382	2901.686	2736.925	2714.728	2638.885	2705.434
320 Grit	3036.624	3111.407	2875.615	2968.303	2988.632	2919.802	3132.610	3082.913	3014.198	3210.745
400 Grit	3910.764	4058.642	3809.489	3766.452	3817.905	3763.814	3782.049	3522.752	3638.125	3764.268
600 Grit	4969.068	4909.716	4697.960	4699.785	4823.740	4969.800	4970.053	4767.281	4517.349	4886.028
9.5 Micron	4779.663	5053.689	4990.139	4945.112	4752.878	4902.259	4977.223	4917.104	4739.528	4892.653
1.0 Micron	4714.872	4871.854	4800.102	4774.512	4673.329	4534.148	4628.663	4674.773	4746.604	4738.266
0.3 Micron	3953.283	3805.154	4267.349	4135.862	4121.025	4074.271	4421.149	4622.829	4599.857	4417.959

Table 4-8. FT-IRRS peak height and peak position of the left boundary of the corrected peak area of a 20/10/70 SLS glass for varying levels of polish during block two.

-BLOCK TWO- PH1: Peak Height One (% Reflectance)

Polish										
180 Grit	0.293	0.520	0.313	0.417	0.367	0.228	0.254	0.437	0.381	0.447
240 Grit	0.408	0.403	0.330	0.344	0.301	0.436	0.446	0.355	0.285	0.349
320 Grit	0.339	0.520	0.308	0.090	0.440	0.489	0.164	0.364	0.295	0.411
400 Grit	0.405	0.355	0.255	0.411	0.462	0.416	0.360	0.372	0.318	0.332
600 Grit	0.336	0.430	0.365	0.381	0.647	0.559	0.403	0.280	0.366	0.441
9.5 Micron	0.408	0.521	0.343	0.315	0.519	0.595	0.378	0.357	0.247	0.363
1.0 Micron	0.480	0.503	0.347	0.519	0.401	0.124	0.432	0.353	0.372	0.608
0.3 Micron	0.616	0.395	0.633	0.697	0.597	0.439	0.359	0.393	0.475	0.516

-BLOCK TWO- PP1: Peak Position One (cm^{-1})

Polish										
180 Grit	1239.972	1239.972	1235.562	1237.411	1237.411	1237.411	1237.411	1239.972	1239.972	1237.980
240 Grit	1239.972	1236.771	1236.771	1239.189	1237.411	1237.411	1237.980	1236.771	1235.562	1237.980
320 Grit	1239.971	1241.252	1238.691	1239.971	1239.971	1241.252	1241.252	1239.971	1238.691	1238.691
400 Grit	1239.971	1239.971	1238.691	1239.971	1238.691	1241.252	1239.971	1239.971	1239.971	1241.252
600 Grit	1239.971	1242.532	1239.971	1241.252	1241.252	1238.691	1239.971	1242.532	1241.252	1239.971
9.5 Micron	1239.971	1239.971	1239.971	1238.691	1238.691	1241.252	1239.971	1239.971	1238.691	1239.971
1.0 Micron	1239.971	1240.398	1239.971	1241.252	1240.398	1239.971	1241.252	1241.252	1240.398	1238.691
0.3 Micron	1239.971	1242.532	1242.532	1241.252	1239.971	1239.971	1241.252	1239.971	1238.691	1241.252

Table 4-9. FT-IRRS peak height and peak position of the silica-oxygen stretching vibration within tetrahedra of a 20/10/70 SLS glass for varying levels of polish during block two.

-BLOCK TWO- PH2: Peak Height Two (% Reflectance)

Polish										
180 Grit	8.917	10.010	9.890	9.340	9.640	9.380	9.744	9.966	9.320	9.586
240 Grit	14.978	15.180	14.207	14.881	14.331	14.311	14.685	15.091	16.268	15.834
320 Grit	18.220	18.146	18.042	18.001	18.288	19.272	18.711	18.820	17.064	17.204
400 Grit	21.424	21.171	21.025	20.136	20.139	21.117	20.733	21.062	20.802	20.829
600 Grit	23.140	23.525	23.252	21.992	21.797	23.335	23.258	23.486	22.787	22.947
9.5 Micron	24.572	25.175	25.147	24.247	24.207	24.019	23.692	23.401	23.444	22.998
1.0 Micron	25.905	25.534	25.755	24.460	23.957	24.776	25.009	24.687	24.431	24.135
0.3 Micron	20.688	20.658	20.605	22.030	21.836	22.179	24.124	22.762	22.981	22.724

-BLOCK TWO- PP2: Peak Position Two (cm^{-1})

Polish										
180 Grit	1050.569	1052.987	1051.778	1050.569	1050.569	1051.778	1051.778	1050.569	1050.569	1051.778
240 Grit	1054.196	1052.987	1052.987	1052.987	1052.987	1054.196	1051.778	1054.196	1052.987	1051.778
320 Grit	1051.778	1051.778	1054.196	1054.196	1053.058	1053.058	1053.058	1054.196	1053.058	1054.196
400 Grit	1053.058	1053.058	1053.058	1054.196	1054.196	1054.196	1054.196	1054.196	1053.058	1054.196
600 Grit	1051.778	1053.058	1051.778	1053.058	1053.058	1053.058	1054.339	1054.196	1054.339	1054.339
9.5 Micron	1054.339	1054.339	1055.619	1054.339	1055.619	1053.058	1054.339	1055.619	1055.619	1054.339
1.0 Micron	1054.339	1054.339	1054.339	1054.339	1053.058	1053.058	1054.339	1055.619	1055.619	1054.339
0.3 Micron	1053.058	1053.058	1054.339	1051.778	1053.058	1053.058	1053.058	1054.339	1051.778	1053.058

Table 4-10. FT-IRRS peak height and peak position of the "coupled" region in a 20/10/70 SLS glass for varying levels of polish during block two.

-BLOCK TWO- PH3: Peak Height Three (% Reflectance)

Polish										
180 Grit	8.454	9.352	9.272	8.934	9.189	8.932	9.559	9.330	8.813	8.792
240 Grit	13.790	13.678	13.274	13.811	13.440	13.276	13.615	13.646	14.390	14.343
320 Grit	16.707	16.671	16.653	16.512	16.668	17.466	16.909	16.949	15.280	15.103
400 Grit	19.638	19.691	19.734	18.284	18.482	18.938	18.858	18.979	18.223	18.614
600 Grit	21.118	20.940	21.066	19.776	19.816	21.051	21.104	21.054	20.286	20.508
9.5 Micron	22.584	22.247	22.472	21.703	21.621	21.553	20.982	20.884	21.029	20.360
1.0 Micron	22.757	22.532	22.242	21.785	21.782	21.798	21.880	22.236	21.660	21.836
0.3 Micron	18.795	18.953	18.785	20.260	20.259	20.326	21.810	20.765	20.565	20.886

-BLOCK TWO- PP3: Peak Position Three (cm^{-1})

Polish										
180 Grit	1002.205	1003.129	1002.205	1002.205	1002.205	1003.414	1003.414	1002.205	1002.205	1003.414
240 Grit	1002.215	1003.129	1005.832	1003.414	1002.205	1002.205	1002.205	1002.205	1003.414	1002.205
320 Grit	1002.215	1001.849	1001.849	1001.849	1003.129	1001.849	1001.849	1000.569	1001.849	1001.849
400 Grit	1002.215	1001.849	1001.849	1003.129	1001.849	1001.849	1003.129	1001.849	1001.849	1003.129
600 Grit	1003.129	1003.129	1001.849	1003.129	1003.129	1001.849	1000.569	1003.129	1001.849	1001.849
9.5 Micron	1001.849	1001.849	1001.849	1001.849	1001.849	1001.849	1003.129	1003.129	1003.129	1003.129
1.0 Micron	1001.849	1003.129	1003.129	1000.569	1003.129	1001.849	1001.849	1001.849	1003.129	1003.129
0.3 Micron	1003.129	1004.410	1003.129	1004.410	1003.129	1003.129	1003.129	1003.129	1003.129	1001.849

Table 4-11. FT-IRRS peak height and peak position of the silica-nonbridging oxygen stretching vibration in a 20/10/70 SLS glass for varying levels of polish during block two.

-BLOCK TWO- PH4: Peak Height Four (% Reflectance)

Polish										
180 Grit	9.924	10.663	10.329	10.324	9.999	10.086	10.480	10.396	9.896	9.929
240 Grit	15.098	15.411	14.649	15.024	14.696	14.702	14.658	15.008	15.771	16.040
320 Grit	18.254	17.698	18.246	17.741	18.029	18.974	18.413	18.015	17.055	17.013
400 Grit	20.210	20.923	20.957	19.747	19.392	20.175	20.109	20.130	19.675	19.729
600 Grit	21.975	22.086	21.683	20.924	20.300	22.111	22.176	22.116	21.699	21.342
9.5 Micron	23.487	22.903	23.221	22.424	22.291	22.154	21.783	22.145	21.614	21.619
1.0 Micron	23.102	23.514	23.335	22.445	22.486	22.399	22.190	22.689	21.883	22.006
0.3 Micron	21.173	20.841	20.661	21.529	21.137	21.450	22.746	21.980	21.678	21.549

-BLOCK TWO- PP4: Peak Position Four (cm^{-1})

Polish										
180 Grit	944.168	946.586	945.377	945.377	945.377	946.586	946.586	946.586	946.586	946.586
240 Grit	951.422	952.642	950.640	949.004	951.422	947.795	950.640	950.640	950.640	949.004
320 Grit	953.201	953.201	951.920	953.201	953.201	951.920	950.640	950.640	953.201	951.920
400 Grit	955.761	957.041	955.761	957.041	957.041	955.761	954.481	954.481	957.041	958.322
600 Grit	957.041	957.041	959.602	957.041	959.602	957.041	959.602	957.041	957.041	958.321
9.5 Micron	960.882	960.882	959.602	960.882	960.882	959.602	959.602	959.602	960.882	960.882
1.0 Micron	960.882	962.162	960.882	962.162	959.602	960.882	960.882	962.162	962.162	960.882
0.3 Micron	953.201	951.920	953.201	958.321	957.041	957.041	959.602	959.602	959.602	957.041

Table 4-12. FT-IRRS peak height and peak position of the right boundary of the corrected peak area in a 20/10/70 SLS glass for varying levels of polish during block two.

-BLOCK TWO- PH5: Peak Height Five (% Reflectance)

Polish										
180 Grit	4.173	4.263	3.793	3.926	4.093	3.622	4.288	4.038	3.719	4.195
240 Grit	5.684	5.307	5.347	5.718	5.983	5.600	5.306	5.067	5.828	6.367
320 Grit	6.192	6.715	6.123	6.611	6.255	7.083	6.363	7.075	6.789	5.924
400 Grit	7.278	6.821	6.940	6.785	6.397	7.291	7.599	6.986	6.793	6.939
600 Grit	6.929	7.236	7.083	6.514	6.607	7.125	7.591	7.312	7.132	6.539
9.5 Micron	7.778	7.703	7.406	7.184	7.169	7.210	7.105	7.033	6.739	6.756
1.0 Micron	7.543	7.504	7.443	7.252	6.808	7.728	7.662	7.200	6.987	6.933
0.3 Micron	8.441	8.218	8.155	8.129	8.215	7.639	8.291	7.532	7.630	8.045

-BLOCK TWO- PP5: Peak Position Five (cm^{-1})

Polish										
180 Grit	807.539	807.539	807.255	811.166	805.121	807.255	811.166	807.539	811.166	808.748
240 Grit	809.815	811.166	809.917	811.166	808.748	812.376	807.255	811.166	808.748	809.917
320 Grit	808.535	807.255	807.255	805.974	808.535	805.974	805.974	807.255	805.974	802.134
400 Grit	807.255	805.974	808.535	808.535	807.255	805.974	808.535	809.815	808.535	807.255
600 Grit	808.535	809.815	809.815	809.815	808.535	809.815	808.535	808.535	807.255	808.535
9.5 Micron	807.255	808.535	809.815	809.815	807.255	811.095	808.535	809.815	807.255	808.535
1.0 Micron	808.535	809.815	808.535	807.255	809.815	808.535	811.095	811.095	809.815	808.535
0.3 Micron	811.095	807.255	811.095	807.255	807.255	811.095	808.535	811.095	811.095	811.095

Table 4-13. FT-IRRS peak height and peak position of the silica-bridging oxygen stretching vibration between tetrahedra in a 20/10/70 SLS glass for varying levels of polish during block two.

-BLOCK TWO- PH6: Peak Height Six (% Reflectance)

Polish										
180 Grit	5.733	5.932	6.215	5.725	5.266	5.756	5.588	5.899	5.264	5.855
240 Grit	7.438	7.177	7.251	7.580	7.158	7.631	7.654	7.420	7.884	7.720
320 Grit	8.422	7.740	7.774	8.250	8.106	8.783	8.881	8.710	7.722	7.705
400 Grit	9.000	9.284	8.886	8.524	8.634	8.900	8.489	8.429	8.735	8.962
600 Grit	9.730	9.484	8.829	8.214	8.201	8.894	8.566	8.822	8.497	8.488
9.5 Micron	8.592	9.208	8.996	9.103	9.177	8.324	8.701	8.595	8.462	8.523
1.0 Micron	8.784	8.811	8.666	8.504	8.496	8.842	8.666	8.669	9.197	8.361
0.3 Micron	10.096	10.548	10.143	10.142	10.116	10.298	9.845	10.100	9.657	10.258

-BLOCK TWO- PP6: Peak Position Six (cm^{-1})

Polish										
180 Grit	733.784	744.666	741.038	743.457	737.411	744.666	742.247	742.247	744.666	744.666
240 Grit	750.711	750.711	749.502	748.293	745.875	748.293	747.084	745.875	744.666	749.502
320 Grit	749.644	745.804	745.804	747.084	748.364	744.524	747.084	745.804	749.644	747.084
400 Grit	745.804	748.364	747.084	748.364	748.364	747.084	747.084	749.644	748.364	748.364
600 Grit	747.084	748.364	747.084	749.644	749.644	749.644	749.644	748.364	747.084	749.644
9.5 Micron	749.644	750.925	749.644	748.364	748.364	749.644	749.644	747.084	748.364	748.364
1.0 Micron	749.644	748.364	749.644	748.364	749.644	747.084	749.644	748.364	748.364	749.644
0.3 Micron	747.084	748.364	749.644	747.084	749.644	749.644	748.364	748.364	749.644	747.084

Table 4-14. The corrected peak area in a 20/10/70 SLS glass for varying levels of polish during block two.

-BLOCK TWO- Corrected Peak Area

Polish										
180 Grit	1961.693	2036.515	2087.574	1937.337	2070.250	1946.043	2017.435	2016.957	1980.805	2020.483
240 Grit	3134.500	3080.120	3003.069	3195.398	3054.042	3012.887	3125.089	3065.940	3289.127	3239.119
320 Grit	3866.347	3776.641	3798.271	3730.986	3753.521	4019.273	3864.669	3835.738	3624.924	3567.701
400 Grit	4425.095	4583.705	4469.275	4271.070	4252.126	4409.910	4402.212	4362.902	4395.521	4292.813
600 Grit	4946.471	4872.414	4912.141	4653.339	4749.543	4922.521	4902.490	4920.535	4821.978	4904.633
9.5 Micron	5203.622	5309.094	5241.261	5063.749	5106.195	5021.767	4966.247	5016.567	4901.266	4915.965
1.0 Micron	5237.785	5258.598	5245.583	5192.188	5147.848	5135.652	5209.786	5151.162	5077.180	5083.682
0.3 Micron	4240.163	4247.689	4166.709	4550.296	4548.809	4467.592	4896.187	4559.168	4647.895	4608.061

Table 4-15. FT-IRRS peak height and peak position of the left boundary of the corrected peak area of a 20/10/70 SLS glass for varying levels of polish during block three.

-BLOCK THREE- PH1: Peak Height One (% Reflectance)

Polish										
180 Grit	0.396	0.395	0.299	0.416	0.437	0.540	0.434	0.543	0.484	0.499
240 Grit	0.439	0.562	0.295	0.347	0.414	0.519	0.463	0.313	0.374	0.233
320 Grit	0.362	0.421	0.222	0.421	0.292	0.432	0.335	0.270	0.346	0.299
400 Grit	0.401	0.474	0.216	0.243	0.317	0.490	0.324	0.364	0.185	0.238
600 Grit	0.219	0.272	0.392	0.429	0.276	0.387	0.519	0.523	0.295	0.175
9.5 Micron	0.160	0.329	0.395	0.437	0.342	0.259	0.519	0.479	0.528	0.622
1.0 Micron	0.247	0.579	0.397	0.490	0.441	0.524	0.595	0.536	0.428	0.266
0.3 Micron	0.525	0.564	0.261	0.364	0.518	0.233	0.589	0.533	0.427	0.684

-BLOCK THREE- PP1: Peak Position One (cm^{-1})

Polish										
180 Grit	1237.411	1237.411	1237.411	1239.972	1237.411	1237.411	1237.411	1239.972	1239.972	1238.692
240 Grit	1241.252	1239.971	1241.252	1238.691	1241.252	1239.971	1241.252	1241.252	1239.971	1239.971
320 Grit	1239.971	1238.692	1239.971	1239.971	1238.692	1238.692	1239.971	1239.971	1239.971	1239.971
400 Grit	1238.692	1241.252	1241.252	1239.971	1241.252	1239.971	1241.252	1239.971	1239.971	1241.252
600 Grit	1239.971	1239.971	1238.691	1241.252	1239.971	1238.691	1239.971	1238.691	1241.252	1239.971
9.5 Micron	1238.692	1238.692	1239.971	1238.692	1239.971	1239.971	1239.971	1239.971	1239.971	1241.252
1.0 Micron	1238.692	1239.971	1240.398	1239.971	1239.971	1241.252	1239.971	1241.252	1239.971	1239.971
0.3 Micron	1236.131	1238.692	1242.532	1241.252	1238.692	1242.532	1238.692	1241.252	1239.971	1239.971

Table 4-16. FT-IRRS peak height and peak position of the silica-oxygen stretching vibration within tetrahedra of a 20/10/70 SLS glass for varying levels of polish during block three.

-BLOCK THREE- PH2: Peak Height Two (% Reflectance)

Polish										
180 Grit	12.216	12.193	12.700	12.042	12.378	12.211	11.837	12.111	11.891	11.857
240 Grit	19.322	19.347	19.496	19.246	19.823	19.561	19.571	19.107	18.636	17.998
320 Grit	19.444	19.218	17.793	18.439	18.399	18.005	18.051	17.624	19.123	18.924
400 Grit	22.822	22.469	23.369	23.576	23.393	22.476	22.828	22.607	22.396	22.811
600 Grit	24.946	25.153	25.082	25.178	24.700	23.695	23.772	23.773	23.295	23.416
9.5 Micron	23.374	23.282	24.97	24.922	25.148	24.736	23.772	24.364	22.660	23.236
1.0 Micron	24.605	24.785	24.355	24.456	24.031	24.281	24.167	24.685	24.471	24.421
0.3 Micron	21.392	21.328	21.089	22.920	22.937	22.957	21.873	21.855	21.499	21.663

-BLOCK THREE- PP2: Peak Position Two (cm^{-1})

Polish										
180 Grit	1053.058	1053.058	1051.778	1053.058	1054.339	1054.339	1053.058	1053.058	1055.619	1054.339
240 Grit	1050.498	1053.058	1051.778	1051.778	1051.778	1053.058	1051.778	1051.778	1054.339	1051.778
320 Grit	1054.339	1054.339	1053.058	1054.339	1053.058	1054.339	1053.058	1054.339	1053.058	1054.339
400 Grit	1053.058	1053.058	1053.058	1054.339	1053.058	1053.058	1053.058	1054.339	1054.339	1051.778
600 Grit	1055.619	1054.339	1055.619	1054.339	1055.619	1054.339	1055.619	1055.619	1055.619	1055.619
9.5 Micron	1054.339	1055.619	1053.058	1054.339	1055.619	1055.619	1055.619	1053.058	1054.339	1055.619
1.0 Micron	1054.339	1055.619	1054.339	1053.058	1053.058	1054.339	1054.339	1055.619	1054.339	1055.619
0.3 Micron	1051.778	1053.058	1051.778	1053.058	1053.058	1053.058	1053.058	1051.778	1053.058	1053.058

Table 4-17. FT-IRRS peak height and peak position of the "coupled" region in a 20/10/70 SLS glass for varying levels of polish during block three.

-BLOCK TWO- PH3: Peak Height Three (% Reflectance)

Polish										
180 Grit	8.454	9.352	9.272	8.934	9.189	8.932	9.559	9.330	8.813	8.792
240 Grit	13.790	13.678	13.274	13.811	13.440	13.276	13.615	13.646	14.390	14.343
320 Grit	16.707	16.671	16.653	16.512	16.668	17.466	16.909	16.949	15.280	15.103
400 Grit	19.638	19.691	19.734	18.284	18.482	18.938	18.858	18.979	18.223	18.614
600 Grit	21.118	20.940	21.066	19.776	19.816	21.051	21.104	21.054	20.286	20.508
9.5 Micron	22.584	22.247	22.472	21.703	21.621	21.553	20.982	20.884	21.029	20.360
1.0 Micron	22.757	22.532	22.242	21.785	21.782	21.798	21.880	22.236	21.660	21.836
0.3 Micron	18.795	18.953	18.785	20.260	20.259	20.326	21.810	20.765	20.565	20.886

-BLOCK TWO- PP3: Peak Position Three (cm^{-1})

Polish										
180 Grit	1002.205	1003.129	1002.205	1002.205	1002.205	1003.414	1003.414	1002.205	1002.205	1003.414
240 Grit	1002.215	1003.129	1005.832	1003.414	1002.205	1002.205	1002.205	1002.205	1003.414	1002.205
320 Grit	1002.215	1001.849	1001.849	1001.849	1003.129	1001.849	1001.849	1000.569	1001.849	1001.849
400 Grit	1002.215	1001.849	1001.849	1003.129	1001.849	1001.849	1003.129	1001.849	1001.849	1003.129
600 Grit	1003.129	1003.129	1001.849	1003.129	1003.129	1001.849	1000.569	1003.129	1001.849	1001.849
9.5 Micron	1001.849	1001.849	1001.849	1001.849	1001.849	1001.849	1003.129	1003.129	1003.129	1003.129
1.0 Micron	1001.849	1003.129	1003.129	1000.569	1003.129	1001.849	1001.849	1001.849	1003.129	1003.129
0.3 Micron	1003.129	1004.410	1003.129	1004.410	1003.129	1003.129	1003.129	1003.129	1003.129	1001.849

Table 4-18. FT-IRRS peak height and peak position of the silica-nonbridging oxygen stretching vibration in a 20/10/70 SLS glass for varying levels of polish during block three.

-BLOCK THREE- PH4: Peak Height Four (% Reflectance)

Polish										
180 Grit	13.027	13.660	12.657	13.070	12.817	12.511	12.879	12.485	12.202	12.313
240 Grit	18.951	19.172	18.767	18.932	18.936	18.577	18.863	18.547	17.871	17.582
320 Grit	18.512	18.267	18.065	17.693	17.789	17.112	17.169	17.605	18.520	18.407
400 Grit	21.407	21.316	22.194	21.769	21.990	21.125	21.497	21.176	21.162	21.079
600 Grit	23.695	23.765	23.244	23.827	23.966	22.226	22.619	22.757	22.601	22.162
9.5 Micron	21.466	21.652	22.811	22.777	22.757	22.664	22.381	22.484	20.757	21.087
1.0 Micron	22.157	22.064	22.389	22.369	22.049	22.099	22.229	22.151	22.333	22.352
0.3 Micron	21.438	21.108	21.307	22.201	22.212	22.263	21.658	21.374	21.115	20.835

-BLOCK THREE- PP4: Peak Position Four (cm^{-1})

Polish										
180 Grit	948.080	946.799	942.959	944.239	944.239	942.959	945.519	942.959	941.679	941.679
240 Grit	957.041	957.041	957.041	955.761	955.761	954.481	957.041	954.481	955.761	951.920
320 Grit	954.481	955.761	954.481	954.481	954.481	951.920	953.201	953.201	954.481	951.920
400 Grit	958.322	960.882	959.602	958.322	958.322	957.041	958.322	958.322	959.602	959.602
600 Grit	958.322	959.602	959.602	959.602	959.602	959.602	960.882	959.602	959.602	959.602
9.5 Micron	960.882	960.882	960.882	960.882	962.304	960.882	959.602	960.882	960.882	962.304
1.0 Micron	959.602	962.304	962.304	962.304	962.304	960.882	963.442	960.882	962.304	960.882
0.3 Micron	954.481	953.201	954.481	955.761	955.761	955.761	957.041	955.761	955.761	955.761

Table 4-19. FT-IRRS peak height and peak position of the right boundary of the corrected peak area in a 20/10/70 SLS glass for varying levels of polish during block three.

-BLOCK THREE- PH5: Peak Height Five (% Reflectance)

Polish										
180 Grit	5.700	5.289	5.646	5.529	5.622	5.466	4.655	4.731	5.063	5.337
240 Grit	6.904	7.243	7.087	6.819	6.557	7.111	6.231	7.183	6.284	6.152
320 Grit	6.813	6.359	6.596	7.038	6.549	6.519	6.343	6.099	7.105	6.844
400 Grit	7.378	6.983	7.607	7.306	7.650	7.552	7.310	7.648	7.035	6.755
600 Grit	7.772	7.804	7.872	7.727	7.753	7.525	7.553	7.396	7.070	7.488
9.5 Micron	6.496	6.882	7.704	7.552	7.318	7.664	7.553	7.402	6.279	6.614
1.0 Micron	6.903	7.532	7.107	7.508	6.947	7.181	6.762	6.842	7.262	6.844
0.3 Micron	8.217	8.128	8.207	8.737	8.395	8.978	8.393	8.452	7.957	7.900

-BLOCK THREE- PP5: Peak Position Five (cm^{-1})

Polish										
180 Grit	805.974	809.815	809.815	807.255	807.255	805.974	811.095	811.095	809.815	807.255
240 Grit	808.535	807.255	808.535	807.255	809.815	811.095	808.535	809.815	808.535	808.535
320 Grit	811.095	811.095	809.815	807.255	811.095	808.535	808.535	808.535	808.535	809.815
400 Grit	811.095	807.255	807.255	808.535	808.535	809.815	808.535	808.535	807.255	807.255
600 Grit	808.535	809.815	811.095	807.255	807.255	808.535	811.095	808.535	809.815	809.815
9.5 Micron	809.815	807.255	808.535	809.815	808.535	811.095	811.095	808.535	809.815	809.815
1.0 Micron	809.815	807.255	809.815	808.535	807.255	809.815	807.255	807.255	811.095	809.815
0.3 Micron	808.535	807.255	805.974	811.095	807.255	807.255	809.815	807.255	807.255	807.255

Table 4-20. FT-IRRS peak height and peak position of the silica-bridging oxygen stretching vibration between tetrahedra in a 20/10/70 SLS glass for varying levels of polish during block three.

-BLOCK THREE- PH6: Peak Height Six (% Reflectance)

Polish										
180 Grit	7.006	7.011	6.396	6.618	7.521	6.980	6.000	7.096	6.844	7.126
240 Grit	8.541	8.145	8.775	8.352	9.129	8.436	8.721	8.318	8.010	7.934
320 Grit	8.273	7.896	8.030	7.768	7.977	7.920	7.899	7.814	8.254	8.398
400 Grit	8.637	8.964	9.230	8.739	8.551	8.783	8.899	8.555	8.791	8.225
600 Grit	9.227	9.457	9.748	9.384	9.275	9.029	8.984	8.365	8.569	8.765
9.5 Micron	8.390	9.009	8.448	8.769	8.777	8.468	8.984	9.028	8.510	8.209
1.0 Micron	8.467	8.856	8.961	8.126	8.388	8.250	8.755	9.467	8.724	8.901
0.3 Micron	10.272	9.485	9.850	10.728	10.471	10.121	9.983	10.517	9.385	9.668

-BLOCK THREE- PP6: Peak Position Six (cm^{-1})

Polish										
180 Grit	740.683	743.243	740.683	740.683	739.402	740.683	743.243	740.683	743.243	740.683
240 Grit	745.804	748.364	748.364	747.084	748.364	747.084	748.364	743.243	747.084	747.084
320 Grit	747.084	748.364	747.084	748.364	749.644	747.084	747.084	745.804	747.084	745.804
400 Grit	748.364	748.364	748.364	748.364	750.711	749.644	748.364	745.804	747.084	749.644
600 Grit	750.711	749.644	748.364	749.644	749.644	749.644	749.644	748.364	748.364	748.364
9.5 Micron	747.084	750.711	749.644	749.644	748.364	748.364	749.644	749.644	748.364	747.084
1.0 Micron	748.364	750.711	748.364	748.364	750.711	749.644	750.711	748.364	748.364	750.711
0.3 Micron	747.084	749.644	749.644	747.084	749.644	747.084	748.364	747.084	747.084	748.364

Table 4-21. The corrected peak area in a 20/10/70 SLS glass for varying levels of polish during block three.

-BLOCK THREE- Corrected Peak Area

Polish											
180 Grit	2641.389	2678.275	2619.192	2584.469	2583.042	2547.474	2574.025	2533.175	2477.890	2529.941	
240 Grit	4033.276	3979.967	4103.592	4069.880	4125.847	4107.228	4176.800	4105.326	3873.232	3938.377	
320 Grit	4044.288	4030.523	3869.858	3898.339	3885.015	3786.696	3741.125	3736.970	3974.640	4038.014	
400 Grit	4877.328	4833.197	4957.928	4936.042	4975.189	4783.253	4887.015	4711.619	4851.336	4779.603	
600 Grit	5297.704	5274.222	5338.738	5300.408	5288.520	5075.713	5188.231	5090.249	5019.990	5086.862	
9.5 Micron	4980.619	4907.099	5349.013	833.157	5230.602	5129.035	5064.268	5142.292	4812.038	4807.601	
1.0 Micron	5157.435	5111.483	5132.093	5038.781	5113.031	5063.292	5130.657	5189.573	5071.819	5123.988	
0.3 Micron	4312.157	4297.742	4339.942	4707.146	4602.781	4667.923	4546.699	4498.729	4437.728	4464.425	

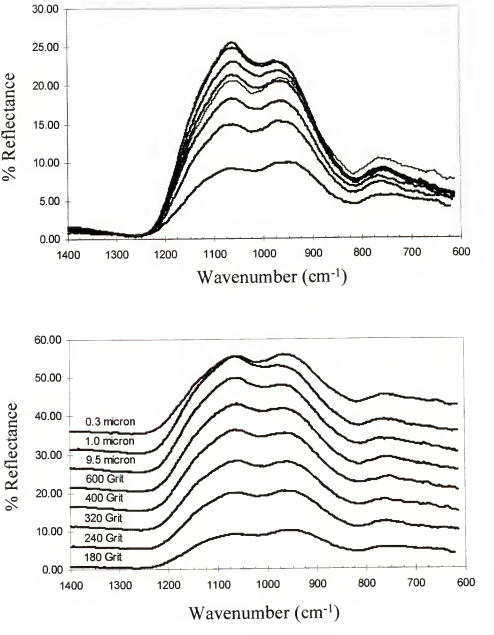

Figure 4-6. FT-IRRS spectra of a 20/10/70 SLS glass as a function of polishing. The spectra are overlaid upon one another in the top figure. The bottom figure offsets spectra by 5% for readability.

Table 4-22. ANOVA table template which was applied to spectral features.

	Variation	Degrees of Freedom	Mean Square	F	F(0.95)	Reject?
Treatment	V_T	a - 1	$S_T^2 = V_T/(a-1)$	S_T^2 / S_I^2	2.03	YES/NO
Block	V_B	b - 1	$S_B^2 = V_B/(b-1)$	S_B^2 / S_I^2	3.03	YES/NO
Interaction	V_I	(a-1)(b-1)	$S_I^2 = \frac{V_I}{(a-1)(b-1)}$	$S_I^2 / *$	1.71	YES/NO
Residual	V_E	ab(c-1)	$S_E^2 = \frac{V_E}{ab(c-1)}$			
Total	V	abc-1				

$$* = \frac{V_I + V_E}{(a-1)(b-1) + ab(c-1)}$$

Table 4-23. ANOVA table for PH1 and PP1.

PH1: Peak Height One

	Variation	Degrees of Freedom	Mean Square	F	F(0.95)	Reject?
Treatment	0.476	7	0.068	5.233	2.03	YES
Block	0.006	2	0.003	0.222	3.03	NO
Interaction	0.182	14	0.013	1.039	1.71	NO
Residual	2.696	216	0.012			
Total	3.359	239				

PP1: Peak Position One

	Variation	Degrees of Freedom	Mean Square	F	F(0.95)	Reject?
Treatment	72.238	7	10.320	2.013	2.03	NO
Block	27.270	2	13.635	2.660	3.03	NO
Interaction	71.759	14	5.126	3.474	1.71	YES
Residual	267.271	216	1.129			
Total	438.888	239				

Table 4-24. ANOVA table for PH2 and PP2.

PH2: Peak Height Two

	Variation	Degrees of Freedom	Mean Square	F	F(0.95)	Reject?
Treatment	5779.839	7	824.548	43.127	2.03	YES
Block	452.961	2	226.480	11.846	3.03	YES
Interaction	267.664	14	19.119	12.047	1.71	YES
Residual	97.364	216	0.451			
Total	6589.828	239				

PP2: Peak Position Two

	Variation	Degrees of Freedom	Mean Square	F	F(0.95)	Reject?
Treatment	163.550	7	23.364	6.528	2.03	YES
Block	6.291	2	3.146	0.879	3.03	NO
Interaction	50.109	14	3.579	3.958	1.71	YES
Residual	157.873	216	0.731			
Total	377.823	239				

Table 4-25. ANOVA table for PH3 and PP3.

PH3: Peak Height Three

	Variation	Degrees of Freedom	Mean Square	F	F(0.95)	Reject?
Treatment	4378.571	7	625.510	42.114	2.03	YES
Block	368.377	2	184.189	12.401	3.03	YES
Interaction	207.938	14	14.853	11.794	1.71	YES
Residual	81.708	216	0.378			
Total	5036.593	239				

PP3: Peak Position Three

	Variation	Degrees of Freedom	Mean Square	F	F(0.95)	Reject?
Treatment	40.464	7	5.781	3.432	2.03	YES
Block	7.680	2	3.840	2.280	3.03	NO
Interaction	23.581	14	1.684	1.176	1.71	YES
Residual	202.151	216	0.936			
Total	237.876	239				

Table 4-26. ANOVA table for PH4 and PP4.

PH4: Peak Height Four

	Variation	Degrees of Freedom	Mean Square	F	F(0.95)	Reject?
Treatment	4159.816	7	594.259	34.297	2.03	YES
Block	369.084	2	184.542	10.651	3.03	YES
Interaction	242.578	14	17.327	12.698	1.71	YES
Residual	71.266	216	0.330			
Total	4842.744	239				

PP4: Peak Position Four

	Variation	Degrees of Freedom	Mean Square	F	F(0.95)	Reject?
Treatment	6412.056	7	916.008	49.782	2.03	YES
Block	104.692	2	52.346	2.845	3.03	NO
Interaction	257.606	14	18.400	6.371	1.71	YES
Residual	406.622	216	1.883			
Total	7180.976	239				

Table 4-27. ANOVA table for PH5 and PP5.

PH5: Peak Height Five

	Variation	Degrees of Freedom	Mean Square	F	F(0.95)	Reject?
Treatment	335.747	7	47.964	20.298	2.03	YES
Block	38.832	2	19.416	8.217	3.03	YES
Interaction	33.083	14	2.363	9.749	1.71	YES
Residual	22.665	216	0.105			
Total	430.327	239				

PP5: Peak Position Five

	Variation	Degrees of Freedom	Mean Square	F	F(0.95)	Reject?
Treatment	33.921	7	4.846	0.575	2.03	NO
Block	23.023	2	11.511	1.366	3.03	NO
Interaction	118.017	14	8.430	3.322	1.71	YES
Residual	465.655	216	2.156			
Total	640.616	239				

Table 4-28. ANOVA table for PH6 and PP6.

PH6: Peak Height Six

	Variation	Degrees of Freedom	Mean Square	F	F(0.95)	Reject?
Treatment	398.194	7	56.885	14.921	2.03	YES
Block	34.879	2	17.440	4.574	3.03	YES
Interaction	53.375	14	3.813	10.912	1.71	YES
Residual	26.986	216	0.125			
Total	513.435	239				

PP6: Peak Position Six

	Variation	Degrees of Freedom	Mean Square	F	F(0.95)	Reject?
Treatment	1012.385	7	144.626	23.621	2.03	YES
Block	30.034	2	15.017	2.453	3.03	NO
Interaction	85.720	14	6.123	1.530	1.71	NO
Residual	834.586	216	3.864			
Total	1962.725	239				

From the ANOVA study, in general the following conclusions may be drawn: (1) surface roughness significantly affects peak height measurement of spectral features, (2) day-to-day variation significantly affects peak height measurement of spectral features, (3) peak position is not affected significantly by day-to-day variation, (4) peak position is affected significantly by surface roughness, and, (5) there appears to be consistently significant interaction effects between treatment and block. Treatment and block interaction effects may be attributed to variability in surface polishing on different days. Normally, F-ratios are calculated with the mean-square of the residual in the denominator, however, if treatment-block interactions are significant, many statisticians recommend using the mean square of the interaction in the denominator instead [SPI99]. Referring back to Table 4-22, this is the method which was used in this study. Now, these surface roughness studies covered a broad range of roughness (from 180 grit polishing to 0.3 micron polishing). Figure 4-7 through Figure 4-15 shows graphically how the means of these treatments over the 3 separate days varied, with 95% confidence bars superimposed. Included in these figures are how the PH2/PH4 peak ratios and PP2/PP4 peak position ratios changed with polishing. Some researchers have used these ratios as a measure of extent of corrosion in silicate glasses [SAL94], [ZHA91]. It can be seen, in general, that the 600 grit SiC polish, the 9.5 micron Al_2O_3 polish and the 1.0 micron Al_2O_3 polish resulted in a similar level of achievable reflectivity from the surface of the samples across the board. Coarser polishing resulted in correspondingly lower reflectivities. It is for this reason that all subsequent corrosion studies were performed with samples which were polished to 9.5 micron Al_2O_3 powder. Peak heights and peak positions corresponding to the 0.3 micron polish appeared to be anomalous. There were divergence's from the

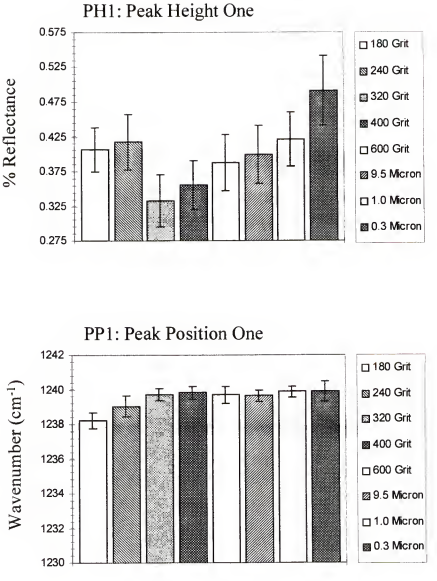

Figure 4-7. The overall 3-day means (30 replicates) of % reflectance and wavenumber (cm^{-1}) for PH1 and PP1, respectively. (95% confidence bars drawn for reference)

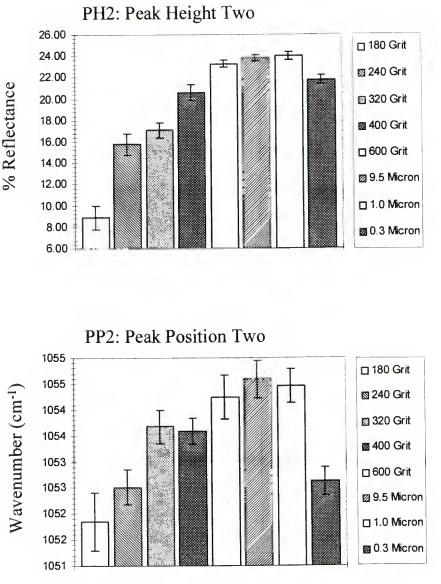

Figure 4-8. The overall 3-day means (30 replicates) of % reflectance and wavenumber (cm^{-1}) for PH2 and PP2, respectively. (95% confidence bars drawn for reference)

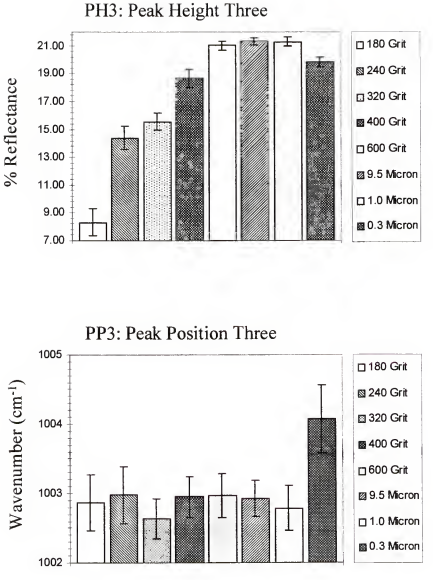

Figure 4-9. The overall 3-day means (30 replicates) of % reflectance and wavenumber (cm^{-1}) for PH3 and PP3, respectively. (95% confidence bars drawn for reference)

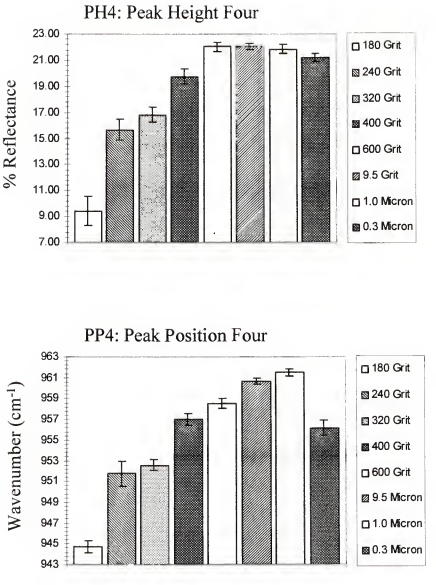

Figure 4-10. The overall 3-day means (30 replicates) of % reflectance and wavenumber (cm^{-1}) for PH4 and PP4, respectively. (95% confidence bars drawn for reference)

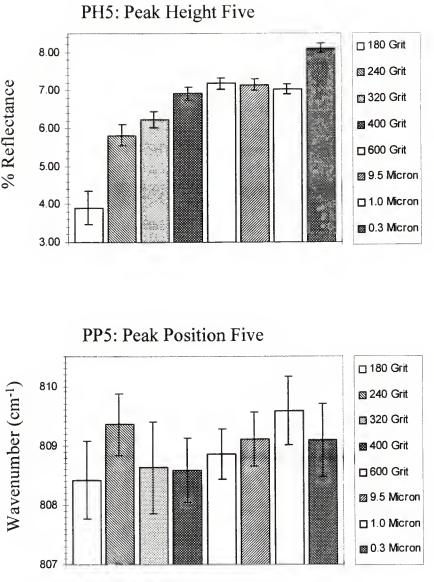

Figure 4-11. The overall 3-day means (30 replicates) of % reflectance and wavenumber (cm^{-1}) for PH5 and PP5, respectively. (95% confidence bars drawn for reference)

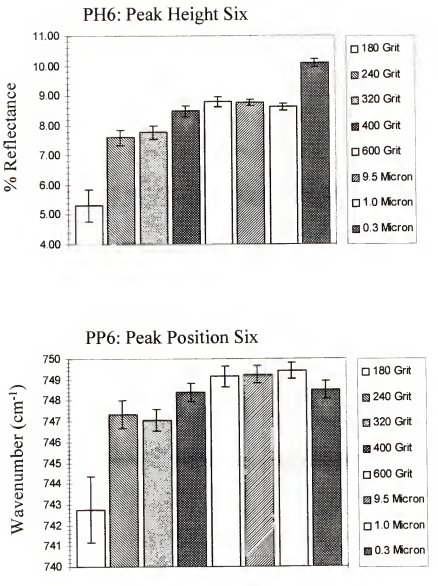

Figure 4-12. The overall 3-day means (30 replicates) of % reflectance and wavenumber (cm^{-1}) for PH6 and PP6, respectively. (95% confidence bars drawn for reference)

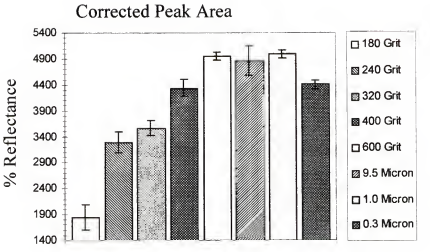

Figure 4-13. The overall 3-day means (30 replicates) of the corrected peak area as a function of polishing.
(95% confidence bars drawn for reference)

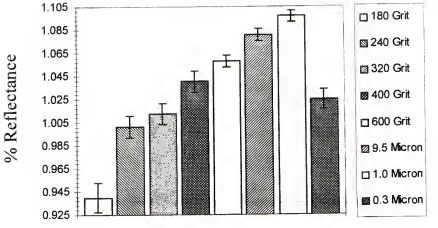

Figure 4-14. The overall 3-day means (30 replicates) of the PH2/PH4 peak height ratio as a function of polishing. (95% confidence bars drawn for reference)

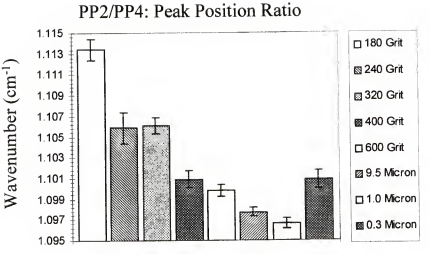

Figure 4-15. The overall 3-day means (30 replicates) the PP2/PP4 peak position ratio as a function of polishing.
(95% confidence bars drawn for reference)

overall trends with the 0.3 micron polish. Surface characterization as a function of level of polish is necessary in order to determine any compositional anomalies as a function of polishing. Optical microscopy (50x) pictures of the surface along with energy dispersive spectroscopy (EDS) measurements of surface composition are displayed in Figure 4-16 through Figure 4-23. Area EDS measurements, as opposed to spot EDS measurements were used to minimize any alkali migration often associated with electron beam techniques.

Upon examination of the optical micrographs, it is evident that the 0.3 micron Al_2O_3 polish introduced alumina agglomerates onto the surface of the sample, which persisted through successive ethanol rinses. A more aggressive wash of the surface may have eliminated these agglomerates, but in doing so, the risk arises of undesirable compositional modification of the surface. Based upon this observation, it may follow that all spectral measurements based upon the 0.3 micron Al_2O_3 polish should be deleted, and the corresponding ANOVA analysis be applied to the 180 grit through 1.0 micron polishes, as significant treatment effects may have arisen from the the 0.3 micron Al_2O_3 polish alone. In fact, it may be reasonable to do successive ANOVA tests from the 180 grit polish to the 1.0 micron polish, eliminating the coarsest polish from each subsequent statistical analysis. The importance in doing these successive ANOVA tests would be to identify the coarsest level of polishing in which blocking and treatment effects disappear in various spectral features. For example, in analyzing surface polishing of 180 grit through 1.0 micron, significant effects of surface treatment were observed in PH2. However, if the analysis of 240 grit through 1.0 micron shows that there are no significant effects of surface treatment in PH2, it can be concluded that PH2 may be used to monitor the

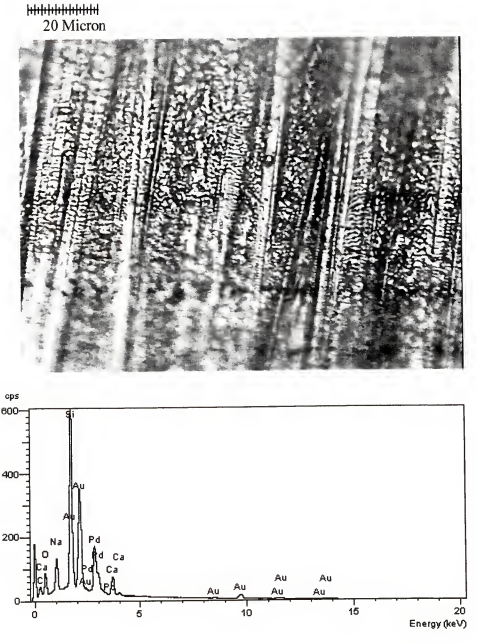

Figure 4-16. Optical microscopy picture of the surface of a 20/10/70 SLS glass polished with 180 grit SiC paper. The EDS spectra shows the presense of Na, Ca and Si as expected. (Samples were coated in Au and Pd)

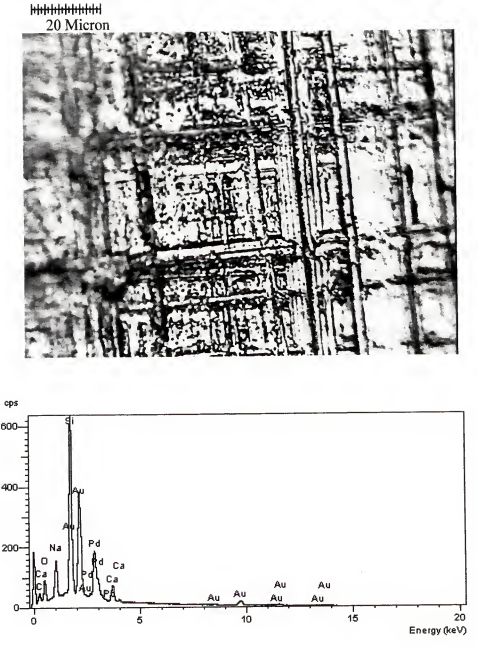

Figure 4-17. Optical microscopy picture of the surface of a 20/10/70 SLS glass polished with 240 grit SiC paper. The EDS spectra shows the presense of Na, Ca and Si as expected. (Samples were coated in Au and Pd)

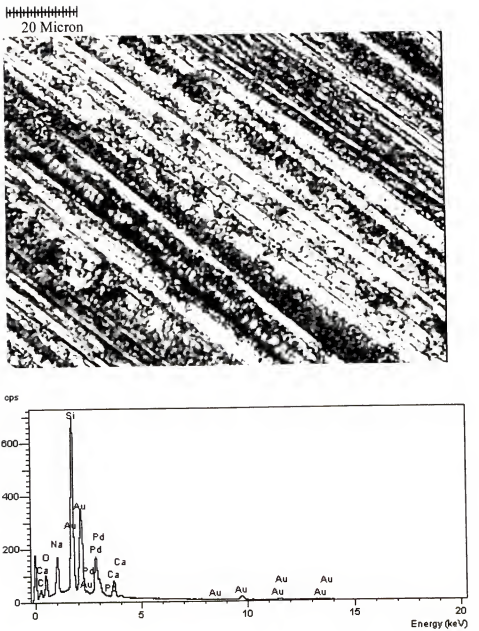

Figure 4-18. Optical microscopy picture of the surface of a 20/10/70 SLS glass polished with 320 grit SiC paper. The EDS spectra shows the presense of Na, Ca and Si as expected. (Samples were coated in Au and Pd)

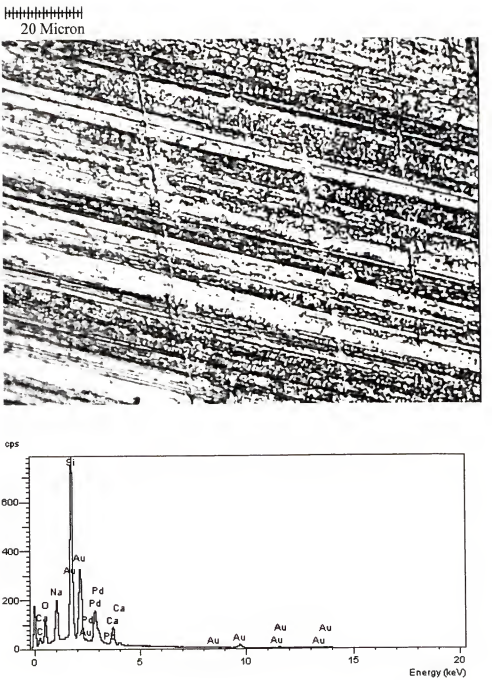

Figure 4-19. Optical microscopy picture of the surface of a 20/10/70 SLS glass polished with 400 grit SiC paper. The EDS spectra shows the presense of Na, Ca and Si as expected. (Samples were coated in Au and Pd)

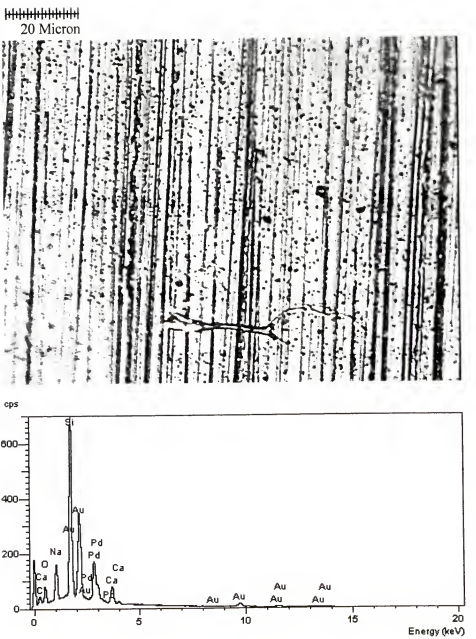

Figure 4-20. Optical microscopy picture of the surface of a 20/10/70 SLS glass polished with 600 grit SiC paper. The EDS spectra shows the presense of Na, Ca and Si as expected. (Samples were coated in Au and Pd)

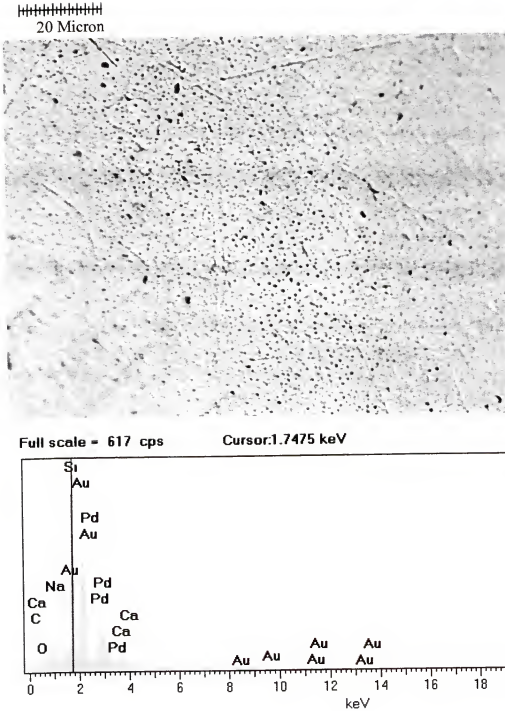

Figure 4-21. Optical microscopy picture of the surface of a 20/10/70 SLS glass polished with 9.5 micron Al_2O_3. The EDS spectra shows the presense of Na, Ca and Si as expected. (Samples were coated in Au and Pd)

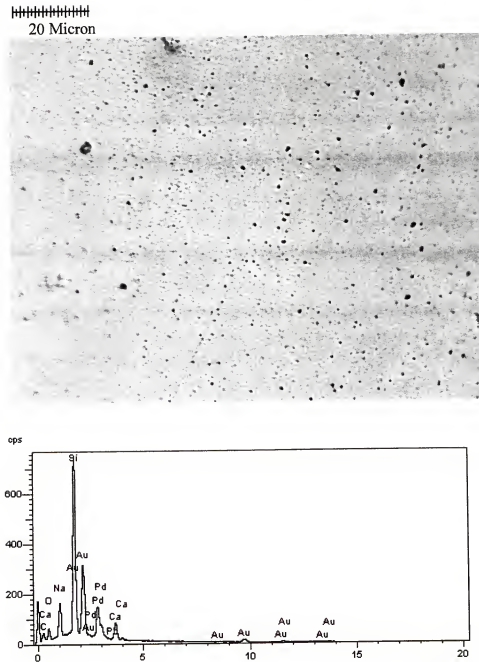

Figure 4-22. Optical microscopy picture of the surface of a 20/10/70 SLS glass polished with 1.0 micron Al_2O_3. The EDS spectra shows the presense of Na, Ca and Si as expected. (Samples were coated in Au and Pd)

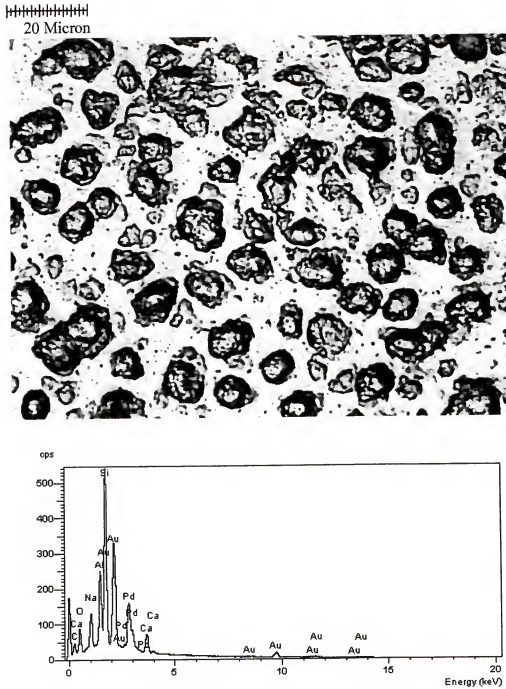

Figure 4-23. Optical microscopy picture of the surface of a 20/10/70 SLS glass polished with 0.3 micron Al_2O_3. The EDS spectra shows the presense of Na, Ca and Si as expected, plus the introduction of Al. (Samples were coated in Au and Pd)

corrosion process as long as the corrosion process did not roughen the surface beyond the equivalent of a 240 grit polish. This analysis was done and the results are represented graphically in figure 4-24 through figure 4-35. If the calculated F-statistic falls below the critical F-statistic line, it can be said with 95% confidence that there is no effect of that particular treatment or block. The dotted lines were drawn only to guide the eye.

In order for a particular spectral feature to be useful in monitoring the corrosion process, it must not display significant effects of treatment and block. Table 4-29 shows in matrix form, based upon this analysis, which spectral features are useful above various levels of coarseness (surface roughness). Therefore, according to Table 4-29, if the corrosion process does not roughen the surface of the glass sample beyond the equivalent of a 320 grit SiC polish, PP2 may be used to monitor changes in composition, with confidence that PP2 is not affected significantly by surface roughness or day-to-day variations. Likewise, if the corrosion process does not roughen the surface of the sample beyond the equivalent of a 600 grit SiC polish, PH1, PH2, PH3, PH4, PH5, PH6, PP1, PP2 and PP5 may be used with confidence to characterize the corrosion process. In order to select which spectral feature(s) could used to characterize glass samples which had been exposed to aqueous corrosion, it was necessary to determine the extent of surface roughening which had occurred in these samples which were corroded. Figure 4-36 through Figure 4-42 are atomic force microscopy (AFM) images of samples polished with 1.0 micron Al_2O_3, 9.5 micron Al_2O_3, 600 grit SiC, 400 grit SiC, 320 grit SiC, 240 grit SiC and 180 grit SiC, respectively. Figure 4-43 is a similar AFM image of a 20/10/70 SLS glass sample corroded in deionized water for 12 hours. The 12 hour aqueous corrosion experiment in deionized water represented the most aggressive corrosion experiment

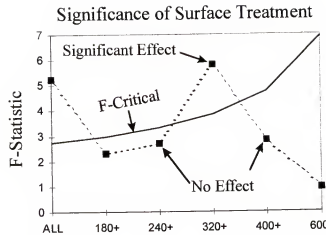

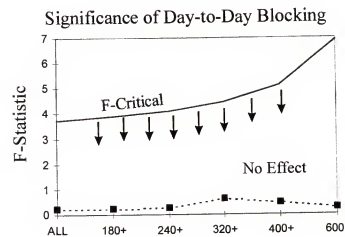

Figure 4-24. Results of successive ANOVA tests on PH1.
(ALL: includes 180 grit through 0.3 micron polishing)
(180+: includes 180 grit through 1.0 micron polishing)
(240+: includes 240 grit through 1.0 micron polishing)
(320+: includes 320 grit through 1.0 micron polishing)
(400+: includes 400 grit through 1.0 micron polishing)
(600+: includes 600 grit through 1.0 micron polishing)

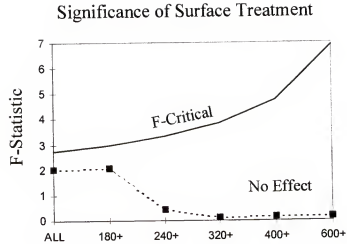

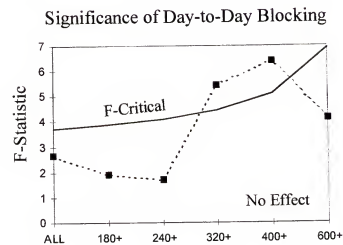

Figure 4-25. Results of successive ANOVA tests on PP1.
(ALL: includes 180 grit through 0.3 micron polishing)
(180+: includes 180 grit through 1.0 micron polishing)
(240+: includes 240 grit through 1.0 micron polishing)
(320+: includes 320 grit through 1.0 micron polishing)
(400+: includes 400 grit through 1.0 micron polishing)
(600+: includes 600 grit through 1.0 micron polishing)

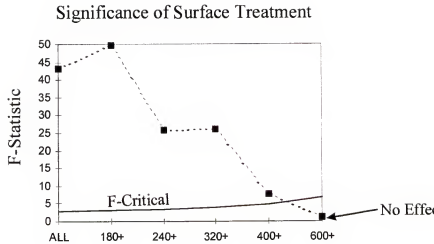

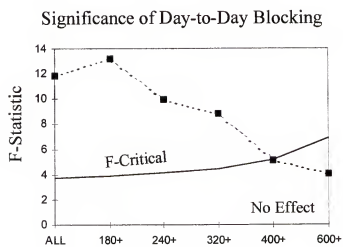

Figure 4-26. Results of successive ANOVA tests on PH2.
(ALL: includes 180 grit through 0.3 micron polishing)
(180+: includes 180 grit through 1.0 micron polishing)
(240+: includes 240 grit through 1.0 micron polishing)
(320+: includes 320 grit through 1.0 micron polishing)
(400+: includes 400 grit through 1.0 micron polishing)
(600+: includes 600 grit through 1.0 micron polishing)

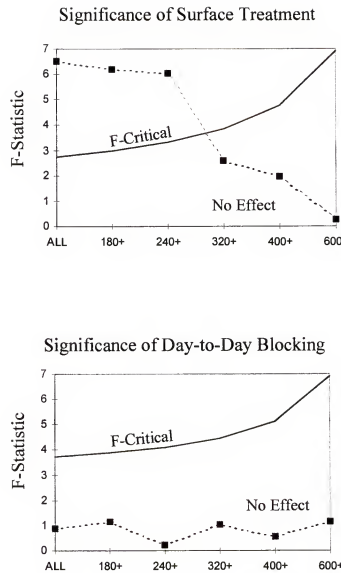

Figure 4-27. Results of successive ANOVA tests on PP2.
(ALL: includes 180 grit through 0.3 micron polishing)
(180+: includes 180 grit through 1.0 micron polishing)
(240+: includes 240 grit through 1.0 micron polishing)
(320+: includes 320 grit through 1.0 micron polishing)
(400+: includes 400 grit through 1.0 micron polishing)
(600+: includes 600 grit through 1.0 micron polishing)

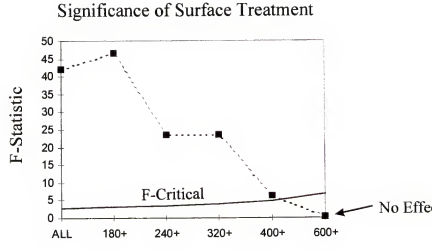

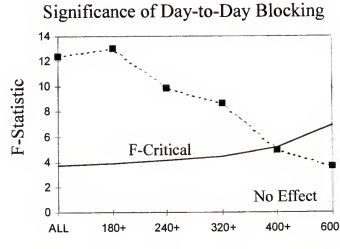

Figure 4-28. Results of successive ANOVA tests on PH3.
(ALL: includes 180 grit through 0.3 micron polishing)
(180+: includes 180 grit through 1.0 micron polishing)
(240+: includes 240 grit through 1.0 micron polishing)
(320+: includes 320 grit through 1.0 micron polishing)
(400+: includes 400 grit through 1.0 micron polishing)
(600+: includes 600 grit through 1.0 micron polishing)

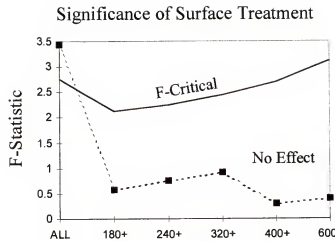

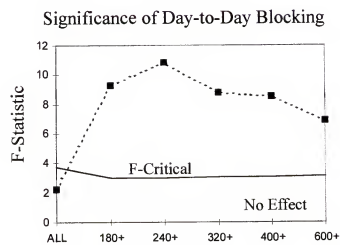

Figure 4-29. Results of successive ANOVA tests on PP3.
(ALL: includes 180 grit through 0.3 micron polishing)
(180+: includes 180 grit through 1.0 micron polishing)
(240+: includes 240 grit through 1.0 micron polishing)
(320+: includes 320 grit through 1.0 micron polishing)
(400+: includes 400 grit through 1.0 micron polishing)
(600+: includes 600 grit through 1.0 micron polishing)

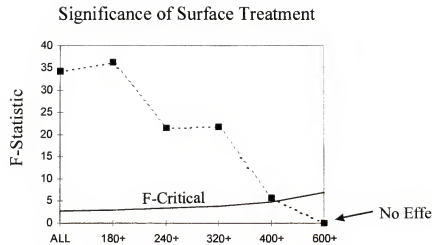

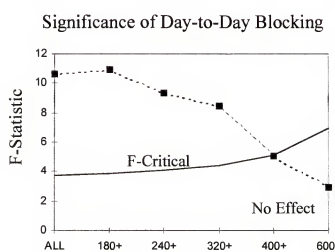

Figure 4-30. Results of successive ANOVA tests on PH4.
(ALL: includes 180 grit through 0.3 micron polishing)
(180+: includes 180 grit through 1.0 micron polishing)
(240+: includes 240 grit through 1.0 micron polishing)
(320+: includes 320 grit through 1.0 micron polishing)
(400+: includes 400 grit through 1.0 micron polishing)
(600+: includes 600 grit through 1.0 micron polishing)

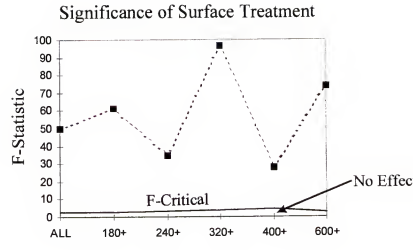

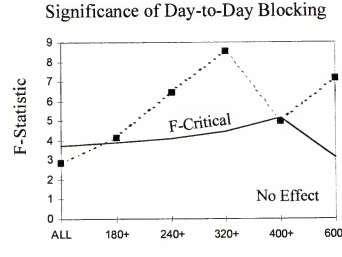

Figure 4-31. Results of successive ANOVA tests on PP4.
(ALL: includes 180 grit through 0.3 micron polishing)
(180+: includes 180 grit through 1.0 micron polishing)
(240+: includes 240 grit through 1.0 micron polishing)
(320+: includes 320 grit through 1.0 micron polishing)
(400+: includes 400 grit through 1.0 micron polishing)
(600+: includes 600 grit through 1.0 micron polishing)

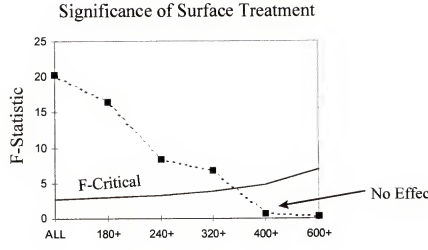

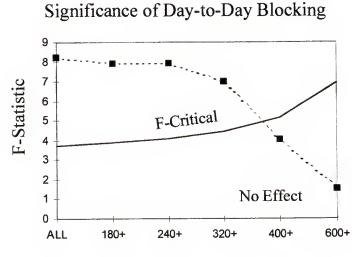

Figure 4-32. Results of successive ANOVA tests on PH5.
(ALL: includes 180 grit through 0.3 micron polishing)
(180+: includes 180 grit through 1.0 micron polishing)
(240+: includes 240 grit through 1.0 micron polishing)
(320+: includes 320 grit through 1.0 micron polishing)
(400+: includes 400 grit through 1.0 micron polishing)
(600+: includes 600 grit through 1.0 micron polishing)

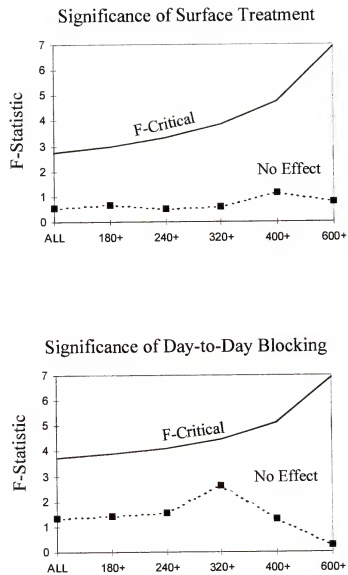

Figure 4-33. Results of successive ANOVA tests on PP5.
(ALL: includes 180 grit through 0.3 micron polishing)
(180+: includes 180 grit through 1.0 micron polishing)
(240+: includes 240 grit through 1.0 micron polishing)
(320+: includes 320 grit through 1.0 micron polishing)
(400+: includes 400 grit through 1.0 micron polishing)
(600+: includes 600 grit through 1.0 micron polishing)

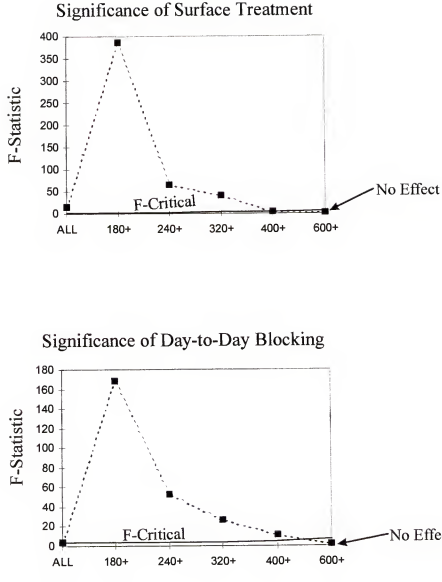

Figure 4-34. Results of successive ANOVA tests on PH6.
(ALL: includes 180 grit through 0.3 micron polishing)
(180+: includes 180 grit through 1.0 micron polishing)
(240+: includes 240 grit through 1.0 micron polishing)
(320+: includes 320 grit through 1.0 micron polishing)
(400+: includes 400 grit through 1.0 micron polishing)
(600+: includes 600 grit through 1.0 micron polishing)

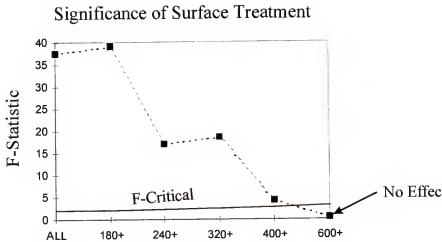

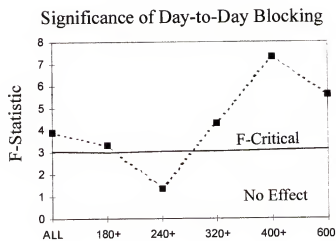

Figure 4-35. Results of successive ANOVA tests on PP6.
(ALL: includes 180 grit through 0.3 micron polishing)
(180+: includes 180 grit through 1.0 micron polishing)
(240+: includes 240 grit through 1.0 micron polishing)
(320+: includes 320 grit through 1.0 micron polishing)
(400+: includes 400 grit through 1.0 micron polishing)
(600+: includes 600 grit through 1.0 micron polishing)

which was performed. Therefore, the surface of this sample should exhibit the most roughening and serve as a benchmark as to which spectral features are used to characterize compositional changes using FT-IRRS. Figure 4-44 through Figure 4-50 show quantitative rms roughness and measurements of features in samples as a function of polishing. Figure 4-51 shows similar information for the corroded sample. As evident from the figures, as polishing becomes finer, the rms roughness decreases. There is some anomalous behavior in that the rms roughness value of the sample polished to 240 grit was less than that polished to 320 grit. This may be explained by the nature of the 240 grit sample's surface. Referring back to Figure 4-17, there is evidence of "cross-polishing" which may have lowered the overall rms roughness value. In general, the samples polished with 180 grit SiC through 600 grit SiC resulted in directional patterns of surface features. This unidirectional orientation of surface scratches was not present in the finer polishing steps (9.5 micron and 1.0 micron). This may be attributed to the nature of the polishing technique. The 180 grit through 600 grit polishing steps were "aggressive," in that the sample was placed into contact with a high rpm polishing wheel. As the sample was removed from the polishing wheel, the characteristic unidirectional scratches remained. The finer polishing steps were not so aggressive, in that fine powders were used, and polishing was done manually on soft felt. As can be seen from the AFM images, surface roughening did occur in the corroded sample, however, it did not exceed the equivalent roughening of a 320 grit SiC polish. The corroded sample resulted in an rms roughness of 133 nm, compared to 143 nm for the 400 grit polish. Here, area rms values are taken, as they would be a better representation of the sample's surface as a whole. Therefore, assuming that the corrosion process did not roughen the surfaces of the glass

samples more than an equivalent 320 grit SiC polish, referring to Table 4-29, PP2 and PP5 may be used to confidently characterize surface compositional changes in those samples following the aqueous experiments. Of the aforementioned spectral features, only PP2 has been noted in the literature as being relevant to the surface composition of silicate glasses (PP2 referring to the silicon-oxygen stretching vibration). Therefore, PP2 was used as the primary spectral feature of interest. Any shifts of PP2 to higher wavenumbers reflected increases in the relative proportion of SiO_2 within the surface of the glasses.

As an exercise, Equation 4-1 was applied in order to extrapolate the rms roughness values required in order to achieve the equivalent spectra which were measured in the polishing study. The spectrum corresponding to the 9.5 micron Al_2O_3 polish was taken to be the maximum reflectance achievable (a perfectly smooth surface), hence R_o in the equation. An iterative procedure was used in order to back out the σ values which would result in spectra corresponding to the actual measured spectra in the polishing study. These spectra are displayed in figures 4-52 through 4-56, along with the σ values determined by curve fitting. The fit with the measured spectra is good, across all wavenumbers, which gives credence to the equation. Notice that in the 180 grit polished sample, the SN peak is greater in magnitude in comparison to the S peak, in both the measured and calculated spectra. As the polishing proceeded to finer grit sizes (decreasing σ values), the S peak overtook the SN peak in relative reflectance in both the measured and calculated spectra and approached what is expected. This may be attributed to the exponential wavelength dependence of Equation 4-1. Referring once again to this equation, a smaller wavelength (higher wavenumber S-peak) will be more affected by changes in surface roughness. The fact that the calculated spectra shows the same

dependence as the measured spectra gives much insight into the spectral dependence on surface roughness. This FT-IRRS spectral dependence on surface roughness is not well covered nor explained in the literature. The rms roughness values calculated, however, do not match those measured via AFM. The calculated values are consistently higher (Figure 4-57). It must be remembered that a qualification of the equation is that a Gaussian surface irregularity distribution must exist. This may not be the case in the polished samples, although unlikely. In addition, the AFM sampling area (400 μm^2) is relatively small in comparison to the FT-IRRS sampling area of 9π mm^2. The FT-IRRS sampling area may include large cracks or imperfections which could raise the effective rms roughness value. Also, the assumption that the 9.5 micron polish represented a "perfectly smooth surface" may have been incorrect. A perfectly smooth surface would have an rms roughness value of zero. However, the previous polishing study indicated that finer polishing beyond 9.5 microns did not result in a statistically significant better reflectance spectrum. It should also be noted that there could exist sources of error in the measurement of rms roughness via AFM. The method by which rms roughness is calculated is by comparing feature heights to a baseline horizontal axis. It is apparent that some samples were "off-horizontal" which may have resulted in erroneous readings. The differences between calculated and measured values were most likely attributed to the scale in which those measurements and calculations were based upon, as well as in the method by which those rms roughness values were calculated.

Table 4-29. A matrix representation of the coarsest surface roughness allowable before effects to spectral features become significant. (YES means that a particular spectral feature is not affected by that level of polish)

	ALL	180+	240+	320+	400+	600+
PH1					YES	YES
PH2						YES
PH3						YES
PH4						YES
PH5					YES	YES
PH6						YES
PP1						YES
PP2				YES	YES	YES
PP3						
PP4						
PP5	YES	YES	YES	YES	YES	YES
PP6						

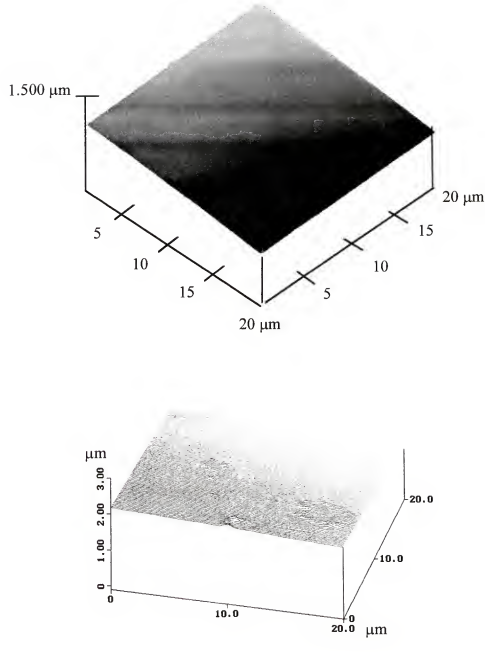

Figure 4-36. The surface of a 20/10/70 SLS glass sample polished with 1.0 micron Al_2O_3 as measured by AFM.

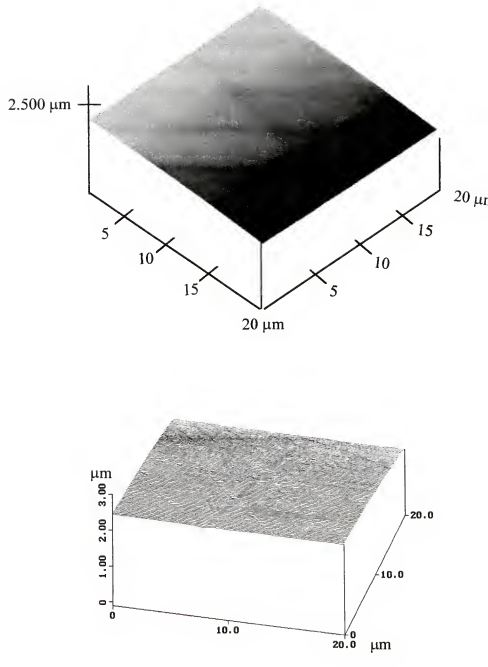

Figure 4-37. The surface of a 20/10/70 SLS glass sample polished with 9.5 micron Al_2O_3 as measured by AFM.

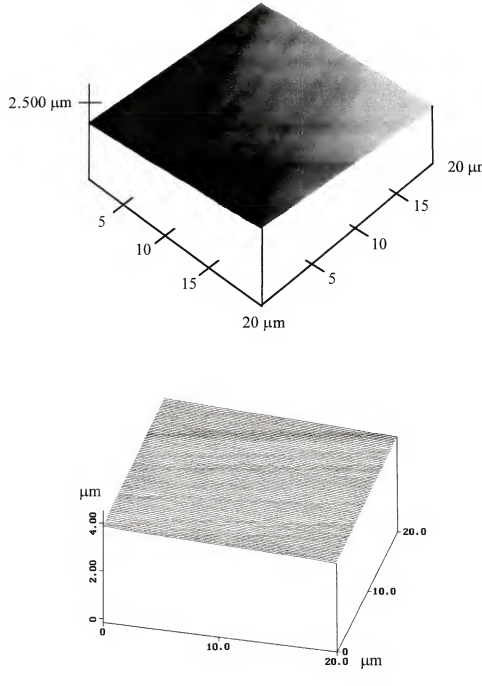

Figure 4-38. The surface of a 20/10/70 SLS glass sample polished with 600 grit SiC as measured by AFM.

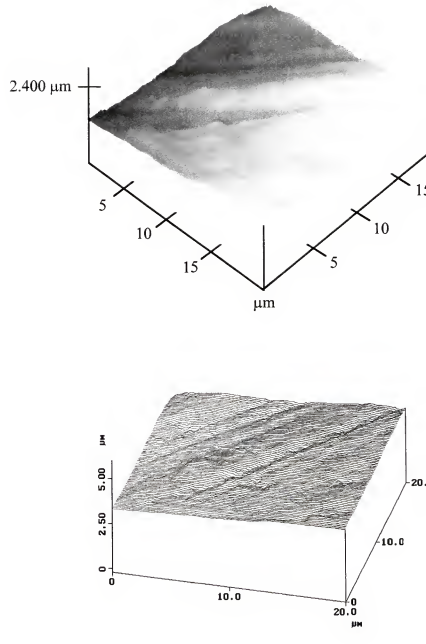

Figure 4-39. The surface of a 20/10/70 SLS glass sample polished with 400 grit SiC as measured by AFM.

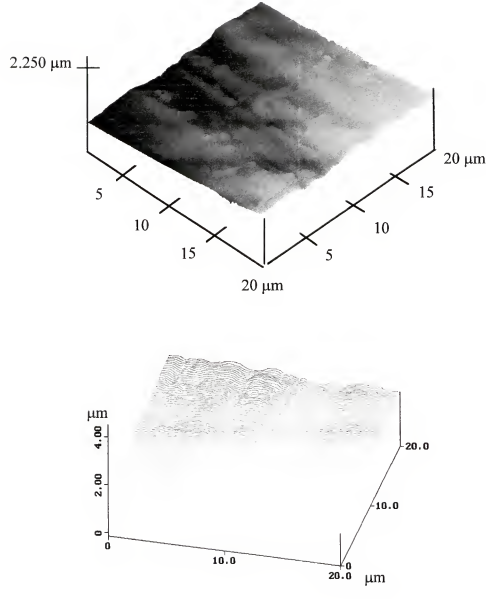

Figure 4-40. The surface of a 20/10/70 SLS glass sample polished with 320 grit SiC as measured by AFM.

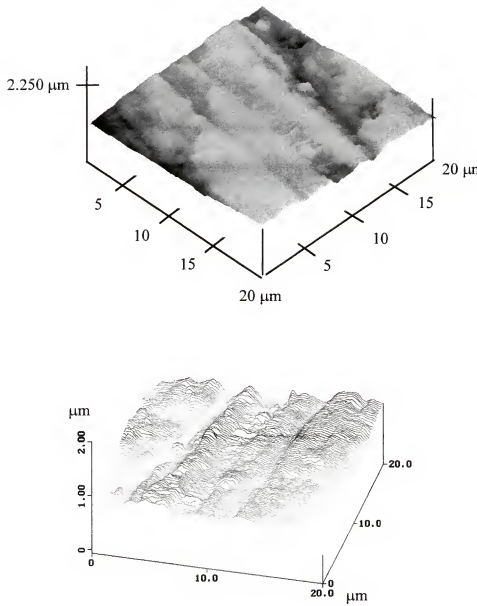

Figure 4-41. The surface of a 20/10/70 SLS glass sample polished with 240 grit SiC as measured by AFM.

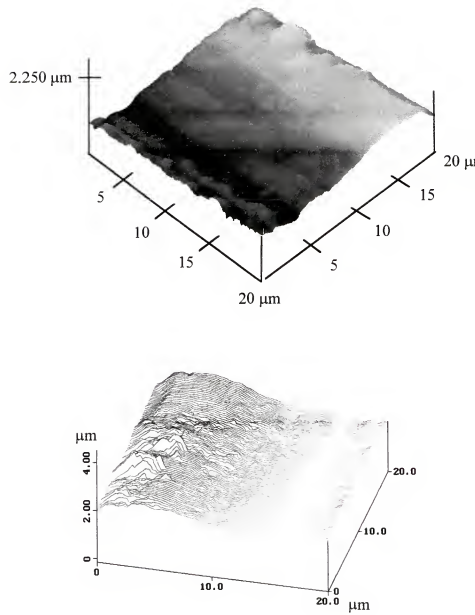

Figure 4-42. The surface of a 20/10/70 SLS glass sample polished with 180 grit SiC as measured by AFM.

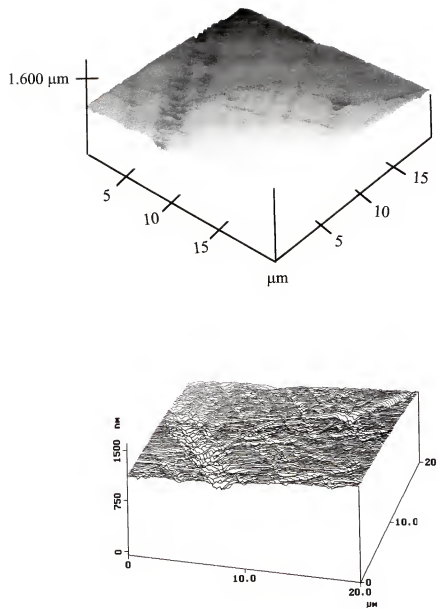

Figure 4-43. The surface of a 20/10/70 SLS glass sample corroded for 12 hours in deionized water as measured by AFM.

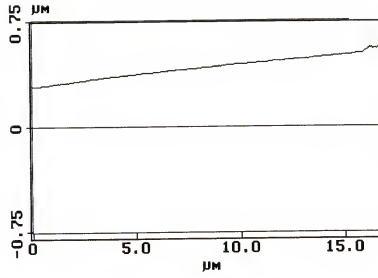

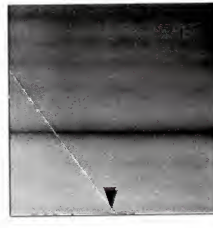

Horizontal Distance:	237.44 nm
Vertical Distance:	5.149 nm
Line RMS Roughness:	9.811 nm
Area RMS Roughness:	21.721 nm
Surface Area:	400.57 μm^2

Figure 4-44. AFM measurements of a 20/10/70 SLS glass sample polished with 1.0 micron Al_2O_3.

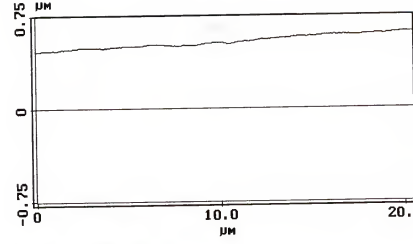

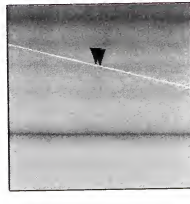

Horizontal Distance:	585.94 nm
Vertical Distance:	13.354 nm
Line RMS Roughness:	5.385 nm
Area RMS Roughness:	14.796 nm
Surface Area:	400.32 μm^2

Figure 4-45. AFM measurements of a 20/10/70 SLS glass sample polished with 9.5 micron Al_2O_3.

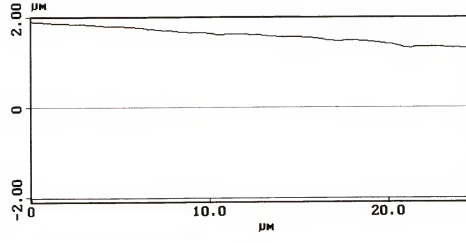

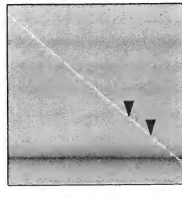

Horizontal Distance:	3.203 µm
Vertical Distance:	166.35 nm
Line RMS Roughness:	51.317 nm
Area RMS Roughness:	83.418 nm
Surface Area:	400.86 µm^2

Figure 4-46. AFM measurements of a 20/10/70 SLS glass sample polished with 600 grit SiC.

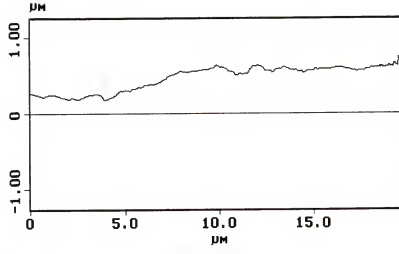

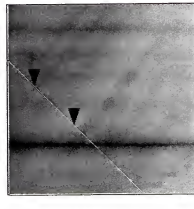

Horizontal Distance:	5.789 µm
Vertical Distance:	422.82 nm
Line RMS Roughness:	126.75 nm
Area RMS Roughness:	110.03 nm
Surface Area:	404.31 μm^2

Figure 4-47. AFM measurements of a 20/10/70 SLS glass sample polished with 400 grit SiC.

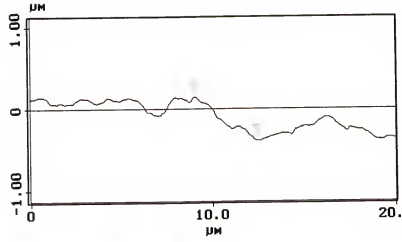

Horizontal Distance:	3.438 µm
Vertical Distance:	525.51 nm
Line RMS Roughness:	157.61 nm
Area RMS Roughness:	143.05 nm
Surface Area:	407.82 μm^2

Figure 4-48. AFM measurements of a 20/10/70 SLS glass sample polished with 320 grit SiC.

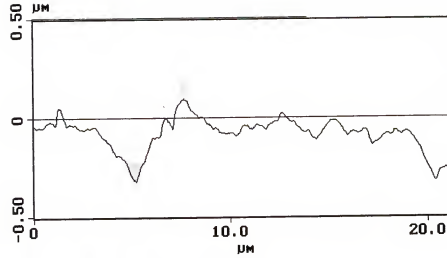

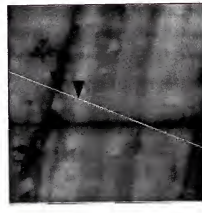

Horizontal Distance:	2.539 µm
Vertical Distance:	413.53 nm
Line RMS Roughness:	118.28 nm
Area RMS Roughness:	107.61 nm
Surface Area:	407.76 μm^2

Figure 4-49. AFM measurements of a 20/10/70 SLS glass sample polished with 240 grit SiC.

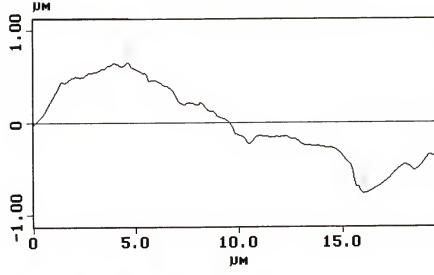

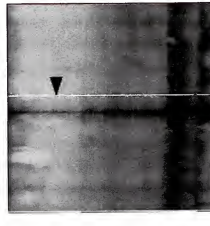

Horizontal Distance:	11.367 µm
Vertical Distance:	1.405 µm
Line RMS:	326.36 nm
Area RMS:	393.79 nm
Surface Area:	424.85 μm^2

Figure 4-50. AFM measurements of a 20/10/70 SLS glass sample polished with 180 grit SiC.

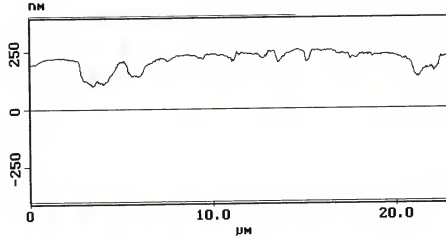

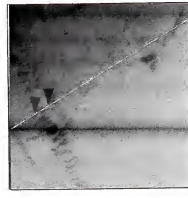

Horizontal Distance:	1.680 μm
Vertical Distance:	105.78 nm
Line RMS:	36.084 nm
Area RMS:	132.61 nm
Surface Area:	404.19 μm^2

Figure 4-51. AFM measurements of a 20/10/70 SLS glass sample corroded for 12 hours in deionized water.

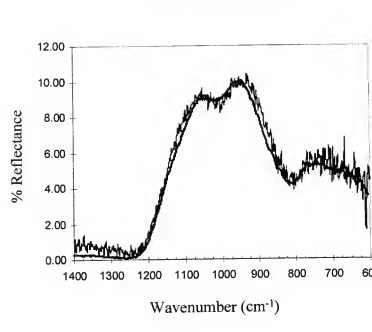

Figure 4-52. Calculated and measured FT-IRRS spectra for a 20/10/70 SLS glass polished at 180 grit.

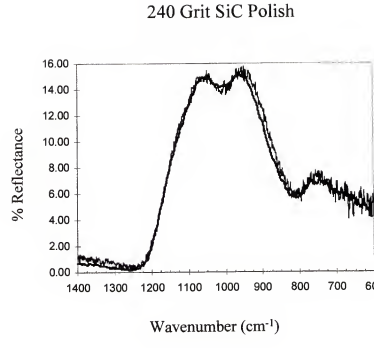

Figure 4-53. Calculated and measured FT-IRRS spectra for a 20/10/70 SLS glass polished at 240 grit.

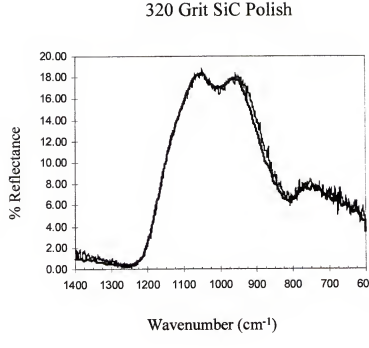

Figure 4-54. Calculated and measured FT-IRRS spectra for a 20/10/70 SLS glass polished at 320 grit.

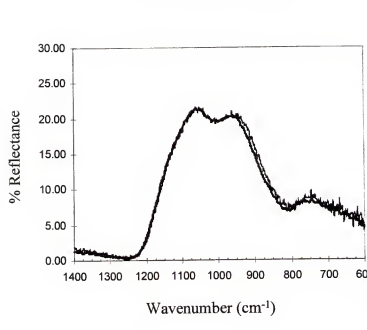

Figure 4-55. Calculated and measured FT-IRRS spectra for a 20/10/70 SLS glass polished at 400 grit.

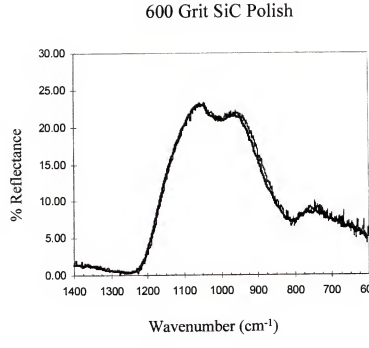

$\sigma = 0.213$ microns

Figure 4-56. Calculated and measured FT-IRRS spectra for a 20/10/70 SLS glass polished at 600 grit.

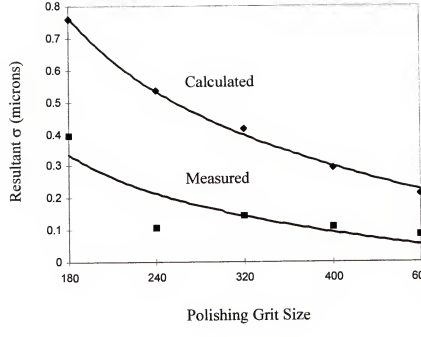

Figure 4-57. Comparison of the measured σ values to those which were calculated via curve fitting.

Discussion

The significance of the study in this chapter points to the usefulness of using FT-IRRS spectral features in characterizing the corrosion process in silicate glasses. When characterizing the corrosion process, in general, only surface compositional changes are of interest. If surface roughening or day-to-day variation significantly affects the characteristics of FT-IRRS spectral features, then confidence is lost in interpreting peak shifts. It was found through statistical analysis that the peak intensities of all spectral features were significantly affected by both surface roughness and day-to-day variation in the measurement. Only the Si-O-Si peak position (cm^{-1}) was unaffected by both day-to-day variation and surface roughening equivalent to a 12 hour aqueous corrosion process. The Si-O-Si peak is a prominent, well defined peak, making the measurement of it's position less error-prone. Although this peak is associated with the relative Si-O-Si bond concentration within the glass surface, shifts in this peak may be related to overall structural and compositional changes occurring within the surface, including the leaching of non-network cations. Therefore, since surface roughening and day-to-day variation may be ignored in the interpretation of the Si-O-Si peak, any shifts may be directly related to structural and compositional changes in the surface. It was this spectral feature (the Si-O-Si stretching vibration) which was used in subsequent FT-IRRS analysis.

Equation 4-1 was also used to transform an FT-IRRS spectrum of a glass sample of "perfectly smooth surface" into those of roughly polished surfaces. Values of rms roughness (σ) were obtained through curve fitting calculated spectra to measured spectra.

The accuracy of these σ values is nonconsequential. The calculated spectra fit well with measured spectra over the entire range of wavelengths, supporting the inherent validity of the Equation 4-1. This provides much insight into the interpretation of FT-IRRS spectra of glass specimens whose surfaces have been roughened through corrosion. It was shown that in the case of a very rough surface, the spectra was distorted significantly. This effect has been observed by others as well, but the spectra arising from such roughening could only be described as "ill-defined" [NEW91]. The results of this study quantifies this observed behavior. Therefore, if information is known in regards to the surface roughness of a glass sample which has undergone a corrosion process, Equation 4-1 could be applied in order to transform the spectrum of the rough glass sample into one of a "perfectly smooth" sample, thereby allowing direct comparison of spectral features in terms of only composition and structure.

CHAPTER 5
EFFECTS OF SOLUTION CHEMISTRY ON LEACHING BEHAVIOR OF SODA-LIME-SILICA GLASS

Introduction

Many studies have been performed examining the effects of solution chemistry on aqueous glass corrosion. Van Lier [VAN65] and Dove [DOV90] observed that salt solutions increase the dissolution rate of quartz. Marshall [MAR80], [MAR80a], [MAR80b] evaluated the effects of salt solutions on the solubility of amorphous silica, and found that as salt concentrations increased, silica solubility decreased. Investigations into the effects and mechanisms of solution chemistry on the corrosion rates of multicomponent glasses were outlined in Chapter 2. It is evident that although much work has been done in this area, the mechanisms of how solution chemistry affects glass corrosion rates are still not well understood.

In general, leach tests involve bringing a sample in contact with an aqueous solution for a period of time, then analyzing the leachant in order to determine the identity and concentrations of the leached material. Often, the leachant analysis is complemented with surface analysis to better understand various leaching mechanisms.

There exists a multitude of standardized leach tests. Many of these were proposed by the Materials Characterization Center (MCC) for the purposes of evaluating the durabilities of glasses used to immobilize radioactive wastes [MEN84]. In general, these

leach test methods may be classified as either being static or dynamic. Static leach tests involve evaluating the corrosion process under stagnant conditions, where the leachant is not refreshed, while dynamic leach tests involve evaluating the corrosion process under flowing conditions, where the leachant is continuously refreshed. The experiments of this study were conducted using the MCC-1P Static Leach Test Method as a guide [MEN83].

Sample Preparation

The soda-lime-silicate (SLS) glasses used for this static leach study were prepared by thoroughly mixing reagent grade carbonates of Na and Ca with 5 μm Min-U-Sil (SiO_2) with the following target composition in mind: 20 mol% Na_2O, 10 mol% CaO, 70 mol% SiO_2 – 20/10/70 SLS. These mixtures were homogenized at 1400°C for 24 hours in a high-temperature electric furnace. After 24 hours of homogenization, the molten glass was cast into approximately 1.30 cm x 1.30 cm x 10 cm bars using a graphite mold. Immediately following casting, the bars were placed into a small annealing furnace, maintained at 450°C for 4 hours and furnace-cooled to room temperature. Following annealing, the cast bars were stored in a drying oven held at 110°C. Melting was carried out in platinum crucibles to minimize potential contamination during the process. Between melts, the platinum crucible was cleaned thoroughly in a 60/40 HF/H_2O bath.

The annealed glass bars were cut into 0.4 cm thick samples using a slow speed diamond-impregnated wafering saw. Prior to each set of leach tests, samples were polished in the following grit sequence: 180 grit SiC, 240 grit SiC, 320 grit SiC, 400 grit SiC, 600 grit SiC and 9.5 μm Al_2O_3. Polishing was done wet through the 400 grit SiC

polish. The 600 grit SiC polish and the 9.5 μm Al_2O_3 were done dry to minimize glass surface interactions with water. Samples not immediately used in an experiment were stored in a drying oven. All corrosion experiments were conducted on the samples polished through 9.5 μm Al_2O_3 based on the results discussed in Chapter 4.

The Leach Test

For the static leach tests, the polished glass samples were suspended inside a 120 ml capacity Teflon corrosion cell, filled with the appropriate leachant solution, and then placed inside a Blue M convection oven held at 90°C as shown in Figure 5-1. The leachant solutions included the following: deionized water, 0.1M KCl, 0.1M KNO_3, 0.1M LiCl, 0.1M $LiNO_3$, 1.0M KCl, 1.0M KNO_3, 1.0M LiCl and 1.0M $LiNO_3$. This selection of aqueous solutions allowed for the evaluation of the effects of electrolyte concentration, electrolyte cation, and electrolyte anion on the kinetics of aqueous corrosion of a 20/10/70 SLS glass sample. Two replicates under each condition were run for confidence. The samples were leached for a period of 12 hours, which would be considered a short-term leach test. On this time scale, ion exchange processes determine the kinetics of the reaction, as opposed to steady-state dissolution kinetics. Therefore the effects of solution chemistry may be examined in regards to this evolving, non-steady state condition. In addition, the short term leach test would result in less surface roughening of the samples, which would allow the use of the FT-IRRS analysis as described in the previous chapters.

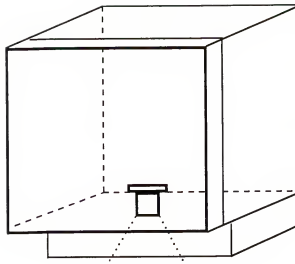

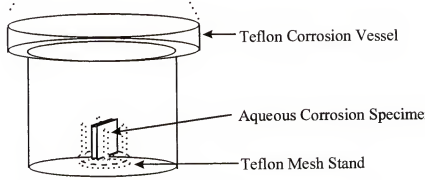

Temperature:	90°C
SA/V:	0.05 cm^{-1}
Time:	Up to 12 hours
Leaching Solutions:	0.1M KCl, 0.1MKNO_3
	0.1M LiCl, 0.1M $LiNO_3$
	1.0M KCl, 1.0M KNO_3
	1.0M LiCl, 1.0M $LiNO_3$
	Deionized Water

Figure 5-1. Schematic of the experimental arrangement for static aqueous leaching.

FT-IRRS Analysis of Glass Corrosion

FT-IRRS spectra were obtained before testing, after 6 hours of immersion in aqueous solution and after 12 hours of immersion. Samples were rinsed in absolute ethanol prior to each measurement to rid the surface of any water. Figure 5-2 through Figure 5-10 are the FT-IRRS spectra obtained for each of the nine immersion conditions. The spectra are offset by 5 degrees each for the sake of readability. Qualitatively, as corrosion proceeds in all cases, the S peak (Si-O-Si stretching vibration at 1055 cm^{-1}) shifts to higher frequencies and the SN peak (Si-Nonbridging Oxygen vibration at 960 cm^{-1}) shifts to lower frequencies. Although the time dependency on aqueous corrosion is obvious, the solution dependency requires a more quantitative approach. Referring to the following equation presented in Chapter 4:

$$R_s = R_o \exp[-(4\pi\sigma/\lambda)^2] \qquad (4\text{-}1)$$

was used to calculate rms roughness values through an iterative procedure that fit calculated spectra to measured spectra. The fits were good, although the calculated rms roughness values did not correspond to those which were measured with AFM. The sampling area, and more importantly, the sample orientation (off horizontal) could have affected measured rms values, as those measured values were based upon a horizontal baseline. One measured parameter which would not have been affected by sample orientation was

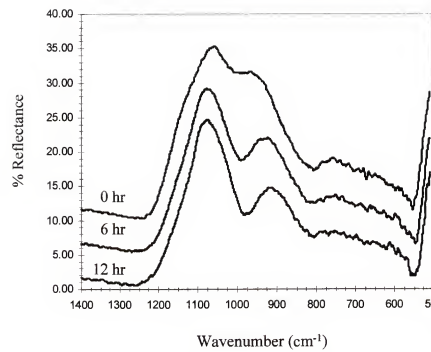

Figure 5-2. FT-IRRS spectra as a function of time for a 20/10/70 SLS glass sample immersed in 0.1M KCl. The spectra have not been transformed to correct for surface roughness resulting from corrosion.

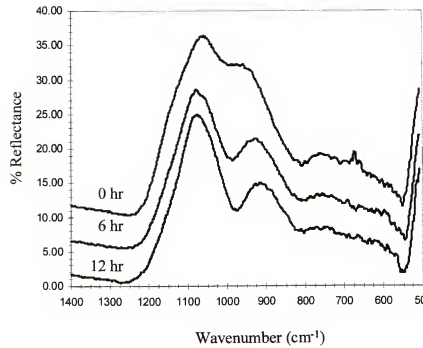

Figure 5-3. FT-IRRS spectra as a function of time for a 20/10/70 SLS glass sample immersed in 0.1M KNO_3. The spectra have not been transformed to correct for surface roughness resulting from corrosion.

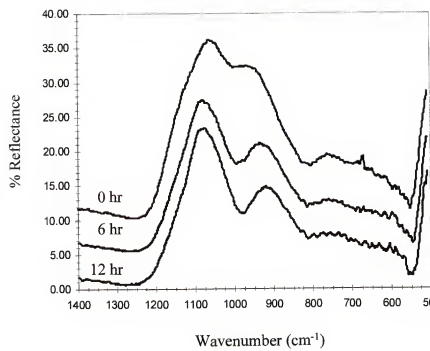

Figure 5-4. FT-IRRS spectra as a function of time for a 20/10/70 SLS glass sample immersed in 0.1M LiCl. The spectra have not been transformed to correct for surface roughness resulting from corrosion.

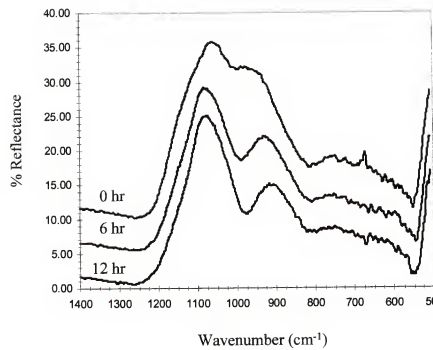

Figure 5-5. FT-IRRS spectra as a function of time for a 20/10/70 SLS glass sample immersed in 0.1M $LiNO_3$. The spectra have not been transformed to correct for surface roughness resulting from corrosion.

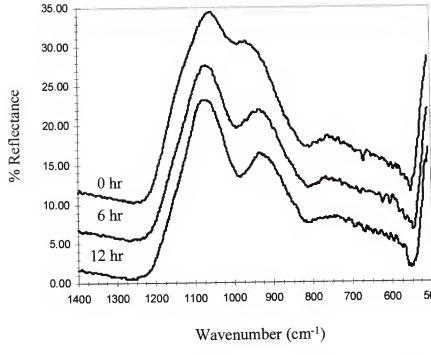

Figure 5-6. FT-IRRS spectra as a function of time for a 20/10/70 SLS glass sample immersed in 1.0M KCl. The spectra have not been transformed to correct for surface roughness resulting from corrosion.

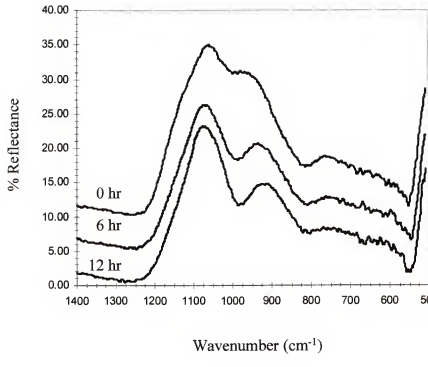

Figure 5-7. FT-IRRS spectra as a function of time for a 20/10/70 SLS glass sample immersed in 1.0M KNO_3. The spectra have not been transformed to correct for surface roughness resulting from corrosion.

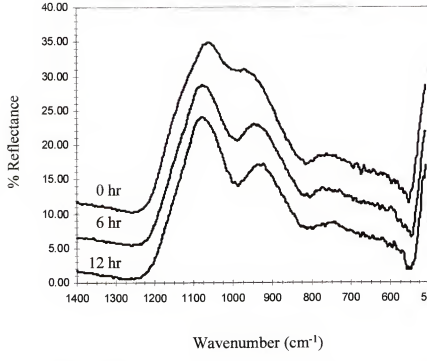

Figure 5-8. FT-IRRS spectra as a function of time for a 20/10/70 SLS glass sample immersed in 1.0M LiCl. The spectra have not been transformed to correct for surface roughness resulting from corrosion.

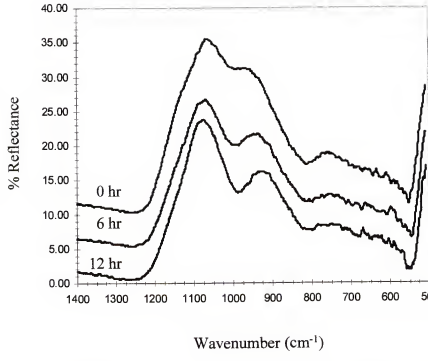

Figure 5-9. FT-IRRS spectra as a function of time for a 20/10/70 SLS glass sample immersed in 1.0M $LiNO_3$. The spectra have not been transformed to correct for surface roughness resulting from corrosion.

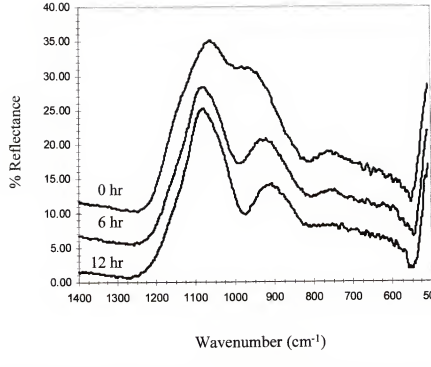

Figure 5-10. FT-IRRS spectra as a function of time for a 20/10/70 SLS glass sample immersed in deionized water. The spectra have not been transformed to correct for surface roughness resulting from corrosion.

the AFM measured surface area. The surface area was determined through an algorithm measuring the intersection of the surface with cubes of decreasing dimension. Such a procedure would not be affected by a sample being off horizontal. Figure 5-11 shows a plot relating the calculated rms roughness (σ) values from Chapter 4 with the corresponding sample surface areas which were measured. This relationship is described by a well correlated fit. Figure 5-12 through figure 5-20 are AFM images of 20/10/70 SLS glasses which have been immersed in each of the nine test conditions for twelve hours. The measured surface area is included. These surface areas may be related through Figure 5-11 to a corresponding rms roughness. This rms roughness may then be used in Equation 4-1 to transform the "roughened" samples' spectra into that of a "perfectly smooth" sample. Since the FT-IRRS spectra are affected by both surface roughness and composition, the consequence of this transformation would be that spectral feature changes may be related more directly to compositional changes. Again, it was assumed that R_o is equal to the reflectance of the respective 9.5 micron polished sample. Figure 5-21 through Figure 5-29 show the transformed FT-IRRS spectra for each of the nine immersion conditions. Included in each figure is the "perfectly smooth" spectra obtained prior to corrosion, and superimposed, the "perfectly smooth" spectra of the twelve-hour immersed sample. Figure 5-30 is a plot of the difference between the twelve-hour corroded peak position (PP2) and that of the unleached sample, for each immersion condition. Confidence bars of 95% are superimposed on the plot. Referring back to Chapter 4, PP2 corresponds to the Si-O-Si stretching vibration peak position, and, as aqueous corrosion proceeds in silicate glasses, PP2 will shift to higher wavenumbers as the

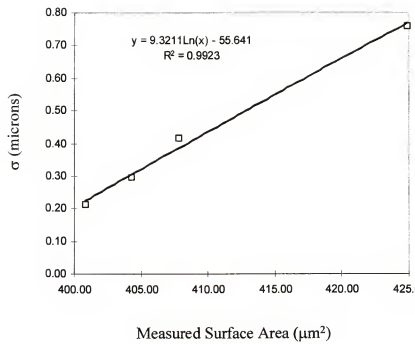

Figure 5-11. Plot of surface area of polished glass samples as measured by AFM versus rms roughness (σ) as calculated for each of the polished samples using Equation 4-1.

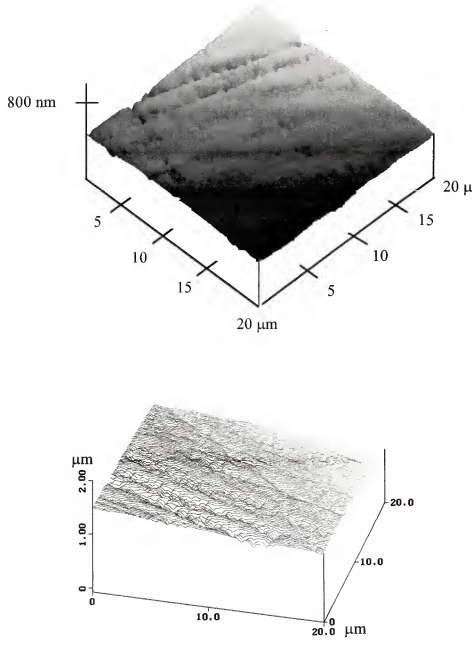

Figure 5-12. The surface of a 20/10/70 SLS glass sample corroded for 12 hours in 0.1M KCl.
Surface Area: 402.77 μm^2

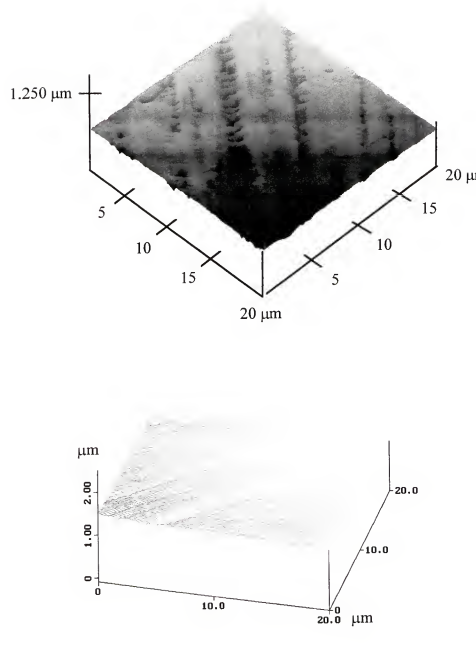

Figure 5-13. The surface of a 20/10/70 SLS glass sample corroded for 12 hours in 0.1M KNO_3.
Surface Area: 405.00 μm^2

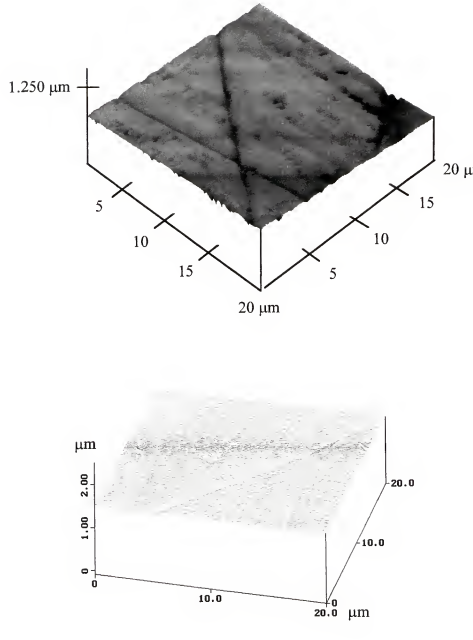

Figure 5-14. The surface of a 20/10/70 SLS glass sample corroded for 12 hours in 0.1M LiCl.
Surface Area: 403.77 μm^2

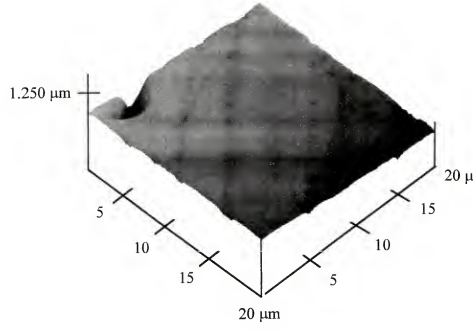

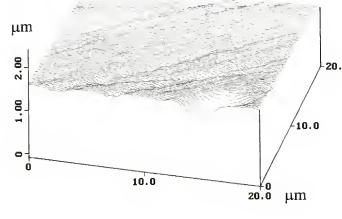

Figure 5-15. The surface of a 20/10/70 SLS glass sample corroded for 12 hours in 0.1M $LiNO_3$.
Surface Area: 403.27 μm^2

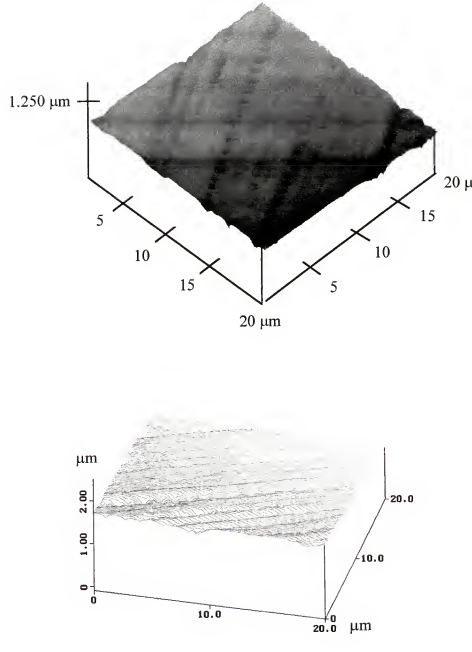

Figure 5-16. The surface of a 20/10/70 SLS glass sample corroded for 12 hours in 1.0M KCl.
Surface Area: 404.45 μm^2

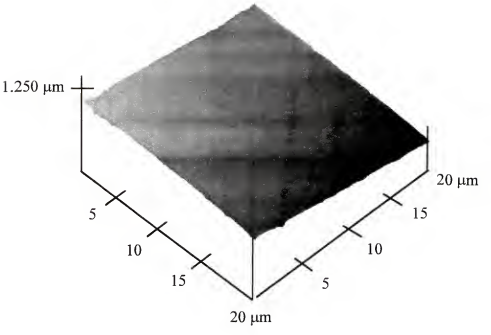

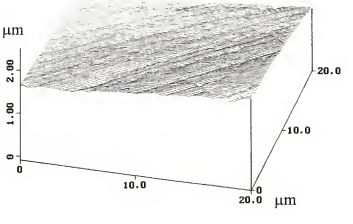

Figure 5-17. The surface of a 20/10/70 SLS glass sample corroded for 12 hours in 1.0M KNO_3.
Surface Area: 401.97 μm^2

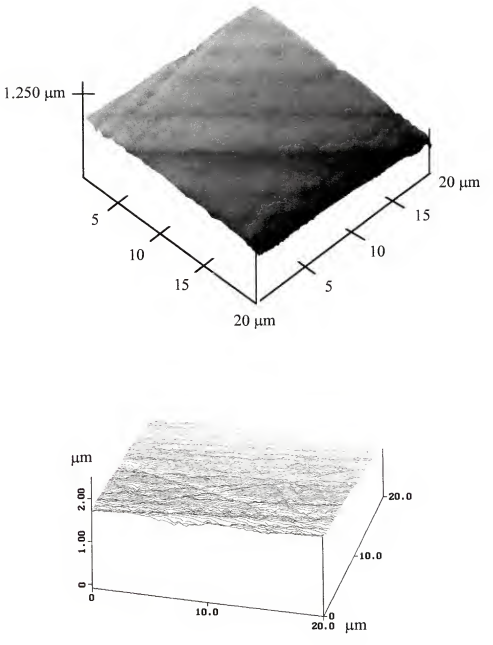

Figure 5-18. The surface of a 20/10/70 SLS glass sample corroded for 12 hours in 1.0M LiCl.
Surface Area: 403.16 μm^2

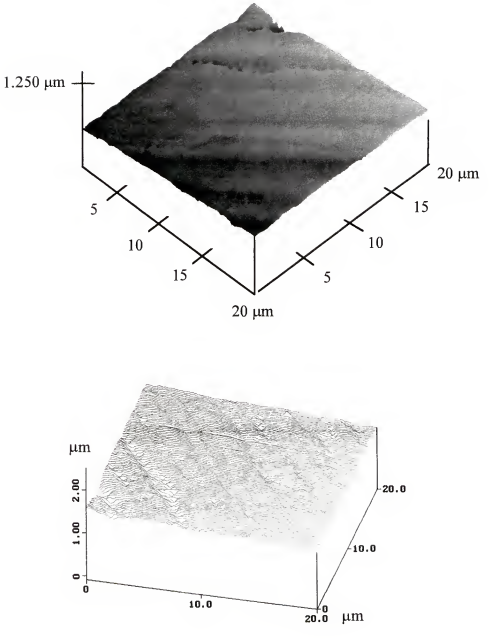

Figure 5-19. The surface of a 20/10/70 SLS glass sample corroded for 12 hours in 1.0M $LiNO_3$.
Surface Area: 402.36 μm^2

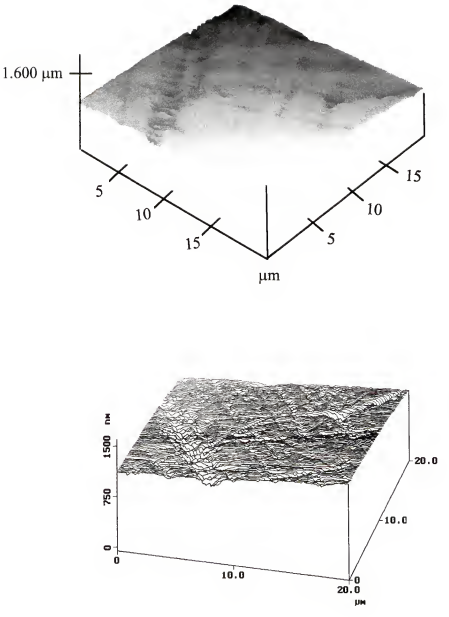

Figure 5-20. The surface of a 20/10/70 SLS glass sample corroded for 12 hours in deionized water. Surface Area: 404.19 μm^2

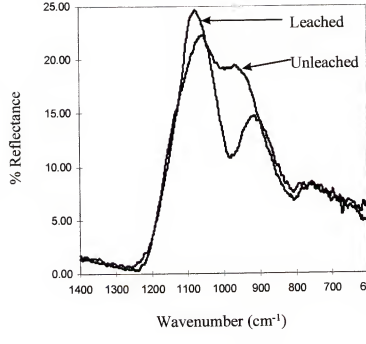

Figure 5-21. FT-IRRS spectrum of the unleached surface polished to 9.5 μm Al_2O_3 compared to the transformed spectrum of the same sample leached in 0.1M KCl for 12 hours.

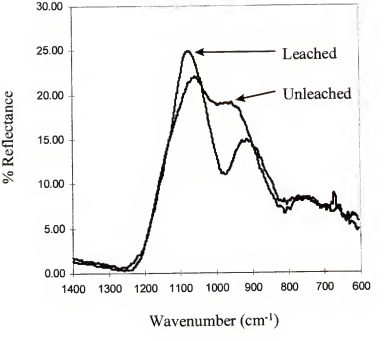

Figure 5-22. FT-IRRS spectrum of the unleached surface polished to 9.5 μm Al_2O_3 compared to the transformed spectrum of the same sample leached in 0.1M KNO_3 for 12 hours.

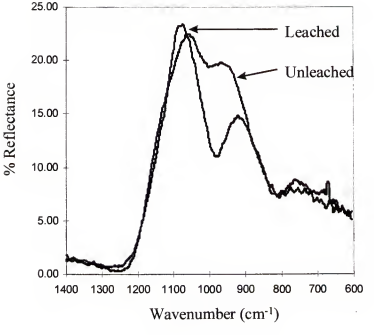

Figure 5-23. FT-IRRS spectrum of the unleached surface polished to 9.5 μm Al_2O_3 compared to the transformed spectrum of the same sample leached in 0.1M LiCl for 12 hours.

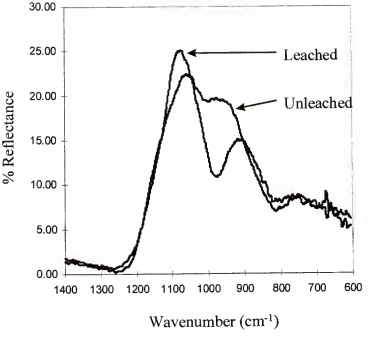

Figure 5-24. FT-IRRS spectrum of the unleached surface polished to 9.5 μm Al_2O_3 compared to the transformed spectrum of the same sample leached in 0.1M $LiNO_3$ for 12 hours.

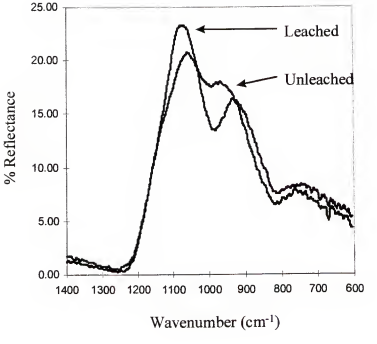

Figure 5-25. FT-IRRS spectrum of the unleached surface polished to 9.5 μm Al_2O_3 compared to the transformed spectrum of the same sample leached in 1.0M KCl for 12 hours.

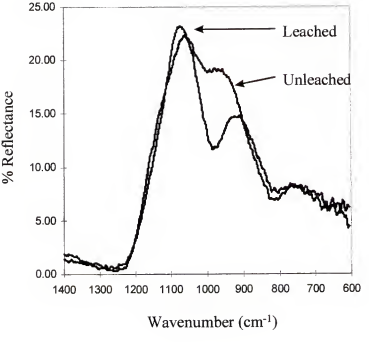

Figure 5-26. FT-IRRS spectrum of the unleached surface polished to 9.5 μm Al_2O_3 compared to the transformed spectrum of the same sample leached in 1.0M KNO_3 for 12 hours.

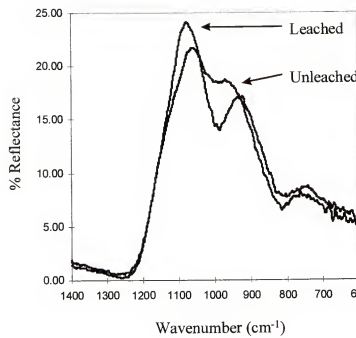

Figure 5-27. FT-IRRS spectrum of the unleached surface polished to 9.5 μm Al_2O_3 compared to the transformed spectrum of the same sample leached in 1.0M LiCl for 12 hours.

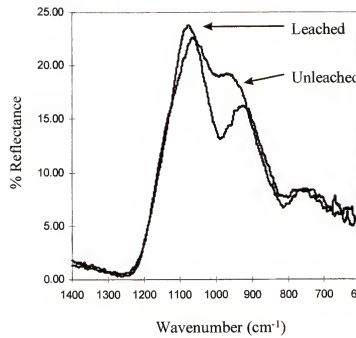

Figure 5-28. FT-IRRS spectrum of the unleached surface polished to 9.5 μm Al_2O_3 compared to the transformed spectrum of the same sample leached in 1.0M $LiNO_3$ for 12 hours.

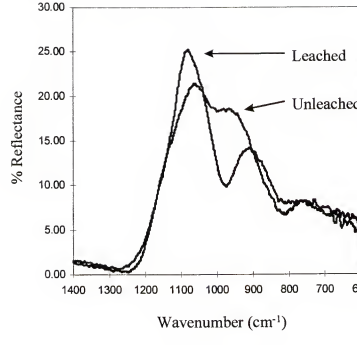

Figure 5-29. FT-IRRS spectrum of the unleached surface polished to 9.5 μm Al_2O_3 compared to the transformed spectrum of the same sample leached in deionized water for 12 hours.

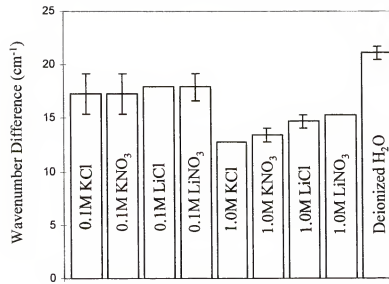

Figure 5-30. Peak position (PP2) differences between the leached glass and the unleached glass with 95% confidence bars superimposed. The error bars for 0.1M LiCl, 1.0M KCl and 1.0M $LiNO_3$ are too small to be seen on the graph.

relative concentration of Si-O-Si bonds increase in the surface. As apparent from Figure 5-30, there is a significant difference in $PP2_{12hr}$ - $PP2_{0hr}$ as a function of electrolyte concentration in solution. From this plot, it cannot be said that there is any significant differences in $PP2_{12hr}$ - $PP2_{0hr}$ as a function of electrolyte anion in solution. Although the data in Figure 5-30 do not show a significant difference in peak shift with respect to the type of cation, they do show a significant effect with respect to cation concentration. The specific cation effect(s) will be addressed later in this chapter. In any case, all of the electrolyte solutions exhibited a lower rate of corrosion as compared to the deionized water case. The exact mechanisms of the concentration effect and possible cation effect cannot be expressed from FT-IRRS analysis alone. However, FT-IRRS analysis may give much insight into the possible mechanisms. Recall the following reactions as described in Chapter 2:

$$\equiv SiO\text{-}M + H^+ = \equiv SiO\text{-}H + M^+ \qquad (2\text{-}1a)$$

$$\equiv SiOSi + H_2O = \equiv SiOH + HO\text{-}Si \qquad (2\text{-}2)$$

where M represents the alkali leaching out of the glass. Consider the case of silicate glass leaching in deionized water. SiOH groups are formed both through the ion exchange process as well as through the direct infiltration of water. As the samples are dried, or dehydrated, prior to FT-IRRS measurement, there exists a driving force for the reverse of the reaction represented by Equation 2-2. This would result in an increase in PH2 and a corresponding shift of PP2 to higher wavenumbers, as the relative concentration of Si-O-

Si would be increasing. Now, consider the case of silicate glass leaching in electrolyte solutions. The following ion exchange reaction must be considered:

$$\equiv SiO\text{-}M + M_s^+ = \equiv SiO\text{-}M_s + M^+ \qquad (5\text{-}1)$$

where M_s represents the electrolyte alkali in solution. As with proton exchange with glass alkali, there exists the opportunity for electrolyte alkali exchange as well. The result would be a decrease in SiOH within the surface of the glass. The consequence of this is that as the surface is dehydrated prior to FT-IRRS measurement, not as much Si-O-Si will be reformed, resulting in less of a shift in PP2. This is indeed what is observed, however, it would be careless to attribute this observation to the above mechanism without complementary characterization. It must be understood that another possibility for the observed behavior is simply that the driving force for proton exchange is reduced in concentrated electrolytes.

pH Analysis

As proton exchange with alkali within a glass occurs (Equation 2-1a), the concentration of H^+ in the leachant will decrease, resulting in an increase in pH. Table 5-1 shows the pH measurements of the various leachants after twelve hours of immersion. Measurement of pH is complicated in electrolyte solutions because both the liquid junction potential of the reference electrode and the hydrogen ion activity coefficient change as a function of electrolyte concentration [BAT81]. This complication was resolved by

defining a pH scale relative to a value assigned to a standard solution. The following procedure as well as Equation 5-2 was adapted from a similar technique employed by Pederson et al. [PED93], where they established a hydrogen ion concentration scale by titration. Electrolyte solutions were of 200 ml volume, and a similar volume of deionized water was titrated with 0.1M NaOH, recording the observed pH. The pH electrode was standardized against reference buffers at pH 7.00 and 10.00. The below relationship was used to correct the pH's measured in the electrolyte solutions:

$$pH = pH_e + Q \qquad (5\text{-}2)$$

where pH is the reported pH, pH_e is the measured pH of the electrolyte and Q is the correction term. Q is simply equal to the difference between the pH of the electrolyte and the corresponding pH of deionized water titrated with the same amount of NaOH. Approximately 1.0 ml of 0.1M NaOH was titrated into these solutions, resulting in an alteration of solution concentration of about 0.5%. Figure 5-31 shows plots of these calibration curves. Overall, there was no statistically significant differences in pH among the various leachant solutions. The only remarkable difference is in the pH after twelve hours of immersion in the 0.1M KCl solution. The pH of this solution was significantly lower than that of the rest. It is also interesting to note that the peak position difference of PP2 (Figure 5-30) of the sample immersed in the 0.1M KCl solution was significantly lower than the rest as well. Apparently, proton exchange was not occurring in this case on the same scale as the other cases. The pH prior to the leaching experiment of the deionized water was measured to be 6.20. It should be noted that the pH of pure water in

Table 5-1. pH after 12 hours of leaching in various solutions. (95% confidence limits are included)

Leachant Solution	pH after 12 hours of immersion
0.1M KCl	7.41 +/- 0.001
0.1M KNO_3	7.40 +/- 0.035
0.1M LiCl	7.64 +/- 0.177
0.1M $LiNO_3$	7.76 +/- 0.177
1.0M KCl	6.96 +/- 0.106
1.0M KNO_3	7.57 +/- 0.106
1.0M LiCl	7.64 +/- 0.141
1.0M $LiNO_3$	7.51 +/- 0.106
D.I. Water	7.73 +/- 0.247

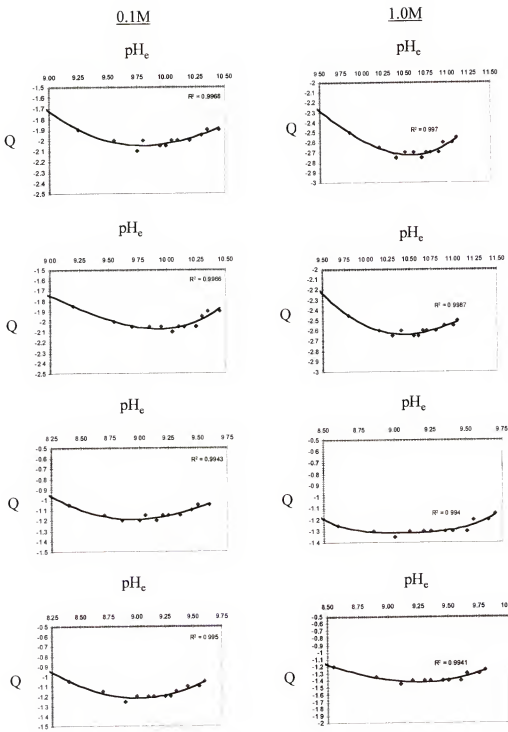

Figure 5-31. pH correction curves for the various electrolyte solutions.

equilibrium with atmospheric CO_2 at 25°C may be calculated to be pH 5.66 [BUT98]. Since the deionized water was measured to have pH 6.20, due to how the electrolyte solutions' pH were corrected for, their pH was assumed to be the same as deionized water prior to leaching. This assumption has its deficiencies, as the ionic strength of solutions may alter the solubility products of the dissolved species, namely CO_2. This is by no means trivial to model, but it should at least be mentioned. The pH's measured in the solutions of this study should be looked at with a cautious eye. Elemental analysis of the leachant solution will determine whether or not a similar amount of alkali is leaching out of the glass immersed in 1.0M KCl as compared to the other cases.

Solution Analysis

The concentrations of various elements present in the solution after twelve hours of leaching were measured with inductively coupled plasma atomic emission spectrometry (ICP-AE). In regards to ICP, the solution is introduced into a spray chamber with the assistance of a nebulizer. A high temperature plasma dissociates the nebulized droplets into individual atoms and ions. They are excited to emit light at wavelengths characteristic of the element, which is then analyzed by the spectrometer. With careful calibration, spectral intensities may be quantified into elemental concentrations. The instrument used in this experiment was a Perkin-Elmer Optima 3200 ICP. Figure 5-32 through figure 5-34 show plots of the normalized mass loss into the various solutions for Na, Ca and Si, respectively. Raw data is obtained in the form of parts per million (ppm), which is

equivalent to milligrams per liter. The following equation is used to convert this raw data into normalized mass loss:

$$(C / f) \times (V / SA) = g / m^2 \qquad (5\text{-}2)$$

where C is the ppm of element in solution (g/m^3), f is the fraction of element present in the uncorroded glass, V is the volume of the solution (m^3) and SA is the surface area of the glass (m^2). The MCC recommends reporting such data in terms of normalized mass loss because it may be used to compare rates of corrosion between glasses of different composition and may also give an indication of the mechanism of corrosion.

Referring to figure 5-32, Na release appears to be similar in all solutions with the exception of the 1.0M KCl solution. The 20/10/70 SLS glasses immersed in 1.0M KCl appear to exhibit approximately twice the Na release as compared with all other solutions. Keeping in mind that the lowest pH and lowest PP2 shift were observed in the 1.0M KCl case, there must be a significant amount of ion exchange between the Na in the glass and the K in the solution. In regards to Ca release (figure 5-33) there appears to be no remarkable trends as a function of solution chemistry. Figure 5-34 shows the Si release as a function of solution chemistry. The results here are interesting. According to this data, the concentration of electrolyte solution does not affect significantly the release of Si into solution, nor does the anion (Cl^-, NO_3^-). However, electrolyte cation appears to have a significant effect on Si release. The electrolyte solutions containing Li appear to result in an increase in the normalized mass loss of Si from the glass. It is believed that under

neutral and alkaline conditions, Si is released into solution as a result of the following network dissolution reaction which was described in Chapter 2[EBE94]:

$$\equiv SiO\text{-}Si(OH)_3 + OH^- = \equiv SiO^- + H_4SiO_4\ (aq) \qquad (2\text{-}3)$$

According to this reaction, the higher the pH of the solution, the greater the driving force to form H_4SiO_4 (aq). This may indicate that the pH's of solutions containing the Li cation were higher than those containing the K cation. This would point to greater proton exchange in electrolyte solutions containing Li^+ as compared to those containing K^+. However, statistically there was no significant differences in pH between all solutions (with exception of the 1.0M KCl case). Therefore, pH may not explain the normalized mass loss behavior of Si in these solutions. This is assuming, of course, that the pH values measured are valid. Another thought is that an increase in terminal $-Si(OH)_3$ groups could result in an increase in driving force to form H_4SiO_4 (aq). If this is the case, then, according to Figure 5-34, electrolyte solutions containing the Li cation resulted in glass surfaces containing more terminal $-Si(OH)_3$ groups. This is a less obvious cause, and may therefore be quite a stretch in reasoning. Elemental depth profiling into the surface of these glasses may provide more insight into the effects of these electrolytes on the corrosion mechanisms.

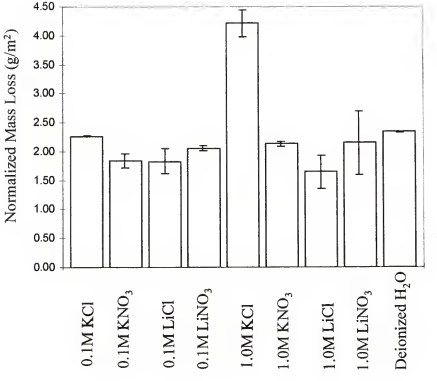

Figure 5-32. Normalized mass loss of Na after 12 hours of immersion in various solutions.

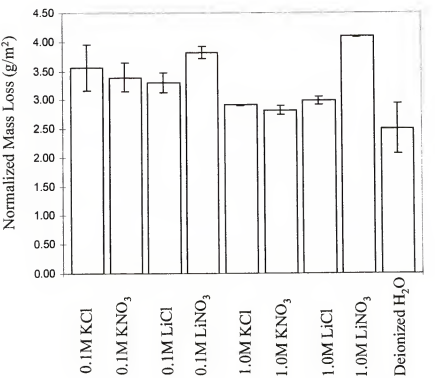

Figure 5-33. Normalized mass loss of Ca after 12 hours of immersion in various solutions.

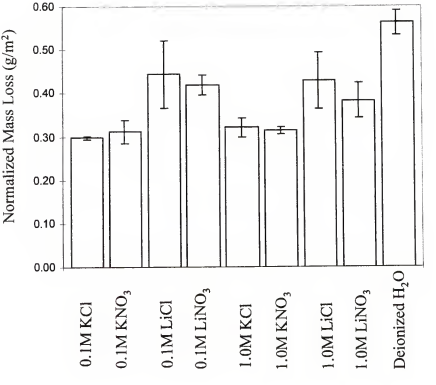

Figure 5-34. Normalized mass loss of Si after 12 hours of immersion in various solutions.

Depth Profiling

Secondary ion mass spectrometry (SIMS) was used in order to obtain elemental depth profiling into the surfaces of the glass samples which were immersed in the various aqueous solutions. SIMS is based upon the bombardment (or sputtering) of the sample surface by energetic primary ions, and the subsequent mass analysis of the ionized sputter products [CLA92]. For this study, the SIMS depth profiles were obtained with a 6 KeV oxygen primary ion beam with a raster size of 100 μm. The elements monitored for were lithium, oxygen, sodium, silicon, potassium, calcium and hydrogen. Figure 5-35 through Figure 5-43 represent SIMS depth profiles plotted as intensity (counts/second) versus sputter time (seconds). Normally the crater depth formed via the sputtering process is measured and sputter time may therefore be correlated to a depth measurement. For this study, however, the crater depth was not measurable, therefore only sputter time is presented. The sputtering times to depth correlation should not deviate significantly from sample to sample, so a qualitative assessment comparing samples should be permissible. In addition, standards were not used to correlate intensity to a concentration of species. In order to compare impurity levels between samples, their signal intensities were ratio'ed to a constant matrix ion intensity, in this case silicon. This is a standard procedure, as in SIMS, impurities or dopants are strongly matrix dependent, in that the same impurity in different matrices will have different apparent yields. The ratio'ing of impurity intensity to that of silicon should provide a good basis for qualitative comparison and should be sufficient for the purposes of this study. Therefore, in Figure 5-35 through 5-43, the top

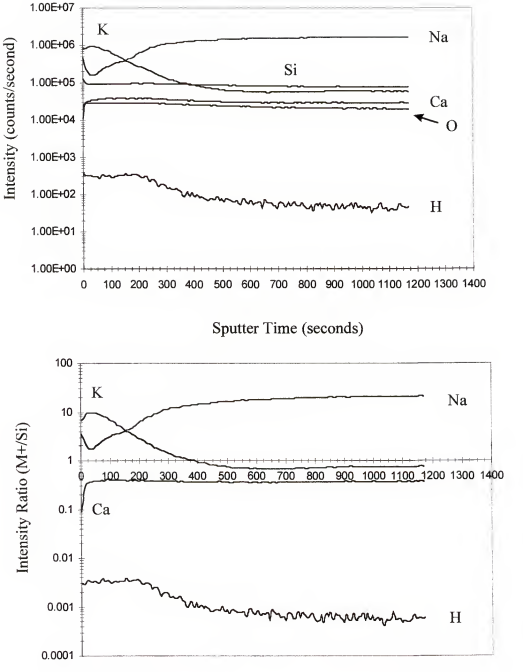

Figure 5-35. SIMS depth profiling of a 20/10/70 SLS glass sample immersed in 0.1M KCl for 12 hours

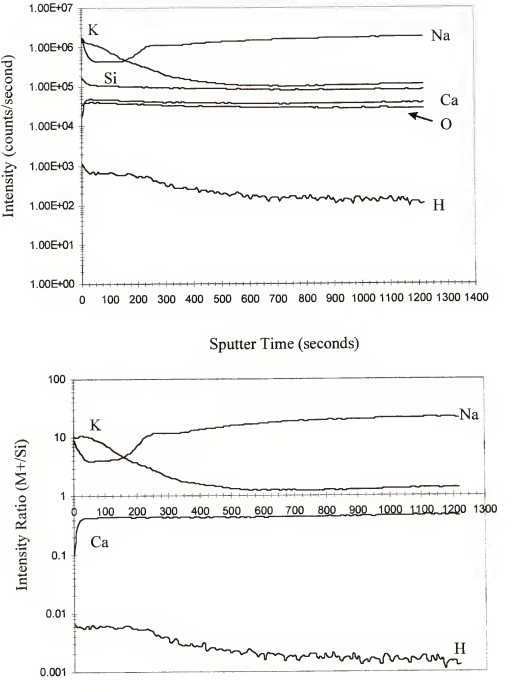

Figure 5-36. SIMS depth profiling of a 20/10/70 SLS glass sample immersed in 0.1M KNO_3 for 12 hours

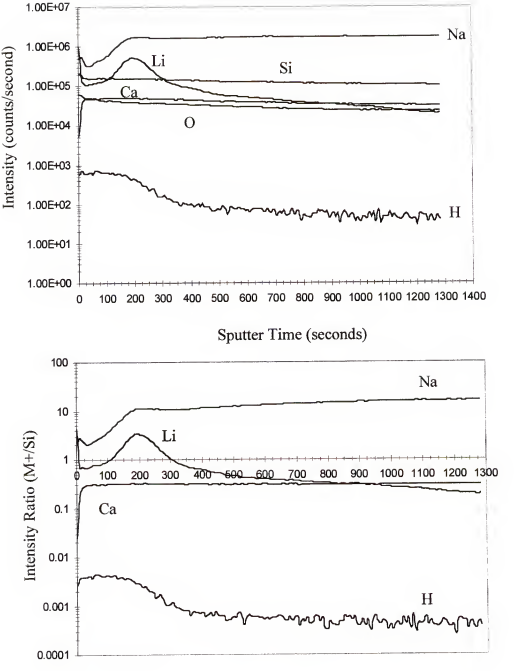

Figure 5-37. SIMS depth profiling of a 20/10/70 SLS glass sample immersed in 0.1M LiCl for 12 hours

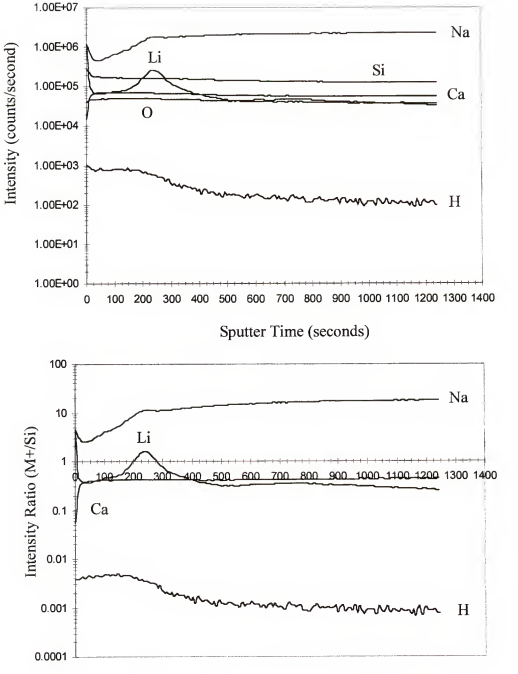

Figure 5-38. SIMS depth profiling of a 20/10/70 SLS glass sample immersed in 0.1M $LiNO_3$ for 12 hours

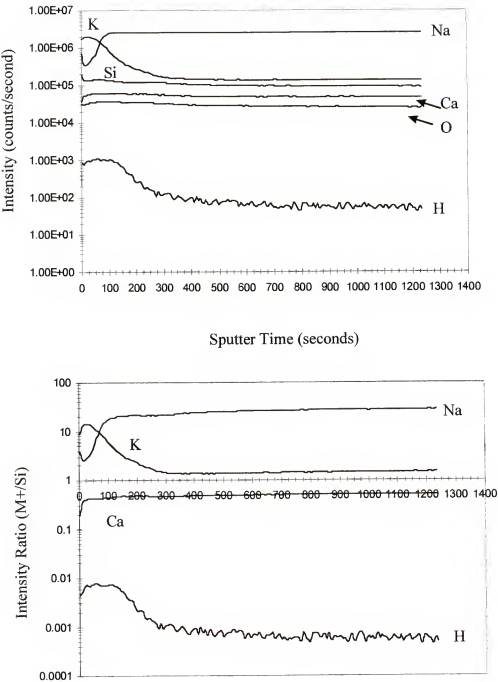

Figure 5-39. SIMS depth profiling of a 20/10/70 SLS glass sample immersed in 1.0M KCl for 12 hours

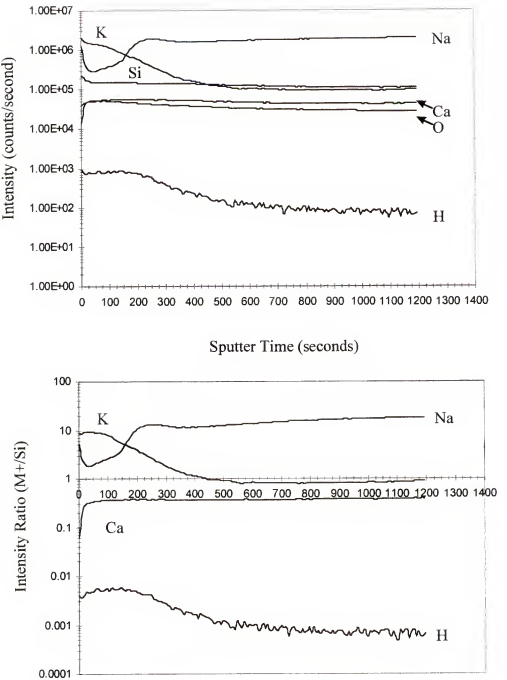

Figure 5-40. SIMS depth profiling of a 20/10/70 SLS glass sample immersed in 1.0M KNO_3 for 12 hours

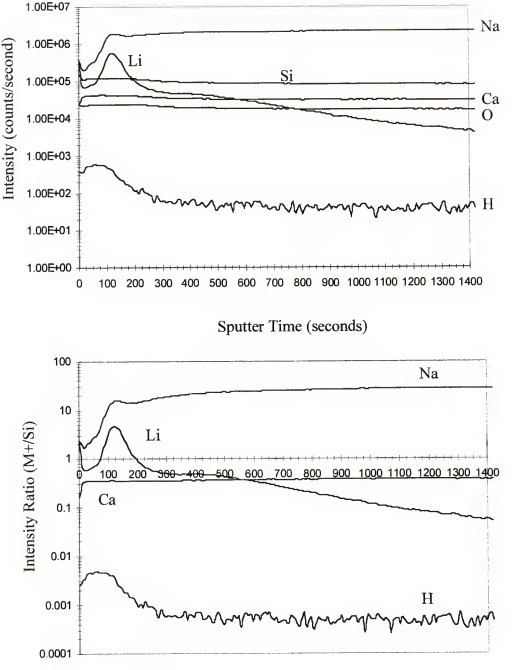

Figure 5-41. SIMS depth profiling of a 20/10/70 SLS glass sample immersed in 1.0M LiCl for 12 hours

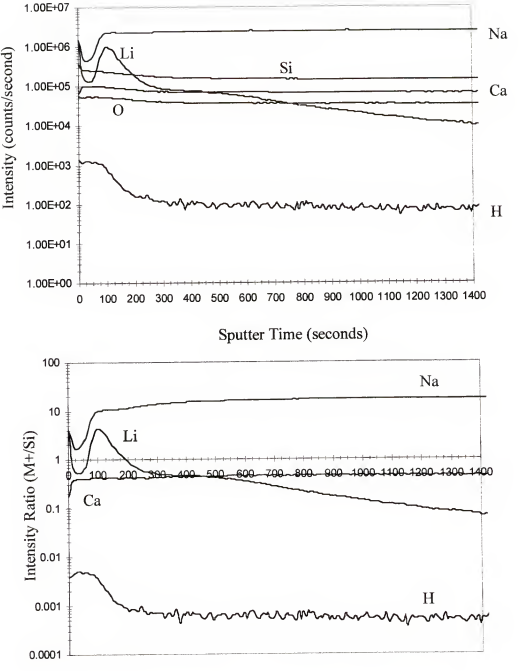

Figure 5-42. SIMS depth profiling of a 20/10/70 SLS glass sample immersed in 1.0M $LiNO_3$ for 12 hours

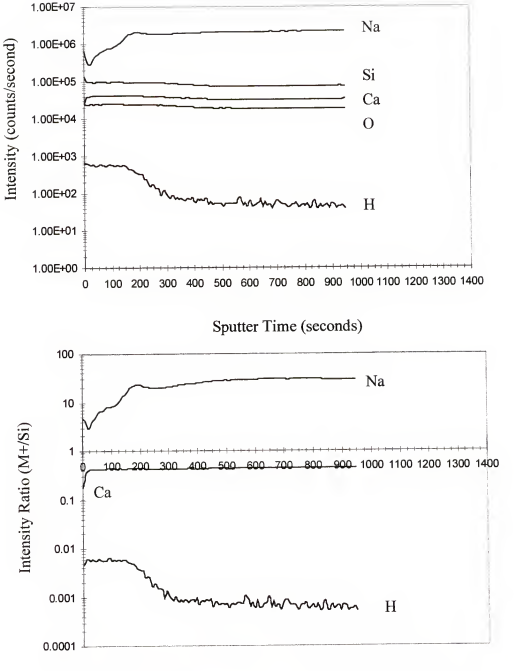

Figure 5-43. SIMS depth profiling of a 20/10/70 SLS glass sample immersed in deionized water for 12 hours

plot is a plot of the raw SIMS data, and the bottom plot is a plot of the ratio of impurity intensity to that of the matrix (silicon). Referring to these figures, it is apparent that cations from the electrolyte solutions are present in the surfaces of these samples. The mechanism by which these electrolyte cations diffuse into the surface is most likely through an ion exchange process with Ca, and more likely, Na. It should be noted that unlike the potassium profiles, the lithium profiles show the appearance of a "hump" at some distance into the sample. It is unlikely that the lithium ions are accumulating at this depth. A more likely reason for this phenomenon is due to the migration of lithium due to surface charging effects from the SIMS measurement technique itself. In general, it is observed that electrolyte concentration affects the depth of corrosion (depletion of Na and penetration of H, or electrolyte cation). The depths of corrosion in the 0.1M solutions are nearly twice that of the 1.0M solutions. This is in agreement with the FT-IRRS analysis as presented in Figure 5-30. The FT-IRRS analysis shows that the peak position difference of PP2 between the unleached and leached conditions are significantly more pronounced in the 0.1M solutions. This would indicate a greater relative concentration of Si-O-Si bonds in the surface of these samples, which may be correlated to an increased depth of corrosion of these samples. Also, the SIMS analysis shows no signficant differences among similar concentrations of electrolytes as far as depth of corrosion. This too, is in agreement with the FT-IRRS analysis.

Discussion

The study in this chapter employed the quantitative techniques developed in Chapter 4 for the analysis of FT-IRRS spectra in evaluating the effects of solution chemistry on glass corrosion. Complementary characterization techniques were used to either verify or oppose the determinations of the FT-IRRS analysis. All of the spectra of the rough, corroded samples were transformed using Equation 1 into that of "smooth" corroded samples, so that a direct comparison of structural and compositional changes could be made. The results of the FT-IRRS analysis showed that there was a significant effect of electrolyte concentration on aqueous glass corrosion. Samples immersed in 1.0M electrolytes exhibited a lower Si-O-Si peak shift as compared to those immersed in 0.1M electrolytes. These results indicated that proton exchange was not as pronounced in the 1.0M electrolytes. This could be due to either, (1) electrolyte cation exchange taking the place of proton exchange, (2) a reduction in the potential for proton exchange, or, (3) some combination of the above.

ICP analysis showed that the same amount of sodium ions were leaching out of the glass in all cases, except for that of the 1.0M KCl test condition. With the 1.0M KCl test condition, nearly twice as much sodium was leaching out as compared to the other test conditions. The FT-IRRS data of Figure 5-30 showed that the 1.0M KCl test condition resulted in a significantly lower peak shift as compared to the other test conditions. The FT-IRRS data by itself would indicate that corrosion was suppressed in the 1.0M KCl case. The only way that this FT-IRRS data would support the ICP data was if a significant amount of potassium exchange was occuring (instead of proton exchange

which would cause the formation of Si-OH groups). Looking at the intensity ratios of the SIMS plots, Figure 5-39 shows a K/Si ratio of approximately 13, as compared to 10 for all other cases in which the samples were immersed in concentrated electrolytes containing the potassium ion. Qualitatively, the SIMS analysis shows that there was indeed a greater amount of potassium diffusing (exchanging) into the glass surface. This gives credence to the otherwise contradictory ICP and FT-IRRS results.

SIMS analysis also showed that there was a significant effect of electrolyte concentration on the depth of corrosion in these samples. Samples immersed in 0.1M electrolytes resulted in a leached layer depth about twice that of the 1.0M electrolytes. The FT-IRRS data of Figure 5-30 showed the same trend; the more concentrated electrolytes resulted in a decreased Si-O-Si peak shift. Recall, that this observation could mean either (1) electrolyte cation exchange was taking the place of proton exchange, (2) a reduction in the potential for proton exchange altogether, or, (3) some combination of the above. Coupled with the SIMS analysis results of the dependence of leached layer depth on the concentration of electrolytes in the leaching solution, it appears that there is some combination of cation exchange and the reduction in potential for exchange itself. The reduction in leached layer depth in more concentrated electrolytes points to a mechanism of reduced ion exchange. The presence of electrolytes is known to decrease the electrical charge on an oxide surface immersed in water [HEA77]. A decrease of the negative surface potential of the glass surface through an increase in electrolyte concentration could lower the near surface concentration of hydrogen ions, decreasing the rate of proton exchange. Since electrolyte cations were also observed to have taken part in ion exchange, this would even further lower the rate of proton exchange in electrolyte

solutions. The ion-exchanged electrolyte cations could even serve as a diffusion barrier to further exchange. It needs to be noted that the ICP analysis showed similar amounts of sodium leaching out of the glass regardless of concentration. This appears to be somewhat of a contradiction to the varying leach depths as measured by SIMS, as a greater leach depth should correlate to more sodium in solution. In the SIMS plots, it was assumed that the glasses were ion-milled at the same rate, allowing a comparison and correlation of sputtering times to leaching depth under the various test conditions. The fact that the correlation of electrolyte concentration on leaching depth existed as well as the fact that identical sputtering parameters were used for every glass seems to bolster the validity of that assumption. Zeta potential measurements of these glasses immersed in the various electrolytes would help to confirm this proposed mechanism.

CHAPTER 6
SUMMARY AND CONCLUSIONS

The mechanisms and kinetics of the aqueous corrosion of glass have been studied for the past several decades. There exists two generally accepted mechanisms of the interaction of water with a glass surface. The first is an ion exchange process, whereby alkali ions from the glass are exchanged for proton or hydronium ions in the solution. The second mechanism relates to the attack of the structural bonds in the glass by hydroxyl ions in the solution, resulting in network dissolution. This study was focused on the former mechanism. Many factors may affect the rate of aqueous corrosion. These include temperature effects, glass composition effects, pH effects, flow rate and the surface area of the glass exposed to a volume of solution. One important factor which is not well understood is the effect of solution chemistry on the rate of aqueous corrosion of glass. Much work has been done in both the monitoring and modeling of glass corrosion as a function of solution chemistry. A number of mechanisms have been proposed, of varying scope, into the last decade, but still, the mechanism(s) is still not well understood.

One of the problems associated with characterizing the aqueous corrosion of glasses is that a surface analytical technique is required. Many of the widely used surface analytical techniques employ the use of energetic particles which must bombard and interact with the surface of the sample. The non-network cations in the glass surface may

be significantly affected by the surface charging developed by such techniques, leading to results which are in question. One surface analytical technique which avoids this problem altogether is Fourier transform infrared reflection spectroscopy (FT-IRRS). FT-IRRS has been used quite extensively over the past three decades in characterizing glass surface modification. FT-IRRS offers many advantages over other surface analytical techniques in that it is rapid, it requires little or no sample preparation, it does not require a vacuum, it avoids the issue of surface charging of the sample, it is a non-destructive technique, and it is inexpensive. There is, however, some question as to the quality of data that FT-IRRS may provide. It has been shown by many authors that aqueous glass corrosion results in the simultaneous roughening of the glass surface, and this roughening may strongly effect spectral features, causing interpretation of the resultant spectra to be difficult. Consequently FT-IRRS has been used by many as a complementary qualitative analysis tool, rather than a primary analysis tool. The advantages that FT-IRRS provides over other surface analytical techniques would make it a powerful primary analytical tool if the resultant spectra could be analyzed with confidence.

The objectives of this research were the following: (1) obtain statistical data from glass surfaces using Fourier transform infrared reflection spectroscopy (FT-IRRS), (2) to develop a quantitative model of the effects of surface roughness on infrared reflection, (3) to apply this quantitative technique to evaluate the effects of solution electrolyte chemistry on glass corrosion, (4) to verify the validity of this quantitative data with complementary characterization techniques, and, (5) to evaluate the general mechanisms of corrosion when a glass is immersed in solutions of varying electrolytes and ionic strength.

Statistical Analysis of FT-IRRS Data

In Chapter 4 a comprehensive statistical analysis of FT-IRRS spectral features was carried out. The purpose of this study was to identify certain spectral features which were not significantly affected by day-to-day variation and surface roughening, given a constant composition. If such spectral features exist, they may then be used to confidently characterize a sample's surface, as any changes to that spectral feature may be directly attributed to structural and compositional changes. It was found in this study that the peak position of the Si-O-Si stretching vibration (~1055 cm^{-1}) was unaffected by both day-to-day variation and by surface roughening equivalent to that of a 12 hour aqueous corrosion experiment. With knowledge of the types of hydrolytic reactions which take place at the glass surface during corrosion, frequency shifts in this peak alone could be used to describe the probable mechanisms of corrosion.

A more quantitative evaluation of the effects of surface roughness on FT-IRRS spectral features was also performed. Equation 4-1 was used to transform an FT-IRRS spectrum taken from a "perfectly smooth" sample into those of increasing surface roughness. An iterative technique to curve fit calculated spectra to measured spectra of samples of varying levels of polish was used to interpolate the rms roughness (σ) of the glass surfaces at those varying levels of polish. The calculated spectra fit well with the measured spectra over the entire range of wavelengths, which supports the inherent validity of Equation 4-1. This provides much insight into the interpretation of FT-IRRS spectra of glass samples which have undergone extensive corrosion. Extensive corrosion would result in extensive surface roughening. An FT-IRRS spectrum of this sample

would result in what only could be described as an "ill-defined" spectrum. The results of the surface roughness study described in Chapter 4 quantifies this behavior. Therefore, if correlation curves could be generated relating calculated σ values to some real measured quantity, such as surface area of the corroded region, Equation 4-1 could be applied in order to transform the spectrum of the "rough" glass sample into one of a "perfectly smooth" sample. The consequence of this is the ability for direct comparison of spectral features in terms of only composition and structure.

Quantitative FT-IRRS Analysis of the Effects of Solution Chemistry on Glass Corrosion

The study in Chapter 5 employed the quantitative techniques developed in Chapter 4 in analyzing the effects of solution chemistry on glass corrosion, using FT-IRRS as the primary characterization technique. The surface areas of samples of varying level of polish were measured with AFM. These surface area values were related to the interpolated σ values which resulted from the curve fitting of Equation 4-1 to the corresponding measured spectra. Hence, a well correlated surface area versus σ plot was obtained. The surface areas of the rough, corroded samples were also measured with AFM. With the previous surface area versus σ relation obtained, σ values could be estimated for the corroded samples. The σ values for each of the corroded samples was entered into Equation 4-1 in order to transform the spectra of those "rough," corroded samples into that of "smooth," corroded samples. This allowed for a direct comparison of structural and compositional changes between the unleached and leached spectra.

The results of this analysis showed that there was a significant effect of electrolyte concentration on aqueous glass corrosion. Samples immersed in 1.0M electrolytes exhibited a lower Si-O-Si peak shift as compared to those immersed in 0.1M electrolytes. These results indicated that proton exchange was decreased in the 1.0M electrolytes. The possible reasons for this decrease in proton exchange could be due to either, (1) electrolyte cation exchange taking the place of proton exchange, (2) some reduction in the potential for proton exchange, or, (3) some combination of the above. Complementary characterization techniques were used in order to elaborate on the possible mechanisms, and to verify whether or not the results of the FT-IRRS analysis are indeed valid.

Verification of the Validity of the FT-IRRS Data

ICP analysis showed that the same amount of sodium ions were leaching out of the glass under all test conditions, with the exception of the 1.0M KCl condition. The 1.0M KCl test condition resulted in nearly twice as much sodium leaching out as compared to the other test conditions. The FT-IRRS data (Figure 5-30) showed a similar anomaly in that the 1.0M KCl test condition resulted in a significantly lower peak shift as compared to the other test conditions, even at the same concentration. The FT-IRRS data by itself would indicate that corrosion was suppressed in the 1.0M KCl case. A possible mechanism by which the 1.0M KCl case would result in both, a minimum Si-O-Si peak shift and a maximum sodium release is if there is a substantial amount of potassium exchange occurring in place of proton exchange. Upon analysis of the SIMS depth profiles, it was observed that the K/Si ratio in the 1.0M KCl case was approximately 30%

higher than in all other cases in which the samples were immersed in concentrated electrolytes containing potassium. Qualitatively, the SIMS analysis shows that there was indeed a greater amount of potassium diffusing (ion exchanging) into the glass surface. This gives credence to the otherwise contradictory ICP and FT-IRRS results.

The SIMS analysis also pointed to a significant effect of electrolyte concentration on the depth of corrosion in these samples. According to the analysis, samples immersed in 0.1M electrolytes resulted in a leached layer depth of about twice that the 1.0M electrolytes. The FT-IRRS data showed the same trend. The 1.0M electrolytes resulted in a smaller Si-O-Si peak shift. Both the ICP and SIMS support the data obtained by FT-IRRS.

Mechanisms of Glass Corrosion in Concentrated Electrolyte Solutions

The FT-IRRS data alone showed a significant difference in Si-O-Si peak shift between the 0.1M electrolytes and the 1.0M electrolytes. The observed peak shifts were only dependent on concentration. Electrolyte anions and electrolyte cations appeared to have no significant effect on these peak shifts. Knowing that the dehydration reaction:

$$\text{Si-OH} + \text{HO-Si} = \text{H}_2\text{O} + \text{Si-O-Si} \qquad (6\text{-}1)$$

has been attributed to the increase in reflection of the Si-O-Si peak, and that with these short-term leaching tests, proton exchange is the dominant mechanism for Si-OH formation, it may be said that proton exchange is reduced in glasses exposed to

electrolytes of higher concentration. The following ion exchange reaction was introduced in Chapter 5:

$$\equiv SiO\text{-}M + M_s^+ = \equiv SiO\text{-}M_s + M^+ \qquad (5\text{-}1)$$

where M_s represents the electrolyte alkali in solution. If sufficient M_s^+ exchange is occurring instead of proton exchange, it could lead to the observed result, as obtained by FT-IRRS. However, if no M_s^+ exchange had occurred in the glass samples, the mechanism of reduced proton exchange would have to be different. It would likely be related to a decrease in negative surface potential of the glass surface, resulting in the lowering of the near surface concentration of hydrogen ions. This would require extensive zeta potential analysis to confirm. If M_s^+ exchange could be confirmed, it would support the mechanism of reduced proton exchange through the substitution of M_s^+. SIMS analysis indeed shows the presence of electrolyte alkali diffused into the surface of the glass. The depth of this diffusion is similar to the depth of sodium depletion, indicating an ion exchange process with sodium. If the concentrated electrolyte alkali are exchanging with sodium from the glass, it would reduce the relative amount of protons exchanging with sodium, and those electrolyte alkali could serve as a diffusion barrier to further exchange.

The conclusions of this research are outlined in Table 6-1 for clarification.

Table 6-1. Conclusions of this study.

1. The Si-O-Si peak position in a soda-lime-silicate glass is not significantly affected by day-to-day variation or surface roughnesses coarser than an equivalent 320 grit SiC polish, and may be used to confidently evaluate aqueous corrosion kinetics if the corrosion process does not roughen the surface beyond the equivalent of a 320 grit SiC polish.

2. The equation, $R_s = R_o \exp[-(4\pi\sigma/\lambda)^2]$, describes spectral intensity shifts well, as a function of surface roughness, and may be used to transform spectra from rough samples so that a more confident comparison may be made to uncorroded smooth spectra.

3. FT-IRRS may be used confidently as a primary surface characterization tool, when the appropriate statistical analysis of spectral features is employed, and the effects of surface roughness (as a function of wavelength) are understood.

4. Ion exchange occurs between glass alkali and electrolyte cations, which reduces the proclivity for proton exchange, and results in less Si-OH groups which are formed in the short-term leach test.

Future Work

There is still much which may be studied as a result of this research. It would be interesting to further develop the scattering equation (Equation 4-1), as applied to FT-IRRS spectra, so that it may yield accurate quantitative measurements of rms roughness. This could result in the ability to use FT-IRRS to not only characterize the structure and composition of surfaces, but also the morphology (roughness). It would also be interesting to do extensive zeta potential measurements soda-lime-silica glass in the different electrolyte solutions studied in this research. It would be beneficial to see if any changes in surface potential correlated with what was observed in this study. A long-term leach test may be informative as well. It would be interesting to see if a long-term leach test in the varying electrolyte solutions would result in the same, or different, steady-state conditions, in terms of leached layer depth. The kinetics have been demonstrated to be dependent at least on electrolyte composition. Whether or not this applies to the long-term is unknown.

REFERENCES

ADV98 Advocat, T., J.L. Chouchan, J.L. Crovisier, C. Guy, V. Daux, C. Jegou, S. Gin and E. Vernaz, Materials Research Society Symposia Proceedings, Vol. 506, pp. 63-70, (1998).

AHM97 Ahmed, A.A. and I.M. Youssof, Glass Science and Technology, Vol. 70, No. 3, pp. 76-85 March (1997).

ASM86 ASM Handbook, Volume 10, Materials Characterization, pp. 109-125 (1986).

BAT81 Bates, R.G., Critical reviews in analytical chemistry, Vol. 10, No. 3 CRC Press, Boca Raton, FL, p. 247 (1981).

BEC63 Beckmann, P. And A. Spizzichino, The Scattering of Electromagnetic Waves from Rough Surfaces, Pergamon Press, New York (1963).

BOS57 Bostock, J. And Riley, H.T. (translation), "The Natural History of Pliny," 6, 379, Henry G. Bohn, London (1857).

BOU94 Bourcier, William L., Materials Research Society Symposia Proceedings, Vol. 333, pp. 69-82, (1994).

BUT98 Butler, J.N. and D.R. Cogley, Ionic Equilibrium: Solubility and pH Calculations, John Wiley & Sons, Inc., New York (1998).

CLA77 Clark, D.E., E.C. Etheridge, M.F. Dilmore and L.L. Hench, Glass Technology, Volume 18, No. 4, August (1977).

CLA92 Clark, David E. and Bruce K. Zoitos, in Corrosion of Glass, Ceramics and Ceramic Superconductors: Principles, Testing, Characterization and Applications, edited by D.E. Clark and B.K. Zoitos (Noyes Publications, Park Ridge, NJ, 1992) pp. 51-97; W. White, ibid., pp. 2-28; B. Grambow, ibid., pp. 124-148; C.M. Jantzen, ibid., pp. 153-216; G.G. Wicks, ibid., pp. 218-260 (1992).

CLA94 Clark, D.E., R.L. Shulz, G.G. Wicks and A.R. Lodding, Materials Research Society Symposia Proceedings, Vol. 333, pp. 107-122, (1994).

CON66 Connes, J. and P. Connes, Journal of the Optical Society of America, Volume 56, p. 896 (1966).

DOR73 Doremus, R.H., Glass Science, John Wiley & Sons, Inc. (1973).

DOV90 Dove, P.M. and D.A. Crerar, Geochimica et Cosmochimica Acta, Vol. 54, pp. 955-969 (1990).

DUN87 Dunken, H. and R.H. Doremus, Journal of Non-Crystalline Solids, 92, 61-72 (1987).

EBE94 Ebert, W.L. and J.J. Mazer, Materials Research Society Symposia Proceedings, Vol. 333, pp. 27-35, (1994).

EIS67 Eisenman, G., Glass Electrodes for Hydrogen and Other Cations, Marcel Dekker, Inc. (1967).

ELS72 El-Shamy, T.M. and R.W. Douglas, Glass Technology, Vol. 13, pp. 77-80, (1972).

ELS72a El-Shamy, T.M., J. Lewins and R.W. Douglas, Glass Technology, Vol. 13, pp. 81-87, (1972).

FAR30 Faraday, M., Trans. Roy. Soc., London, part 1, 1 (1830).

FEL58 Felgett, P., J. Phys. Radium, Volume 19, p. 187 (1958).

FEN94 Feng, X. and I.L. Pegg, Physics and Chemistry of Glasses, Volume 35, No. 2, pp. 98-103, April (1994).

FER78 Ferraro, J.R. and L.J. Basile, Fourier Transform Infrared Spectroscopy: Applications to Chemical Systems, Volume 1, Academic Press (1978).

GRA85 Grambow, B., Materials Research Society Symposia Proceedings, Vol. 44, pp. 15-27, (1985).

HEA77 Healy, T.W., D.E. Yates, L.R. White and D. Chan, Journal of Electroanalytical Chemistry, 80, 57 (1977).

HUN71 Hunter, R.J. and H.J.L. Wright, Journal of Colloid Interface Science, 37, 564 (1971).

HUS90 Husung, R.D. and R.H. Doremus, Journal of Materials Research, Volume 5, No. 10, October (1990).

JAC60 Jacquinot, P., Rep. Prog. Phys., Volume 23, p. 267 (1960).

JAN83 Jantzen, C.M. and M.J. Plodinec, Journal of Non-Crystalline Solids, Vol. 67, No. 1-3, pp. 207-223, (Sep. 1983).

KIN76 Kingery, W.D., H.K. Bowen and D.R. Uhlmann, Introduction to Ceramics, A Wiley-Interscience Publication, pp. 91-124, (1976).

KIS08 Kisa, A., Das Glas im Alterthum, 1, Leipzig (1908).

LEE86 Lee, C, "Surface and solution chemistry of glass/water interactions," A Dissertation Presented to the Graduate School of the University of Florida, Gainesville, FL (1986).

MAR69 Marinksky, J.A., Ion Exchange, Volume 2, Marcel Dekker, Inc. (1969).

MAR80 Marshall, W.L., Geochimica et Cosmochimica Acta, Vol. 44, pp. 907-913 (1980).

MAR80a Marshall, W.L., Geochimica et Cosmochimica Acta, Vol. 44, pp. 915-924 (1980).

MAR80b Marshall, W.L., Geochimica et Cosmochimica Acta, Vol. 44, pp. 925-931 (1980).

MEN83 Mendel, J.E., Nuclear Waste Materials Handbook: Test Methods, MCC-1P Static Leach Test Method, Pacific Northwest Laboratory, Richland, WA, DOE DE-AC06-76RLO 1830 (1983).

MEN84 Mendel, J.E., Final Report of the Defense High-Level Waste Leaching Mechanisms Program, Battelle Pacific Northwest Laboratory, Richland, WA, Report PNL-5157, (1984).

MOR38 Morey, G.W., The Properties of Glass, American Chemical Society Monograph Series, Reinhold Publishing Corporation (1938).

MUL79 Mularie, W.M., W.F. Furth, and A.R.C. Westwood, Journal of Materials Science, 14, 1979, pp. 2659-2664.

NER12	Neri, A., L'Arte Vetraria, Florence (1612) English translation, Merrett (1662).
NEW80	Newton, R.G. and A. Paul, Glass Technology, Vol. 21, p. 307, (1980).
NEW91	Newton, R.G. and A.B. Seddon, Corrosion Science, Vol. 33, No. 4, pp. 617-626 (1992).
OLB82	Olbert, B.H. and R.H. Doremus, Journal of the American Ceramic Society, Vol. 66, No. 3, pp. 163-166 (1982).
PAU90	Paul, A., Chemistry of Glasses, Second Edition, Chapman and Hall (1990).
PED83	Pederson, L.R., C.Q. Buckwalter and G.L. McVay, Sci. asis for Nuclear Waste Management, Vol. 6, (1983).
PED93	Pederson, L.R., McGrail, B.P., McVay, G.L., Petersen-Villalobos, D.A. and Settles, N.S., Physics and Chemistry of Glasses, Vol. 34, No. 4, August 1993, pp. 140-148.
PET25	Petrie, Sir W.M. Flinders, Trans. Newcomen Society, 5, 72 (1924-1925).
RAN61	Rana, M.A. and R.W. Douglas, Physical Chemistry of Glasses, Vol. 2, pp. 179-205, (1961).
SAL94	Salem, A.A., R. Kellner and M. Grasserbauer, Glass Technology, Volume 35, No. 3, June (1994).
SAN72	Sanders, D.M., W.B. Person and L.L. Hench, Applied Spectroscopy, Volume 26, No. 5 (1972).
SAN74	Sanders, D.M., W.B. Person and L.L. Hench, Applied Spectroscopy, Vol. 21, No. 3, pp. 247-255, (May-June 1974).
SPI99	Spiegel, M.R. and L.J. Stephens, Theory and Problems of Statistics, Third Edition, Schaum's Outlines (1999).
SUL83	Sullivan, T.M. and A.J. Machiels, Journal of Non-Crystalline Solids, 55, 1983, pp. 269-282.
VAN65	Van Lier, J.A., The Solubility of Quartz, Drukkerji en Uitgeversmij v/h Kemink en Zoon, n.v. Dem Plein, Utrecht, Netherlands (1965).

VAR94 Varshneya, A.K., Fundamentals of Inorganic Glasses, Academic Press, Inc. (1994).

VEL78 Velain, Ch., Bull. Franc. Soc. Mineral., 1, 113 (1878).

VOL88 Volf, M.B., Mathematical Approach to Glass, Elsevier (1988).

WAL83 Wallace, R. and G. Wicks, Sci. Basis for Nuclear Waste Management, Vol. 6, pp. 23-28, (1983).

WAR38 Warren, B.E. and co-workers, Journal of the American Ceramics Society, 17, 249 (1934).

WIN21 Winlock, H.E., "Bulletin of the Metropolitan Museum of Art," New York, Part 2 (1921).

ZAC32 Zachariasen, W.H., Journal of the American Ceramics Society, 54, 3481 (1932).

ZHA91 Zhang, Z., N. Soga and K. Hirao, Journal of Non-Crystalline Solids, 135, pp. 55-61 (1991).

BIOGRAPHICAL SKETCH

Greg Darby was born October 5, 1972, in Taipei, Taiwan. He received his Bachelor of Science degree in 1995 from the Department of Materials Science and Engineering at the University of Florida, Gainesville, Florida. He was accepted into graduate school at the University of Florida in 1995. Since then, he has been pursuing a Doctor of Philosophy degree. Greg is a member of the American Ceramic Society (ACerS) and Keramos.

I certify that I have read this study and that in my opinion it conforms to acceptable standards of scholarly presentation and is fully adequate, in scope and quality, as a dissertation for the degree of Doctor of Philosophy.

David E. Clark, Chairman
Professor of Materials Science and Engineering

I certify that I have read this study and that in my opinion it conforms to acceptable standards of scholarly presentation and is fully adequate, in scope and quality, as a dissertation for the degree of Doctor of Philosophy.

E. Dow Whitney
Professor of Materials Science and Engineering

I certify that I have read this study and that in my opinion it conforms to acceptable standards of scholarly presentation and is fully adequate, in scope and quality, as a dissertation for the degree of Doctor of Philosophy.

John J. Mecholsky, Jr.
Professor of Materials Science and Engineering

I certify that I have read this study and that in my opinion it conforms to acceptable standards of scholarly presentation and is fully adequate, in scope and quality, as a dissertation for the degree of Doctor of Philosophy.

Wolfgang M. Sigmund
Professor of Materials Science and Engineering

I certify that I have read this study and that in my opinion it conforms to acceptable standards of scholarly presentation and is fully adequate, in scope and quality, as a dissertation for the degree of Doctor of Philosophy.

J. Erik Enholm
Professor of Chemistry

This dissertation was submitted to the Graduate Faculty of the College of Engineering and to the Graduate School, and was accepted as partial fulfillment of the requirements for the degree of Doctor of Philosophy.

December 2000

M. Jack Ohanian
Dean, College of Engineering

Winfred M. Phillips
Dean, Graduate School